THESIS FOR THE DEGREE OF DOCTOR OF PHILOSOPHY

The cyanobacterial pigments scytonemin and nostodione A

Synthesis, photophysicochemical behavior and biological studies

ANDREAS EKEBERGH

Department of Chemical and Biological Engineering

CHALMERS UNIVERSITY OF TECHNOLOGY

Gothenburg, Sweden 2014

The cyanobacterial pigments scytonemin and nostodione A

Synthesis, photophysicochemical behavior and biological studies

Andreas Ekebergh
ISBN 978-91-7597-125-4

Doktorsavhandlingar vid Chalmers tekniska högskola
Ny serie nr 3806
ISSN 0346-718X

Department of Chemical and Biological Engineering
Chalmers University of Technology
SE-412 96 Gothenburg
Sweden
Telephone + 46 (0)31-772 1000

Cover: *Top:* Response surface map displaying the ligand effect on a cascade Heck-Suzuki reaction. *Middle:* Cells treated with monomer **70e** together with its structure. *Bottom:* Absorption spectra for the photo-decay of scytonemin together with its structure.

Printed by Chalmers Reproservice
Gothenburg, Sweden 2014

The cyanobacterial pigments scytonemin and nostodione A

Synthesis, photophysicochemical behavior and biological studies

ANDREAS EKEBERGH

Department of Chemical and Biological Engineering
Chalmers University of Technology

ABSTRACT

The natural UV-screener scytonemin is found in a plethora of cyanobacterial species. Its UV-protective ability allows the bacteria to thrive in inhospitable locations exposed to intense solar radiation. Scytonemin has a dimeric structure consisting of two 1-1' linked 3-(4-hydroxybenzylidene)cyclopenta[*b*]indole-2-one moieties. The cyanobacterial pigment nostodione A consists of the same skeleton, but is not symmetrically appended at C-1. Instead it appears as a 1,2-dione. Both natural products have displayed attractive bioactivity, e.g. inhibition of cancer cell mitosis and *in vitro* reduction of kinase activity.

In this study, flexible synthetic strategies leading to the 3-alkenyl-cyclopenta[*b*]indole-2-one skeleton have been investigated, with focus on different ring-closing methods for the annulation of indoles. In particular, statistical experimental design has been utilized to successfully optimize a cascade Heck-Suzuki reaction. Here, the cyclopentanone is fused onto the indole with the concurrent assembly of the exocyclic alkenyl moiety. The route has been employed to construct a number of 3-alkenyl-cyclopenta[*b*]indole-2-one containing compounds with various substituents around the exocyclic double bond. Both the total synthesis of scytonemin and of nostodione A could be completed from suitable 3-alkenyl-cyclopenta[*b*]indole-2-one fragments, the former via an oxidative enolate coupling of two monomers and the latter via a selective oxidation.

A number of relevant derivatives were synthesized via the developed synthetic route and used to investigate the photophysicochemical properties of scytonemin. Scytonemin demonstrated a low photo-stability in organic solvents, contradictory to its reported behavior *in vivo*. In cyanobacterial colonies, scytonemin is located in the extra cellular polysaccharide matrix, which likely has a stabilizing effect on scytonemin.

Lastly, elaboration of the 3-alkenyl-cyclopenta[*b*]indole-2-one skeleton into kinase inhibitors relevant for combating melanoma was pursued. The kinase inhibiting properties of 17 substances, including scytonemin and nostodione A, were studied. Activity against the clinically proven melanoma target BRAF V600E was found and the most promising compound also displayed favorable properties in cell studies.

Keywords: Scytonemin, nostodione A, UV-screeners, photo-stability, design of experiments, palladium catalysis, cascade reactions, gold catalysis, ligand effect, kinase inhibitor.

List of publications

This thesis is based on the following papers, as well as some unpublished results. The papers are referred to in the text by their roman numerals.

I. **Oxidative Coupling as a Biomimetic Approach to the Synthesis of Scytonemin**

A. Ekebergh, I. Karlsson, R. Mete, Y. Pan, A. Börje and J. Mårtensson
Organic Letters, 2011, **13**, 4458-4461

II. **Total Synthesis of Nostodione A, a Cyanobacterial Metabolite**

A. Ekebergh, A. Börje and J. Mårtensson
Organic Letters, 2012, **14**, 6274-6277

III. **Exploring a cascade Heck-Suzuki reaction based route to kinase inhibitors using Design of Experiments**

A. Ekebergh, C. Lingblom, P. Sandin, C. Wennerås and J. Mårtensson
Submitted

IV. **On the Photostability of Scytonemin, Analogues thereof and their Monomeric Counter-Parts**

A. Ekebergh, P. Sandin and J. Mårtensson
Manuscript

The author has published the following paper which is not included in this thesis.

V. **Ketoprofen-induced formation of amino acid photoadducts: Possible explanation for photocontact allergy to ketoprofen**

I. Karlsson, E. Persson, A. Ekebergh, J. Mårtensson and A. Börje.
Chemical Research in Toxicology, 2014, **27**, 1294-1303

Contribution report

The author made following contributions to the papers presented in this thesis.

Paper I: Performed all reported experimental work except elemental analyses and high resolution mass analyses. Wrote minor parts of the manuscript. Wrote the supporting information.

Paper II: Planned and performed all experimental work, except high resolution mass analyses. Wrote major parts of the manuscript. Wrote the supporting information.

Paper III: Planned and performed the Design of Experiments study. Performed all reported synthesis and characterization, except high resolution mass analyses. Assisted with the planning and execution of the cell studies. Wrote the manuscript. Wrote the supporting information, except experimental procedures for the cellular assays.

Paper IV. Performed the synthesis and HPLC-MS analyses. Assisted with interpretation of the photophysical measurements. Wrote parts of the manuscript.

List of abbreviations

Ac	Acetyl
ANOVA	Analysis of variance
Ar	Aryl
ATP	Adenosine triphosphate
C	Concentration
CCF	Central face composite
dba	Dibenzylideneacetone
DDQ	2,3-dichloro-5,6-dicyano-1,4-benzoquinone
DMF	Dimethylformamide
DoE	Design of experiments
Et	Ethyl
h	The Planck constant
HOMO	Highest occupied molecular orbital
HPLC	High performance liquid chromatography
IC	Internal conversion
ICT	Internal charge transfer
i-Pr	Isopropyl
ISC	Intersystem crossing
L	Ligand
LDA	Lithium diisopropylamide
LUMO	Lowest unoccupied molecular orbital
Me	Methyl
Me-THF	2-methyltetrahydrofuran
ν	Frequency
NMM	*N*-methylmorpholine
Nu	Nucleophile
OTf	Trifluoromethanesulfonate
OVAT	One variable at a time
PACD	Photo-allergic contact dermatitis
PCA	Principal component analysis
Ph	Phenyl
PMB	*Para*-methoxybenzyl
rt	Room temperature
SET	Single electron transfer
T	Temperature
t	Time
TBAF	Tetrabutylammonium fluoride
TBS	Tertbutyldimethylsilyl
t-Bu	Tertbutyl
THF	Tetrahydrofuran
TIPS	Triisopropylsilyl
TMS	Trimethylsilyl

UV	Ultra violet
X	Halide or pseudo halide

Contents

1 Introduction and background

1.1 Introduction to organic chemistry and synthesis of natural products

In the beginning of the nineteenth century, it was believed that organic compounds (substances containing carbons and hydrogens) could not be synthesized, but had to be obtained directly from living organisms.[1] Looking at the vast field of organic chemistry, which today consists of more methods for creating and manipulating organic molecules than any one person can comprehend, such a belief seem distant. The significance of organic chemistry, and consequently the high research interest, is easily understood considering how it contributes both to fundamentally understanding our surrounding as well as concretely giving us means to create new materials and pharmaceuticals.

Organic chemistry can be split into several subfields, one being the total synthesis of natural products. Natural products, also known as secondary metabolites, are small organic molecules found in living organisms. They are distinguished from compounds that are essential to all life, primary metabolites, which consequently are found in all life forms. Instead, different natural products are found in different types of organisms, i.e. a particular natural product is found exclusively in a particular organism. For a long time, natural products were thought to have no explicit role in the organism in which it was produced. Today, numerous natural products have been established to assist with important functions, such as attracting pollinators (for plants) and preventing infections, ultimately enhancing the organisms survivability.[2-4]

The synthesis of natural products has attracted the attention of many an organic chemists. One rationale to the attention lies in the chemical complexity found in numerous natural products. The synthesis of such targets have led to many innovative solutions of synthetic problems and brought novel knowledge to the field. Further, to quote K.C. Nicolaou and S.A. Snyder, "they also provide one of the best forums in which to identify synthetic inadequacies worthy of further methodological development".[5] Another rationale relates to the biological activity frequently encountered among natural products.[6] Synthesizing natural products, and analogues of them, can be used as a platform for developing new bioactive compounds, i.e.

pharmaceuticals. Today, the majority of total synthesis reported concerns natural products with inherent bioactivity.

1.2 Scytonemin and nostodione A

1.2.1 Occurrence, isolation and structure

Scytonemin (**1**) and nostodione A (**2**) are pigments found exclusively in cyanobacteria. Scytonemin was reported already in 1849 by Nägeli,[7] and was subsequently mentioned in several papers during the 20:th century. The compound was however not isolated until 1991 when Garcia-Pichel and Castenholz did a first in depth study of it.[8] They identified it in over 30 species of cyanobacteria, where it mainly occurred in the extracellular matrix, which consists mostly of high molecular weight polysaccharides, but also different proteins.[9, 10] Scytonemin was early on demonstrated to strongly absorb UV-light.[8] The absorbance is strongest in the UVA-(315-400nm) and UVC-regions (100-280nm), while less pronounced in the UVB-region (280-315nm). Scytonemin was also demonstrated to exist in two different forms, a predominant oxidized green/brown form and a reduced red form. The two could be interconverted by reducing/oxidizing agents. The unique dimeric structure of scytonemin (Figure 1) was determined in 1993 along with its reduced form (**3**).[11] The structure consists of a cyclopenta[*b*]indole-2-one system, appended with a phenol substituted alkenyl group in the three position. Scytonemin has since then been explored in many different types of studies, *vide infra*.

Nostodione A (**2**), having a close structural resemblance to scytonemin, has received far less attention. It was first isolated from cyanobacteria in 1994 by Kobayashi who characterized it as a pair of rapidly interconverting stereo-isomers (Figure 1).[12] This was however not the first report of nostodione A. Unknowingly, a semi-total synthesis of the natural product was performed in 1993 when ozonolysis of reduced scytonemin (**3**) yielded nostodione A during the scytonemin characterization campaign.[11] Two additional reports on the isolation of nostodione A have since then been published.[13, 14] Apart from scytonemin and nostodione A, single reports on the isolation of five additional closely related natural products have been accounted for (Figure 1).[13, 15, 16]

1.2.2 Biological role

In their study from 1991, Garcia-Pichel and Castenholz proposed that scytonemin (**1**) is a part of a UV-protective strategy adopted by cyanobacteria.[8] The proposed function was validated by the same researchers only a year later when mats of cyanobacteria were grown in a light controlled environment. The experiment revealed that scytonemin synthesis was triggered by UV-light and that cyanobacteria containing scytonemin were more resilient toward UV-light than those without.[17] Further, scytonemin has been proposed to have an ancient origin, being present as a cyanobacterial sun protective metabolite already during the Precambrian time period (~2×10^9 years ago).[18]

Complementary to these studies, the connection between UV-light, cyanobacteria and scytonemin has been studied on several occasions.[19] However, photo-protection is not the sole

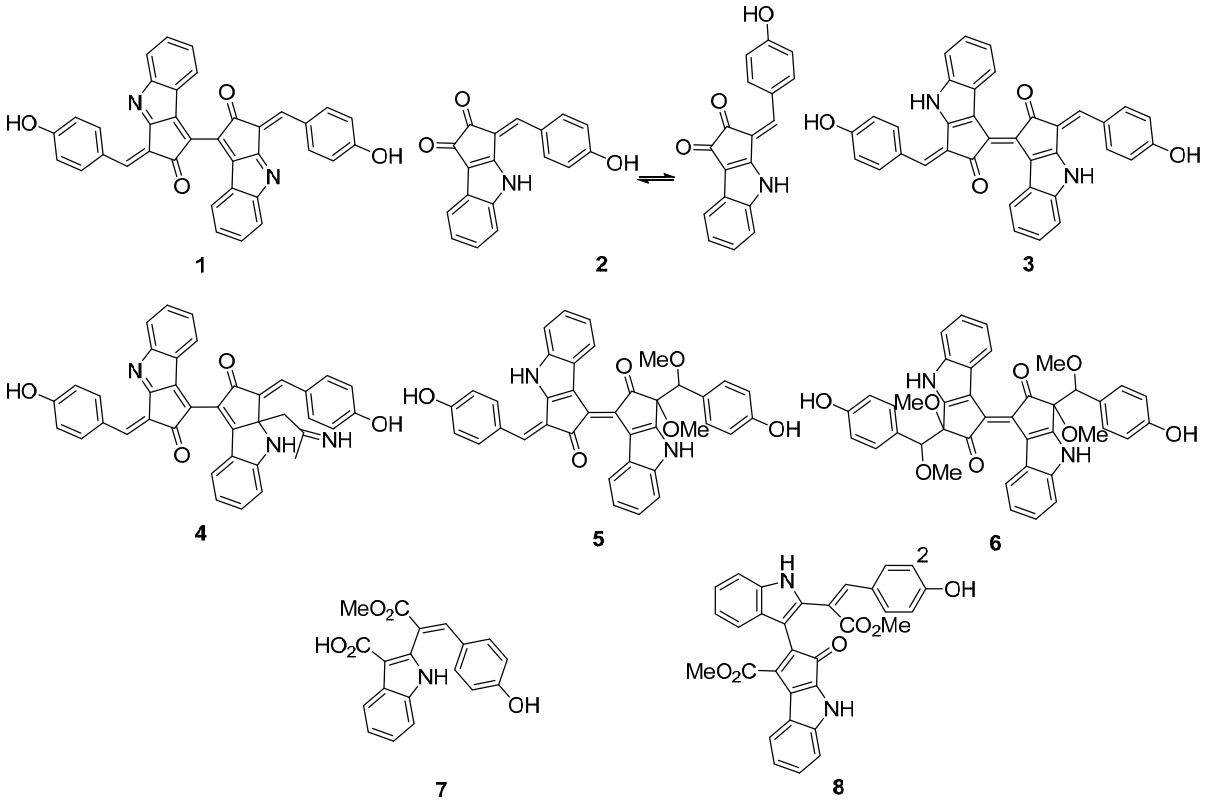

Figure 1. Structures of cyanobacterial metabolites: Scytonemin (1), nostodione A (2), reduced scytonemin (3), scytonemin-imin (4), dimethoxyscytonemin (5), tetramethoxyscytonemin (6), prenostodione (7) and scytonine (8).

role of scytonemin, but its function as an antioxidant has also been established. The combination of oxidative stress (reactive oxygen) and UV-light enhance the biosynthesis of scytonemin compared to UV-light alone.[20] Further, isolated scytonemin has demonstrated radical scavenging properties *in vitro* by a conventional assay.[21]

The role of nostodione A (**2**) has yet to be elucidated. It has been proposed as a biosynthetic precursor in the synthesis of scytonemin,[22] which is a credible explanation considering that scytonemin is biosynthetically derived from a monomeric precursor (see chapter 1.2.3 below). Upon its extraction from cyanobacteria, prenostodione (**7**) was suggested to be a precursor to nostodione A, which also explains its name.[13] However, nostodione A is likely constructed via the same pathway as scytonemin, which does not contain prenostodione as an intermediate, making the suggested role questionable. The cyanobacterial production of scytonemin-imin (**4**) has been reported to be dependent on intense UV-radiation. Further, its absorption is red-shifted compared to scytonemin and has therefore been proposed to shield chlorophyll from visible light during intense solar radiation.[16] The same explanation could be adopted for dimethoxy- (**5**) and tetramethoxyscytonemin (**6**) as well, both having a red-shifted absorption. Finally, a degradation pathway from reduced scytonemin has been propositioned for scytonine (**8**).[15]

1.2.3 Biosynthesis

Over the last 7 years, great progresses have been made to understand the biosynthesis of scytonemin (**1**). In 2007, Soule et al. presented a genomic study of the cyanobacteria *Nostoc Punctiforme*, revealing a cluster of 18 genes involved in the synthesis of scytonemin.[23] Several of the genes involved were determined to code for tryptophan and tyrosine synthesis, which are the two amino acid precursors of scytonemin. However, a number of genes were established to have no comparable function in any other organism and were therefore anticipated to be specific for the scytonemin biosynthesis. In 2008, two genes in the cluster were translated into proteins.[24] These were demonstrated *in vitro* to first catalyze the formation of indole-3-pyruvic acid from tryptophan and then to couple it with *p*-hydroxyphenylpyruvic acid, generating **11** (SCHEME 1). The function of a third gene was established one year later.[25] Its corresponding protein catalyzed a ring closing reaction of **11**, forming a monomeric form **(12)** of scytonemin. The functions of the remaining unknown genes are yet to be elucidated, but they should involve an oxidation of **12** and a subsequent coupling of two monomers into the dimeric structure of scytonemin.

SCHEME 1. Initial biosynthetic steps toward scytonemin, catalyzed by the enzymes ScyB, ScyA and ScyC.

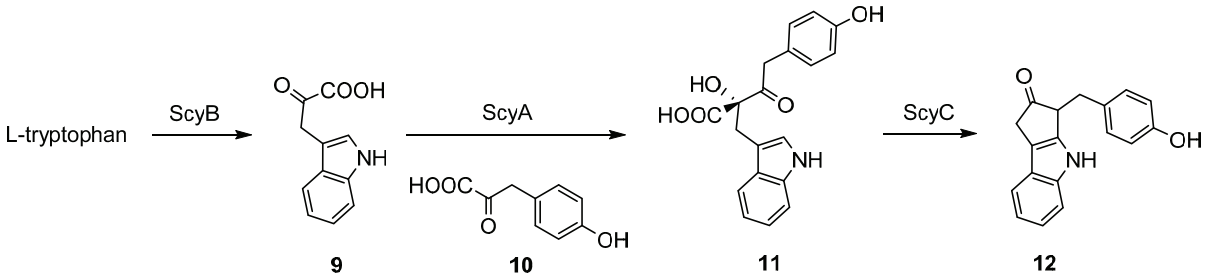

Utilizing the biosynthetic breakthroughs, an attempt to produce scytonemin in *E. Coli* has recently been presented.[26] The gene cluster associated with scytonemin was inserted into the bacteria, giving them the ability to produce an oxidized form of scytonemin monomer **12** together with a number of byproducts, but not scytonemin itself. The results suggest either that additional genes are necessary for the complete synthesis or that the synthesis requires the specific cellular environment of the cyanobacteria.

1.2.4 Artificial synthesis

The cyclopenta[*b*]indole-2-one part of scytonemin (**1**) and nostodione A (**2**) has been synthesized via various methods.[27-33] However, apart from our accounts on the total syntheses of scytonemin (2011) and nostodione A (2012),[34, 35] only one synthesis has been reported of the cyclopenta[*b*]indole-2-one system with an exocyclic double bond in position three.[36] In their report, McNulty and co-workers present an elegant route to nostodione A. The route is designed around an acidic phosphonate which is utilized on double occasions, first to ring-close a 2,3-disubstituted indole and then in a Horner-Wadsworth-Emmons reaction to install the exocyclic double bond. The route was used to synthesize a number of derivatives which were assayed against the parasite *Toxoplasma gondii*.

1.2.5 Biological activity

The bioactivity of scytonemin (**1**) has been evaluated in several studies. It was in 2002 characterized as a possible antiproliferative pharmacophore, demonstrating the ability to inhibit several kinases involved in the cell cycle regulatory mechanism.[37] In agreement with cell-cycle inhibition, tumor cells treated with scytonemin were shown to undergo apoptosis while non-proliferating cells treated with scytonemin remained intact. Since then, its antiproliferative effect on a number of cancer cell types has been established.[38-41] Scytonemin has also been characterized as an anti-inflammatory agent, reducing induced ear edema and skin inflammation in mice.[42, 43] A suggested mechanism involves inhibition of the NF-κB transcription factor, which activity is regulated by kinases.

The ability of nostodione A (**2**) to inhibit cell-division of sea urchin eggs was established concurrent with its first isolation in 1994.[12] The ability originated from a destructive interaction with the mitotic spindle during cell mitosis. Later, nostodione A was also found to inhibit proteasomes and the parasite *Toxoplasma gondii*.[14, 36]

1.3 Sunscreens, skin cancer and allergy

Exposure of the human body to solar UV-radiation has both beneficial and harmful effects. Production of vitamin D, necessary for several body functions, is well known to be dependent on UV-radiation.[44, 45] Too much sun exposure has on the other hand been linked to the development of the three most common types of skin cancers; squamous cell cancer, basal cell cancer and melanoma. The two first skin cancer types are associated with chronic UV exposure, while melanoma has been related to intermittent and intense UV exposure, especially when exposed at a younger age. [46, 47]

The use of sunscreens have been reported to reduce the risk of squamous cell cancer, while its effect on basal cell cancer and melanoma is inconclusive.[48] Although beneficial as UV-protection, sunscreens have been associated with negative side-effects, such as photo-allergic contact dermatitis (PACD).[49] PACD originates from sunscreens insufficiently stable toward UV-radiation. While the sunscreen in itself may be safe, the photo-degradation products formed can potentially be allergenic. For instance, it is well known that the commonly used sunscreen avobenzone (**13**) can cause allergy.[50] The allergenic mechanism was investigated in the dissertation thesis of I. Karlsson, who established that avobenzone degrades into benzils (**14**) and arylglyoxals (**15**) upon UV-irradiation (SCHEME 2).[51, 52] The former was shown to be cytotoxic while the latter was strongly allergenic. Thus, the allergenic mechanism of avobenzone is indeed that of photo-allergenic contact dermatitis. Consequently, photo-stability is an important factor to account for in sunscreen design.

SCHEME 2. Photo-degradation of avobenzone (13) into cytotoxic benzils (14) and allergenic arylglyoxals (15).

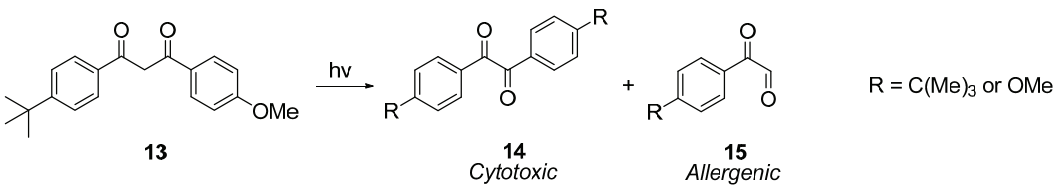

13 **14** *Cytotoxic* **15** *Allergenic*

Nature is often used as an inspirational source to solve problems. The natural UV-screener scytonemin (**1**) has been proposed as a potential sunscreen on several occasions. It has a broad absorption in the UV-region and has also been reported to be photo-stable. With its ancient history,[18] one could also argue that scytonemin is evolutionary favorable, thus having inherent traits which cannot be improved upon further by the evolutionary mechanism. This of course raises the question: Are those traits favorable for sunscreens in a general sense, or simply favorable for the cyanobacteria?

1.4 Advanced melanoma

Melanoma has continuously increased in occurrence over the last 30 years.[53] Despite the negative trend in melanoma incidence, no significant change in mortality has been observed. The development is likely a result of increasingly better methods for early recognition of melanoma, which often results in successful surgical removal of the tumor. However, if not detected in time, melanoma will eventually spread to other parts of the body (advanced melanoma). Once spread, the prognostic outlook is poor with a median survival of about 6 to 10 month, which cannot be improved upon with traditional chemotherapies.[54, 55]

In 2002, Davies et al. found mutations in the gene coding for the kinase BRAF in over 60% of the tested melanoma, with a single mutation, BRAF V600E, found in 52% of the cases.[56] BRAF is part of the mitogen-activated protein kinase (MAPK) pathway, which regulates cellular events such as proliferation, cell cycle regulation and cell survival.[57] External cellular stimuli activate the pathway, which in a cascade event ultimately lead to gene transcription. BRAF is in this sequence activated by the upstream kinase RAS and activates the downstream kinase MEK. However, the BRAF V600E mutant is inherently active, resulting in a constantly active MAPK pathway.[58] Melanoma cancer cells have demonstrated a high dependency on the mutated pathway and selective inhibition of BRAF induces apoptosis.[59]

The new therapeutically relevant information spawned an intense search for selective BRAF-inhibitors with a good therapeutic profile. In 2011, a first inhibitor (vemurafenib) was approved for the treatment of BRAF V600E mutation-positive melanoma. In phase three clinic trials, the BRAF inhibitor displayed a reduction in the risk of death by 63% compared to chemotherapy.[60, 61] However, the treatment is associated with a number of adverse side effects, such as squamous-cell carcinoma and photosensitivity. Another major problem is tumor adaptation resulting in replenished growth of the tumor after a few month of treatment.[58] A number of adaptive mechanisms have been elucidated so far. A common denominator for several mechanisms is a BRAF dimerization process, in which BRAF form new active dimeric complexes together with other proteins, toward which the inhibitor is ineffective. A number of different strategies are emerging to overcome resistance, e.g. combination of different kinase inhibitors and periodical use of BRAF-inhibitors. Another strategy focus on developing inhibitors effective against the mutant BRAF-dimers. Some success in this area have been achieved with a second generation BRAF inhibitors.[62]

2 Objectives

Three main objectives were pursued in this study:

1) To develop a concise, flexible synthetic route to scytonemin, nostodione A and derivatives of them relevant for achieving objectives 2 and 3. Specifically, the route should offer the possibility of constructing derivatives with different substituents around the exocyclic double bond (Figure 2), which is considered to be important in the studies of the photophysical behavior (objective 2) as well as bioactivity (objective 3).

2) To investigate and evaluate the photophysicochemical properties of scytonemin, ultimately to determine its viability as a sun screening compound.

3) To explore the possibility of developing melanoma relevant kinase inhibitors based on the 3-alkenyl-cyclopenta[*b*]indole-2-one skeleton of scytonemin and nostodione A.

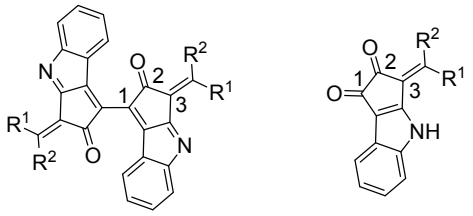

Figure 2. Scytonemin scaffold 16 and nostodione A scaffold 17, which should be conceivable to construct with the synthetic route. Molecule numbering is displayed for the three first positions.

3 Theory and methodology

Theory and methods central to this thesis are reviewed here. These include accounts for palladium- and gold-catalyzed cyclizations, Design of Experiments methodology, chemistry of excited states and ligand-kinase interactions.

3.1 Palladium catalysis: The Suzuki and Heck reactions

Numerous palladium catalyzed methods for creating carbon-carbon bonds have been developed over the last couple of decades.[63] The palladium catalyzed reactions are usually characterized by mild reaction conditions and great selectivity toward the desired chemical outcome. Palladium catalysis recently gained attention when the Nobel prize was awarded to Akira Suzuki, Richard Heck and Ei-ichi Negishi for their work in the field.[64] A short summary of Suzuki and Heck reaction theory is presented here.

3.1.1 Suzuki reaction

The palladium catalyzed reaction between an organoboron compound and an aryl or vinyl halide is known as the Suzuki reaction.[63, 65] The organoboron species is most often a boronic acid or a boronic acid precursor which is hydrolyzed *in situ*. The reaction mechanism is usually described by three discrete steps. First, an oxidative addition of palladium(0) (**18**) to the organohalide (**19**) forms a 16-electron square planar *trans*-palladium(II)-complex (**20**). A subsequent transmetallation, where a carbon migrates from the boronic acid (**22**) to the palladium, generate a new square planar *trans*-complex (**23**). Finally, a *cis*/*trans* isomerization and reductive elimination form the new carbon-carbon bond in product **24** (SCHEME 3). Albeit the 16-electron square planar complex is usually invoked as an intermediate, both 14-electron and 18-electron species are now being proposed as active species, *vide infra*. Typical reaction conditions involve a palladium precatalyst, ligands (most often of a phosphor-donor type), solvent and hydroxide ions or base/water.[63]

The rate of oxidative addition depends strongly on the halide or pseudo halide in the substrate. The relative rate has been established as: PhI >> PhOTf >PhBr >> PhCl.[66, 67] The rate further

SCHEME 3. Simplified mechanism of the Suzuki reaction. I: Oxidative addition, II: Transmetallation, III: Reductive elimination. L: Ligand, X : Halide or pseudo halide. Formed C-C bond in bold.

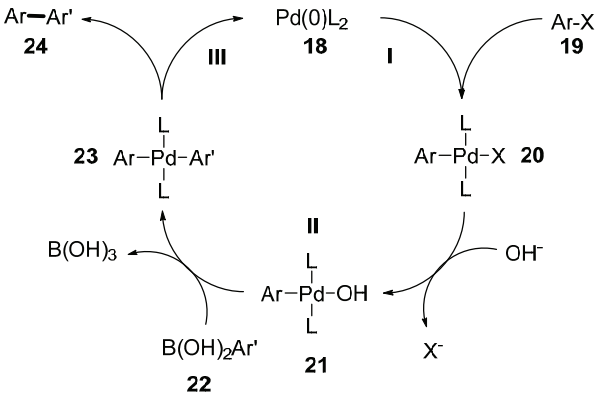

depends on the electron density of the compound. For both *para* substituted PhI and PhOTf, Hammet free-energy relationship studies have demonstrated an increased rate for electron deficient compounds. A recent study of the oxidative addition found that the active palladium(0) species depends on the halide.[68] While iodo-arenes react with a bi-ligated palladium(0) complex, the less reactive chloro-arenes proceed via mono-ligated palladium. The observation is further supported by calculations, where mono-ligated palladium has been put forward as more reactive and as such necessary for activation of unreactive chloro-carbon bonds.[69] It was further demonstrated that ligand bulk affected the active species, but much less so than the halide. Bulky, electron rich ligands can on the other hand stabilize mono-ligated complexes.[70] Consequently, even though the bulk does not affect the oxidative addition transition state, the ability of bulky ligands to force the reaction into a mono-ligated pathway will increase the reaction rate.[71] Further, the pure electronic properties of the ligand have been computationally demonstrated to affect the oxidative addition, with a positive correlation between ligand σ-donating capacity and rate.[72]

The transmetallation is comparably difficult to investigate, and is therefore less studied than oxidative addition. Most efforts have been aimed toward elucidating the role of water. Two pathways have been suggested, the first involves formation of a boronate complex (**25**) prior to transmetallation, and the second involves a palladium hydroxide species (**21**) (SCHEME 4).[73] It is now generally accepted that the latter mechanism is correct, and that the oxophilic organoboron species will coordinate to the hydroxide (**26**) in the transmetallation step.[74, 75] Both electron deficient ligands (better π-acceptors) and substrates (the organohalide and organoboron species) have been proposed by computational studies to accelerate the transmetallation.[72, 76] Ligands with good π-accepting abilities have been suggested to better accommodate the buildup of negative charge on the palladium during carbon migration and thereby reduce the transition state energy (see **27** in SCHEME 4).

A prerequisite condition for reductive elimination is a *cis*-configuration (**28**) of the eliminating species (SCHEME 5). The 16-electron square planar palladium complex is however more stable in a *trans*-configuration, resulting in unfavorable conditions for reductive elimination.[63] Instead, 14-electron mono-ligated T-shaped complexes (**30**) have been suggested in kinetic investigations as the active species.[77, 78] Ligands stabilizing mono-

SCHEME 4. Two proposed pathways of the transmetallation. L : Ligand, X : Halide or pseudo halide.

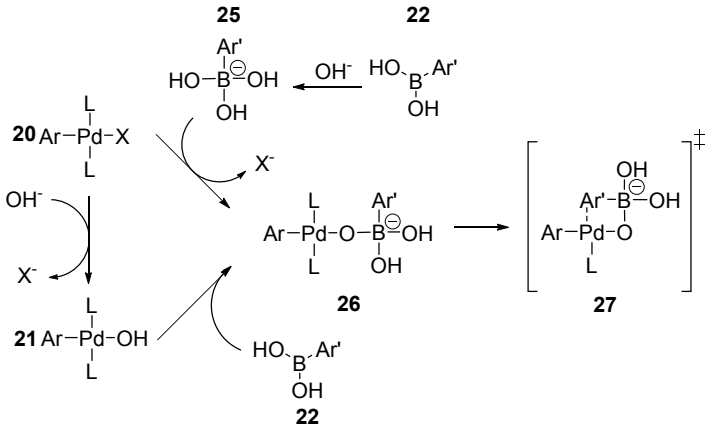

ligated complexes can therefore possibly operate via this mechanism.[70] 18-electron penta-coordinated anionic complexes (**29**) have also been invoked as active species in reductive elimination.[79] In Suzuki couplings, hydroxyl ions have been suggested to coordinate to palladium prior to the reductive elimination, forming such a penta-coordinated complex.[74] The electronic properties of the ligand also affect the reductive elimination, with electron deficient ligands increasing the rate.[80, 81] Electron donating ligands have been suggested to stabilize the electron deficient Pd(II)-complex and thereby increasing the transition energy barrier. An opposite dependence of the substrates have been proposed, thus electron rich substrates accelerate the reductive elimination.[76]

The relative rate of the catalytic steps depends on many factors: electronic and steric properties of substrates and ligands, additives, solvents etc. When using aryl chlorides, it is typically the oxidative addition that is rate limiting. Aryl iodides on the other react fast in oxidative addition and the transmetallation have in a model system been determined as the rate determining step.[74] Regarding ligands, both oxidative addition and reductive elimination have been suggested to benefit from mono-ligated palladium species, which are stabilized by large and electron rich ligands. Both transmetallation and reductive elimination benefit from electron poor ligands, while oxidative addition benefit from electron rich. Taken together, the choice of ligand depends on both steric and electronic properties and the optimal option varies with the substrate.

SCHEME 5. Possible complexes active in the reductive elimination.

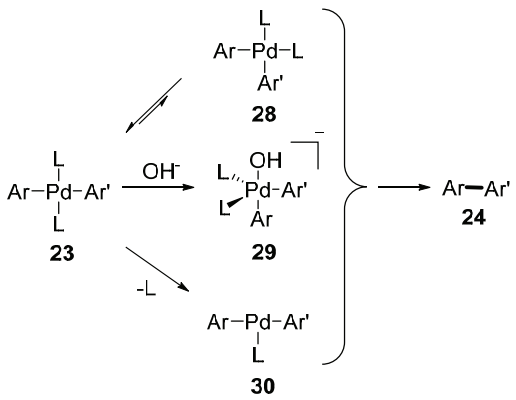

3.1.2 Heck annulations involving alkynes

The Heck reaction[82, 83] is usually described as a catalytic cycle made up by four discrete subreactions (SCHEME 6); an oxidative addition of palladium(0) to an aryl halide **19** (can also be a vinyl halide), a *syn*-carbopalladation of the palladium(II) species **20** to an alkene **31** (can also be an alkyne), a β-hydride elimination of intermediate **32** to produce the organic product **33** and finally a reductive elimination of a hydrogen and a halide to regenerate the active palladium(0).

SCHEME 6. Catalytic cycle of the Heck reaction. I: Oxidative addition, II: Carbopalladation, III: β-hydride elimination, IV: Reductive elimination. L: Ligand, X: Halide or pseudohalide. Formed C-C bond in bold.

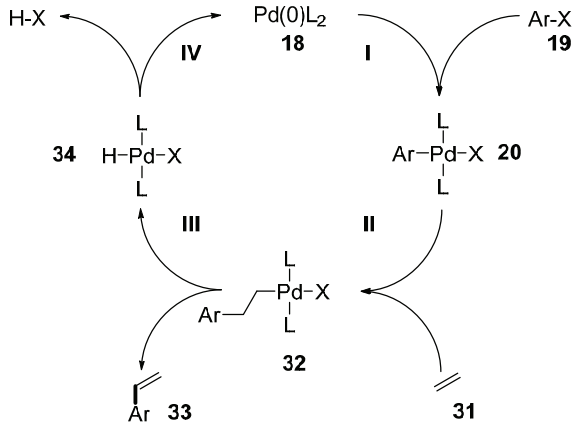

An intramolecular, ring forming Heck reaction is obtained when the alkene/alkyne is tethered to the organohalide. Using alkynes without available β-hydrogens generate a special case in which the reaction cannot proceed past carbopalladation (SCHEME 7).[84-92] Instead, in the presence of a transmetallation reagent **22**, the "trapped" species **37** proceed to form a complex of type **38**. The palladium species **38** can via reductive elimination form product **39** and regenerate the palladium(0)-complex. Two C-C bond forming events take place through the course of the reaction, first in the carbopalladation and then in the reductive elimination. When the transmetallation reagent is a organoboron, the reaction is known as a tandem/cascade Heck-Suzuki reaction. Intramolecular Heck reactions involving alkynes have been used exclusively in this project and the remainder of this chapter will discuss some theoretical aspects of it. Focus will be on carbopalladation as the other elemental steps have been previously discussed in chapter 3.1.1 above.

Intramolecular carbopalladations involving alkynes proceed regiospecifically to form *exo-dig syn*-products.[90] This phenomenon can be explained by the energetically unfavorable transition state associated with a hypothetical *endo-dig syn*-carbopalladation of alkyne **36** (SCHEME 8), which would give the highly strained vinylic intermediate **40**. The alkyne substituent has in some instances been demonstrated as vital for the cyclization.[85] Whereas a terminal alkyne of **41** does not participate in a cyclization event, a methyl group enables the reaction (SCHEME 8). Similarly, introducing a bulky group at the nitrogen of **41** enabled terminal alkynes to participate in the reaction. The necessity of bulky substitutes has been suggested to originate

SCHEME 7. Simplified mechanism of an intramolecular tandem Heck-Suzuki reaction. I: Oxidative addition, II: Carbopalladation, III: Transmetallation, IV: Reductive elimination. L: Ligand, X: Halide or pseudohalide. Formed C-C bonds in bold.

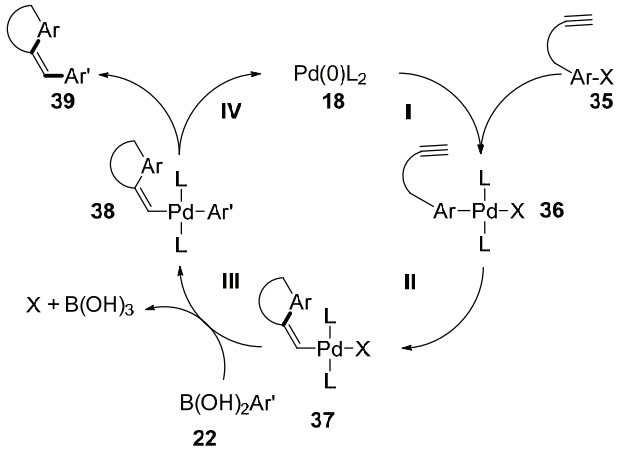

from conformational features of the substrate. A facile carbopalladation require the right conformation of **41**.

The 16-electron *trans*-square planar complex **43** proposed as a product after oxidative addition (see chapter 3.1.1) is unreactive in carbopalladations (SCHEME 9).[93] However, theaddition of acetate ions to preformed complex **43** enables its participation in a reaction with styrene. In this reaction, the palladium(II)-complex **44** has been postulated as the active species during carbopalladation. Whether other ions, such as hydroxyls, also accelerate the carbopalladation is unknown. Further, ligands are well known to affect carbopalladation and have in intermolecular Heck reactions been used to tune the regioselectivity between branched and linear products.[94] Using the literature to elucidate how ligand bulk and electronic properties affect carbopalladation of intramolecular addition to alkynes is however difficult.

SCHEME 8. a) Hypothetical endo syn-carbopalladation. b) Influence of substituents on a tandem Heck-Suzuki reaction. Substituent bulk presumably force the substrate into a favorable rotamer. Formed C-C bonds in bold.

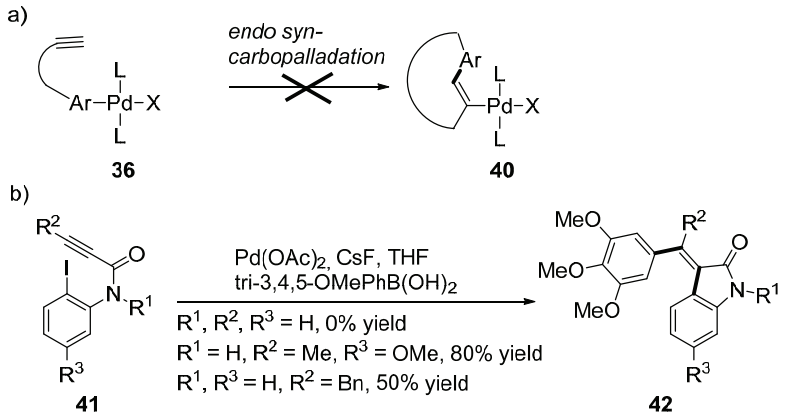

SCHEME 9. Ion effect on carbopalladation. While iodide ligated palladium(II)-species 43 react sluggishly, acetate ligated species 44 reacts swiftly.

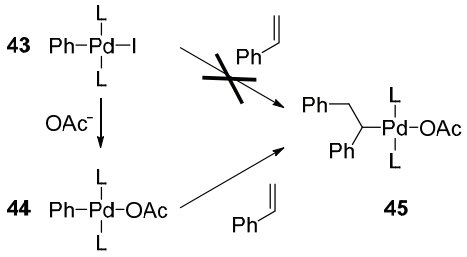

3.2 Gold catalyzed annulation of indoles

Gold(I) is a highly π-acidic metal, a property explained by relativistic effects (which will not be theoretically treated here).[95] It coordinates strongly with alkynes to give a linear ligand-gold-alkyne complex **46** (SCHEME 10). The coordination activates the alkyne toward a nucleophilic attack, which produces a *trans*-alkenyl gold complex **47**. The nature of the nucleophile determines how the gold complex **47** reacts thereafter. It can e.g. rearrange, fragment and add additional nucleophiles. This chapter focuses on the reactivity of alkynes toward indoles.

SCHEME 10. Nucleophilic addition to alkynes catalyzed by gold.

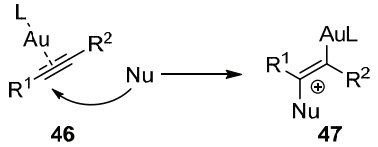

Recently, gold catalyzed annulations of indoles have received attention by several research groups. Indoles tethered with alkynes at C-2 or at C-3 is a common theme for these cyclizations.[96-103] The mechanism of gold mediated annulations of indoles can be exemplified by a catalytic cycle (SCHEME 11). Treating indoles appended with alkynes in the 3-position, e.g. **49,** with gold, produces the activated species **50** which readily undergoes nucleophilic addition by the indole. A 1,2-shift of the spiro intermediate **51** produce species **52**.[97, 103] Indole **52** is the result of a 1,2-shift which retains the initial skeleton connectivity, the 1,2-shift can however occur with rearrangement to produce indole **53**. Deprotonation regenerates the aromatic indole **54**, which after protodemetalation produces the target molecule **55** and regenerates the gold catalyst.

Systems comprised of alkynes tethered to indoles via a two atom chain at C-3 have been reported to cyclize exclusively into 6-membered rings (SCHEME 12).[96, 97, 102, 103] Thus, the 3-appended indole **56** react via the 5-*endo-dig* intermediate **57** to give **58** or **59**. While substrates with two atom tethers have shown only one type of ring-size selectivity so far, substrates with four atom tethers have displayed a selectivity which can be controlled by the catalytic system.[96] A recent investigation into general *dig*-cyclizations showed that 4-*exo* is kinetically favorable to 5-*endo*. However, the energy difference is small and the selectivity is

SCHEME 11. Simplified mechanism of gold catalyzed annulation of 3-appended indoles. I: Gold-alkyne coordination, II: Nucleophilic attack, III: 1,2-shift, IV: Deprotonation, V: Protodemetalation. L: Ligand

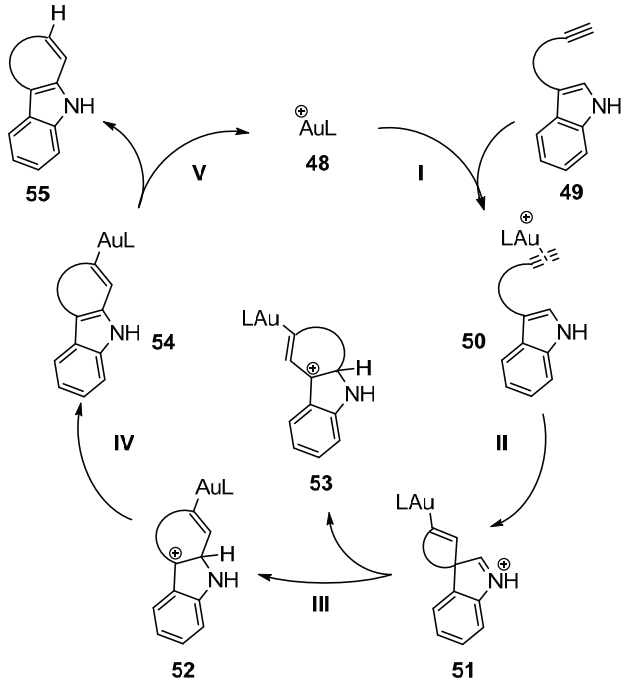

determined by the stereoelectronics of the substrate.[104] This suggests that the 3-appended indole **56** could be forced into the 4-*exo-dig* intermediate **60** through careful choice of substrate and catalytic system. This would, after a 1,2-shift, produce either the 3-alkenyl-cyclopenta[*b*]indole **61** or the 1-alkenyl cyclopenta[*b*]indole **62**.

SCHEME 12. Reactivity of indoles tethered to alkynes via a two carbon chain.

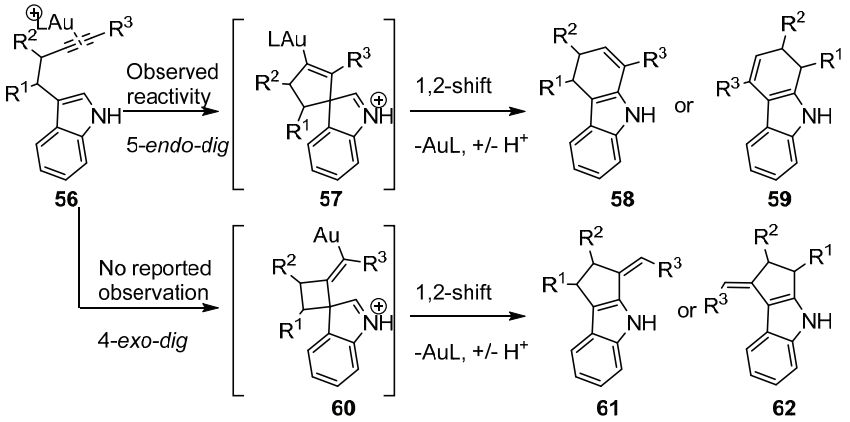

3.3 Design of experiments (DoE)

Experiments constitute the core of research. Whenever a research question is investigated, experiments are conducted to generate information relevant to the study. Design of experiments (or statistical experimental design) is a rational method for designing experiments which will produce as much relevant information as possible. More specifically,

by investigating variables by their simultaneous variation, an information rich quantitative model of the investigated problem is produced.

3.3.1 DoE, step-by-step

The workflow of an experimental design, exemplified by an organic reaction, is briefly outlined below.

1) Defining objective and choosing response variables. Before any experiments can be conducted, it is important to have a well-defined objective of the study. This is closely related to choosing response(s) which are measurable outcomes of the experiments. In a typical organic reaction, the *objective* is often "to obtain as much product as possible" which is quantified by the *response* "yield".

2) Establishing variables affecting the responses. The variables, also known as *factors* in DoE, can either be varied (investigated) or kept constant (non-investigated) during the experiments. As the number of varied factors increase, the experiments necessary to perform will rapidly be amplified. Consequently, the varied factors should if possible be limited to the most influential and interesting ones. In the present exemplar reaction, temperature (T), concentration (C) and time (t) are chosen as investigated variables.

3) Choosing levels of the investigated (varied) factors. Each factor is typically investigated at two levels, a high (+) and a low (-) level. Choosing factor values can be difficult, but initial estimates can often be made based on chemical understanding and previous knowledge. In this example, we choose: T (+) = 100°C, T (-) = 50°C, C (+) = 1 M, C (-) = 0.1 M, t (+) = 10 h and t (-) = 1 h.

4) Choosing an experimental design. The design determines which experiments to perform. Each design aims at producing as much high quality data as possible with as few experiments as possible. Three related experimental designs are briefly described below.

4a) Full factorial design. Here, the factors are investigated in all possible combinations. Both factor main effects and effects due to factor interactions can be elucidated with a full factorial design. The number of experiments necessary to perform is given by 2^k where k is the number of investigated factors. A center point is also included, which have mid-values on all factors. The center point is usually performed three times (triplicate) to determine the experimental error. A center point will also reveal whether the response can be modeled with a linear function or if the inclusion of higher order terms is required, *vide infra*. The present example with three factors (k = 3) will give $2^k = 2^3 = 8$ experiments for factor variations and additional 3 experiments for the center point, totaling 11 experiments. The explored reaction space can be visualized as a cube in a three dimensional coordinate system, confined by the levels of the investigated factors (Figure 3).

With the full factorial design, the reaction model obtained after data fitting has the form:

$$yield = \beta_0 + \beta_T T + \beta_C C + \beta_t t + \beta_{TC} TC + \beta_{Tt} Tt + \beta_{Ct} Ct + \beta_{TCt} TCt + residual \qquad (Eq. 1)$$

Where β_0 is a constant, β_x are factor coefficients and β_{xy} are factor interaction coefficients.

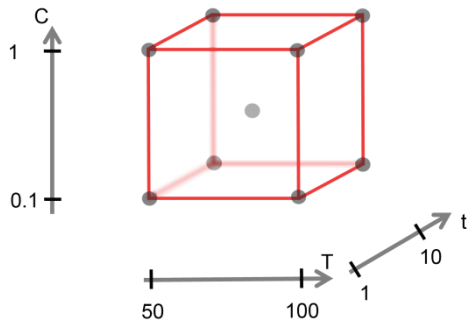

Figure 3. Reaction space visualized as cube defined by the levels of investigated factors (T (+) = 100°C, T (-) = 50°C, C (+) = 1 M, C (-) = 0.1 M, t (+) = 10 h and t (-) = 1 h.) Each experiment is represented by a grey dot.

Eight coefficients are calculated from the full factorial design, one constant, three for main effects, three for second order interaction effects and one for a third order interaction effect.

4b) Fractional factorial design. Studies based on full factorial designs quickly become unrealistic when the number of factors increase; 6 factors = 64 experiments, 10 factors = 1024 experiments (excluding center point). A large number of variables is also associated with many interaction effects of higher order (i.e. interaction effects involving more than two factors). The impact of these effects is usually insignificant and does consequently not need to be modeled. When excluding higher order interaction effects, a model with 6 factors include 1 constant, 6 main effects and 16 second order interaction effects, totaling 23 coefficients. Thus, 23 experiments are enough when excluding interaction effects of higher order, compared to the 64 performed in a full factorial design. In the same way, it may be enough to model main effects in an initial screening process, which in the case with 6 factors would require 7 experiments. *Fractional factorial* designs use a *fraction* of the experiments needed for a full factorial design according to 2^{k-p} where k is the number of factors and p is the size of the fraction (i.e. $1/2^p$ = 1/2, 1/4, 1/8... for p =1, 2, 3...). Using a 2^{3-1} fractional factorial design for the reaction exemplified here would require $1/2^1$ of the original experiments, i.e. 4 experiments for factor variation. Another three experiments should be included for the center point as discussed previously. The experiments are in a fractional factorial design selected to cover a maximal volume of the reaction space (Figure 4).

With the 2^{3-1} fractional factorial design, a model of 4 coefficients is obtained after data fitting:

$$yield = b_0 + b_1T + b_2C + b_3t + residual \qquad (Eq. 2)$$

Where b_0 is a confounded constant and b_x are confounded factor coefficients.

In Eq. 2, the coefficients are labeled as "confounded", which is an effect of using a fractional factorial design. Confounded coefficients are the sums of 2 or more "real" effects and a more accurate way of denoting the model would be:

$$yield = (\beta_0 + \beta_{TCt}) + (\beta_T + \beta_{Ct})T + (\beta_C + \beta_{Tt})C + (\beta_t + \beta_{TC})t + residual \qquad (Eq. 3)$$

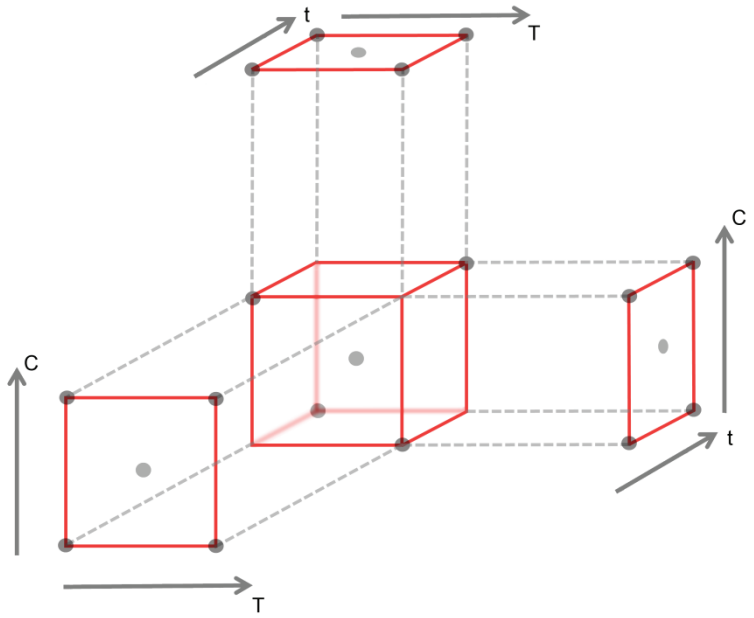

Figure 4. A 2^{3-1} fractional factorial design with the four experiments covering a maximal volume of the reaction space. This can be visualized by projecting the experiments onto lower reaction dimensions. Each of the three reaction planes correspond to a full factorial design.

Where β_0 is a constant, β_x are factor coefficients and β_{xy} are factor interaction coefficients.

Thus, the constant term b_0 in Eq.2 is really the sum of the "true" constant term, β_0, and the higher order interaction coefficient, β_{TCt}. It is also seen from Eq. 3 that the main effect coefficients are the sum of "true" main effects and second order interaction effects.

Consequently, if the model contain a large b_1, one cannot be certain if it is the temperature or an interaction between the concentration and reaction time that strongly affects the yield. The confounding is an obvious weakness of the fractional factorial design used here. Moving into designs with more factors, fractions become more viable. Using 6 factors in a 2^{6-1} design will reduce the number of experiments from 64 to 32 (excluding center point). Yet the main effects are only confounded with the fourth order interaction effects and second order interaction effects with third order interaction effects. The higher order interaction effects rarely contribute and the model terms can reliably be interpreted as main and second order interaction effects.

4c) Central composite face (CCF) designs. As previously mentioned, the center point is used to screen for non-linear effects which cannot be modeled with the interaction equations obtained from previous designs. The center point, having intermediate values on all factors, should consequently have an intermediate response. If the response deviates strongly from what is anticipated, it is an indication that quadratic terms need to be included for one or more factors.

Central composite face (CCF) designs are closely related to factorial designs. However, in addition to elucidating main and interaction effects, CCF designs investigate quadratic relations by isolating and inspecting each of the factors separately. Practically, one factor is inspected by performing experiments at its two extreme values, while maintaining the other

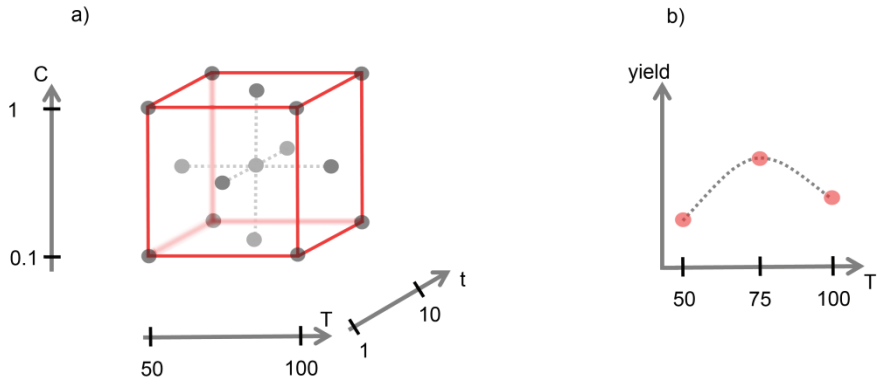

Figure 5. a) Full factorial 2^3 CCF design displaying axial points centered on each side of the cube. b) The quadratic influence of temperature (T) on the yield is inspected. As the factors C and t are kept constant at intermediate values, T can be visualized in a two dimensional coordinate system with the response (yield) on the other axis. Notice how the mid-value of 75°C produces the best yield, indicating a quadratic dependence of the temperature on the yield.

factors at intermediate values (Figure 5). For the reaction example with three factors, a CCF design requires an additional six experiments to investigate all factors for quadratic relations, compared to a factorial design. Once again, a cube can be used to visualize the reaction space (Figure 5). The additional experiments are known as *axial points* and are centered at the sides of the cube. Conveniently, factorial designs can easily be evolved into CCF designs by introducing axial points.

With the 2^3 CCF design, the reaction model obtained after data fitting has the form:

$$yield = \beta_0 + \beta_{TT}T^2 + \beta_{CC}C^2 + \beta_{tt}t^2 + \beta_T T + \beta_C C + \beta_t t + \beta_{TC}TC + \beta_{Tt}Tt + \beta_{Ct}Ct$$

$$+ \beta_{TCt}TCt + residual \qquad (Eq.4)$$

Where β_0 is a constant, β_{xx} are quadratic factor coefficients, β_x are factor coefficients and β_{xy} are factor interaction coefficients.

Fractional factorial CCF designs are also a viable choice. However, the resulting model will contain confounded coefficients as discussed above.

5) Randomizing and running the experiments. Once the experimental design is chosen, the experiments are performed in a random order. Experiments run in a randomized order are considered to be the most impartial way to obtain reliable data.

6) Regression and analysis of model. The size of the factor coefficients are elucidated by fitting the experimental data by regression. As the resulting empirical model will not fit the experimental data perfectly, a residual term (also known as error term) will always accompany the model (as is shown in Eq.1 to Eq.4 above). Factors with coefficients that are not statistically different from zero (0) have insignificant effects on the response and are usually removed from the model.

Analysis of variance (ANOVA) is the common method for determining the reliability of the model. ANOVA make two primary tests. In the first, the total experimental variance is

divided into the variance explained by the model and the residual, non-explained variance. A good model explains most of the observed experimental variance, thus the residual variance is small. In the second test the residual variance is further divided into variance due to model error and variance due to imperfect experimental reproducibility. All experiments are associated with non-perfect reproducibility, which usually is determined by center point replicates in DoE. A good model has a small model error compared to the experimental error, which is known as having *no lack of fit*. Taken together, a good model should have a high explained variance compared to the residual variance, and most of the residual variance should stem from experimental variance due to imperfect reproducibility.

There are a number of parameters, obtained from ANOVA, used to evaluate the reliability of the model. The *explained variation*, R^2, is a common parameter. R^2 adopt values between 0 and 1, where 1 indicates a model which explain all the variation in the data set and 0 a model which does not explain any of the variation. The *predicted variation*, Q^2, is another important parameter. It determines how well the model can predict the outcome of new experiments within the experimental space. Q^2 is determined by cross-validation, in which parts of the experimental data is left out during data fitting. Data points corresponding to the data left out are then predicted and compared with the experimental data. A Q^2 of 1 indicates a model with perfect predictability.

7) Extraction of information from model. With a reliable model in hand, vital information of the investigated response can be obtained. In the results and discussion part of this thesis, a palladium catalyzed reaction is thoroughly analyzed by DoE and good examples of information extracted from the model are given there.

3.3.2 Strengths of DoE

Changing one variable at a time (OVAT) is a common approach when investigating reactions in organic chemistry. The multivariate approach of DoE has several advantages over the classical OVAT approach. Consider an example, where a two factor optimization of a reaction is attempted (Figure 6). Using OVAT, the first variable (T) is optimized with regard to

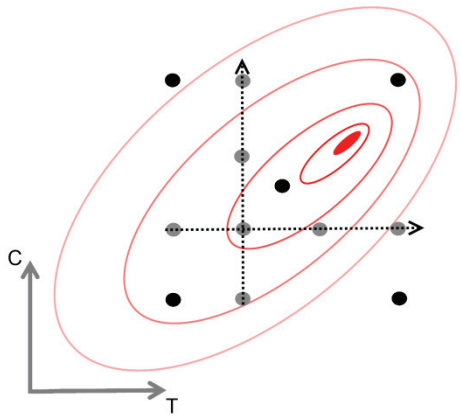

Figure 6. Reaction optimization of two factors (T and C) illustrated with a yield contour map. OVAT experiments represented as grey dots and DoE experiments as black dots. Both approaches span over an equal reaction space when considering the factors individually, but DoE span a larger area due to the even distribution of experiments.

reaction yield. With the optimal temperature, the second variable (C) is optimized. This method clearly misses important features of the reaction landscape, where a gradient is running diagonal to the OVAT coordinate system. With DoE, having experiments evenly distributed over the two dimensional reaction space, this feature will be detected. The center point is recognized as the highest yielding experiment and the initial 2^2 full factorial design can be evolved into a CCF design. Performing the extra axial experiments will after data fitting produce a quantitative model with quadratic terms for both T and C. The model can be used to find the exact maximum within the investigated reaction space.

3.3.3 DoE, discrete variables and principal component analysis (PCA)

So far, only continuous variables have been discussed. In a typical organic reaction, several of the variables are however discrete, e.g. different reagents. Discrete variables can be investigated with DoE in a comparative type of study. It is possible to elucidate how the discrete variables influence the response, but it will not give any information about other "values" of the discrete variable, e.g. investigating two bases in a reaction will reveal their effects, but will not give any information to whether a third base would work even better. Treating reagents as continuous variables, in which each of the reagents have a specific value, would greatly enhance the amount of information obtained from DoE.

Describing a molecule with a single property is difficult and will likely only provide a limited amount of the information necessary to chemically explain it. However, by describing a molecule with many properties, either physical (e.g. melting point, retention times in HPLC etc.) or calculated (e.g. HOMO, LUMO etc.), a more complete picture of its chemical behavior is produced. Each molecular property would however need to be introduced as a separate factor in DoE, which would result in a huge number of experiments. As a solution, the data processing technique *principal component analysis* (PCA) can be used to compress the dataset while maintaining as much of the original information as possible.

To explain PCA, a small dataset containing 13 molecules explained by three properties is used (Figure 7). PCA recognize the directionality of the greatest variance in the three-dimensional dataset and introduce a new variable (known as a latent variable or a principal component) oriented in this direction. The original data will be projected onto the latent variable. The three dimensions have thereby been reduced to a single dimension, explaining as much of the variance (information) in the original dataset as possible. Compressing the data into a single dimension does usually not sufficiently explain the original information, whereby more latent dimensions are introduced. A second latent variable is introduced orthogonal to the first, and oriented to capture as much of the remaining variance as possible. More latent variables can be introduced in the same way. Here, a dataset with three-dimensions (i.e. three variables) has been described for simplicity. In reality, molecules are explained by many more properties, ranging from ten to hundreds of them. The strength of PCA is also best demonstrated when this type of multidimensional datasets are compressed into a few orthogonal variables.

The relation between the original variables and the latent variables can be inspected and used to give the latent variables a physical meaning. For instance, if the first latent variable in Figure 7 would be highly related to melting point and molecular weight, it may be interpreted

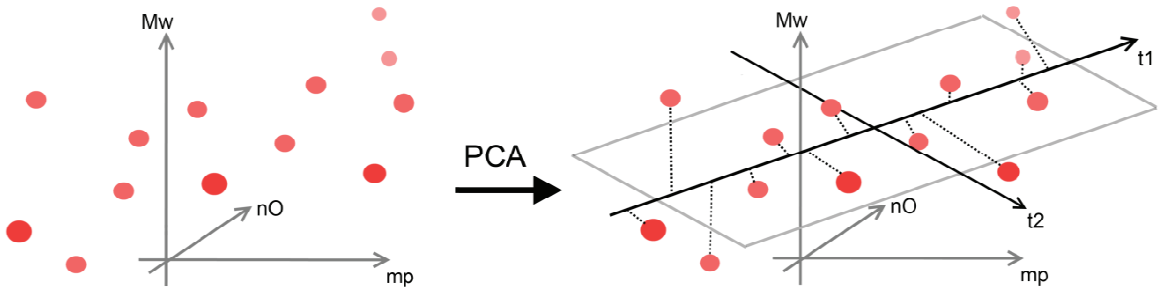

Figure 7. 13 compounds explained by their melting points (mp), molecular weights (Mw) and number of oxygens (nO). PCA introduce a latent variable, t1, which capture as much of the variance as possible within the dataset. The data points (compounds) are projected onto t1. A second latent variable, t2 is introduced orthogonal to t1. t2 is oriented to capture as much of the remaining variance as possible. The data points are projected onto t2 (not shown) and the dimensionality of the dataset has efficiently been reduced from three to two dimensions. The new dimensions generate a plane (grey) described by t1 and t2.

as capturing the size of the molecule.

For more detailed descriptions of DoE and PCA, the reader is referred to more specialized literature.[105-113]

3.4 Chemistry of excited states

Organic molecules can interact with electromagnetic radiation of different wavelengths, i.e. photons of different energies. The absorption of a photon (hν) will force the organic molecule into an energetic excited state. Depending on the energy of the radiation, the transition can for instance be rotational, vibrational or electronic. The latter type of transition is caused by ultra violet and visible light, which are in focus here. The absorption process is from a molecular perspective instantaneous (10^{-15}s), i.e. not even displacement of the nuclei will occur. Once in the excited state, the relaxation back to the ground state is not instantaneous but is sufficiently long for molecular processes such as diffusion and conformational changes to transpire.[114] A few molecular processes affecting the molecular excited state and its relaxation back to the ground state are discussed here.

The Jablonski diagram is a convenient way to represent the most common relaxation processes (Figure 8). A molecule in the ground state, denoted S_0, can be excited to the first, second or even higher electronic states, denoted S_1, S_2 etc. The concurrent vibrational excitations, responsible for the structure of absorption spectra, are also given in the diagram.

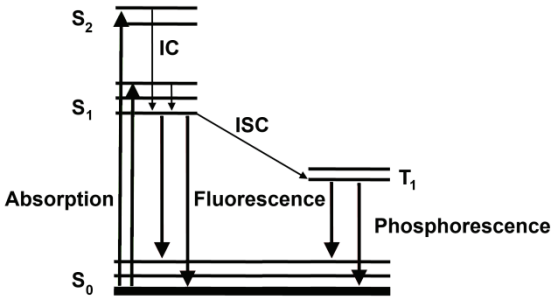

Figure 8. Jablonski diagram. IC: internal conversion, ISC: intersystem crossing.

Once in the excited state, the molecule is quickly relaxed to the lowest lying vibrational state of S_1 by internal conversion (IC). The process of IC typically occurs within 10^{-12}s. In the S_1 state, the molecule can emit a photon, i.e. returning to ground state by fluorescence. It can also proceed via intersystem crossing (ISC), forming a triplet which can return to ground state via emission of a photon, i.e. phosphorescence. Finally, it can return via non-radiative processes. There are a number of non-radiative processes, for instance energy transfer by collisions with other molecules such as oxygen. Quantum yield is used to relate the rate of fluorescence and non-radiative processes according to:

$$Q = \frac{\Gamma}{\Gamma + k_{nr}} \qquad (Eq. 5)$$

Where Q is the quantum yield, Γ is the rate fluorescent emission, k_{nr} is the rate of non-radiative processes.

When the quantum yield is close to one, the non-radiative processes are too slow to compete with the fluorescence and virtually all absorbed photons are re-emitted as light with lower energy.[114]

Molecular conformational and isomerical changes are well known to affect the quantum yield. In fact, fluorescent probes commonly exhibit fast non-radiative excited state decay via conformational changes in solution. When bound to a molecular target, such processes are denied resulting in an increased fluorescence quantum yield, efficiently enabling detection of the target.[114] The relaxation of tetraphenylsilole **63** displays such an environmental dependent behavior. While in solution at room temperature, the molecule is non-emissive. However, it turns brightly fluorescent when the solution is cooled.[115] The behavior is attributed to rotational freedom of the phenyl groups, which relax the excited state. As the solution is cooled, the rotation will eventually be hindered causing the non-radiative relaxation pathway to be turned off. Another classical example is the *trans*/*cis*-isomerization of stilbene **64**. The

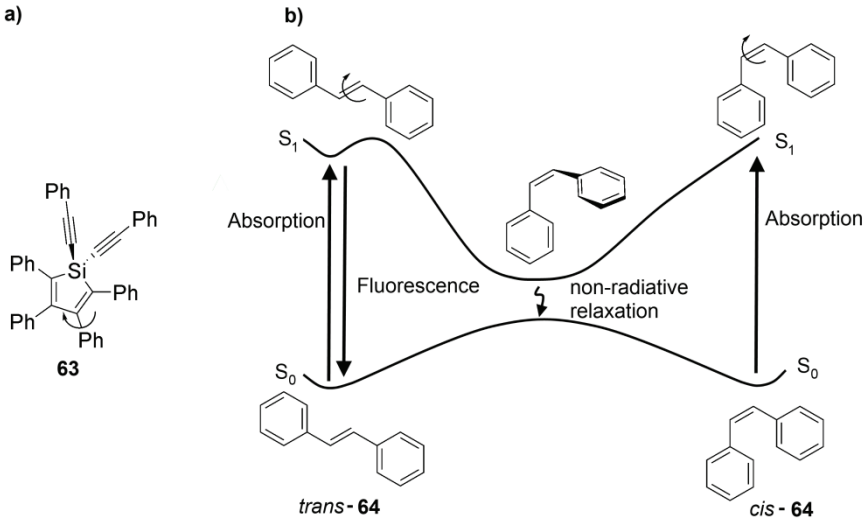

Figure 9. a) Rotational relaxation of tetraphenylsilole. b) trans/cis-isomerization deactivation of stilbene.

double bond is weakened in the excited state, allowing rotation (Figure 9). Both isomers relax swiftly in the excited state by a 90° rotation around the double bond, bringing the potential energy surface of S_1 close to S_0, facilitating a swift non-radiative transition.[116] As the temperature is lowered, the rotational rate in the excited state will decrease, consequentlydecreasing the rate of the non-radiative relaxation pathway. Indeed, fluorescence of *trans*-stilbene is enhanced at lower temperatures.[117]

Internal charge transfer (ICT) is another excited state phenomenon encountered in some species. After a molecule is excited to S_1, it can relax via an ICT to a charge separated state. The charge separated state is energetically favorable in the excited state, but unfavorable in the ground state, brining S_1 and S_0 closer together. The fluorescence observed from ICT is accordingly of longer wavelengths compared to emission from its neutral state (Figure 10). A conjugated electron donating-electron accepting moiety is a typical structural feature for molecules displaying ICT (Figure 10). The phenomenon is very environmental dependent, with polar solvents stabilizing charge separated molecules and apolar destabilizing. As a consequence, molecules usually only display fluorescence from charge separated states in polar solvents.[114]

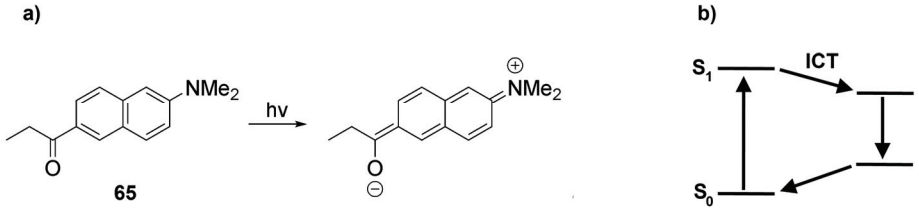

Figure 10. a) Electron donating/accepting system typical for ICT. A charge separated species can form in the excited state. b) Simple Jablonski diagram for the ICT process.

The different electron distributions observed in ground and excited states indicate that the ionization potential of molecules can change upon light absorption. Indeed, phenols are more acidic in the excited state. Excited phenols are known to protonate solvents and subsequently emit fluorescence from the resulting excited phenoxy species.[114, 118] The phenomenon occurs in protic media and is especially favored by an aqueous environment. A special case arises in amphoteric molecules, e.g. **66**, where the phenolic hydroxyl group is conjugated with an

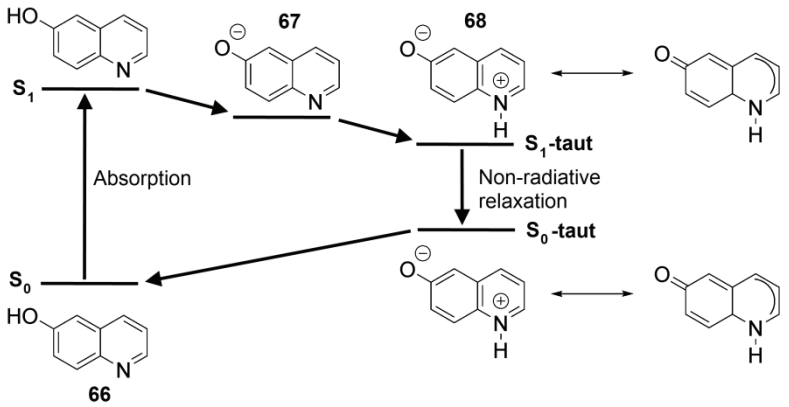

Figure 11. Excitation behavior of amphoteric 6-hydroxyquinolin.

imine (Figure 11). The molecule display a complicated excited state behavior which has been elucidated with time-resolved spectroscopy.[119] In the excited state, a step wise proton transfer is observed. First, deprotonation of the phenol produce an expected phenoxy anion **67**. A subsequent protonation of the imine give the zwitterionic species **68** which is a tautomer of the ground state molecule. The tautomer relaxes radiationless to the ground state. The observed phenomenon was specific for aqueous solutions. In organic solvents (including MeOH), the relaxation was characterized by an intersystem crossing mechanism.

3.5 Kinase inhibition

Protein kinases are phosphorylating enzymes involved in cellular transduction pathways. Kinases are defined by their ability to catalyze the transfer of a phosphate from adenosine triphosphate (ATP) onto a hydroxyl substrate, which are specific amino acids in proteins. Depending on the substrates, kinases are usually divided into two subgroups; tyrosine and serine/threonine. The enzymes have two major conformations, an active and an inactive. The inactive form is converted into the active by selective phosphorylation, which is catalyzed by an upstream kinase. Consequently, kinases are substrates to other kinases.[120, 121]

Inhibition of kinases has during the last decade received a great deal of attention. The human genome codes for more than 500 and almost every signal transduction process is believed to be wired through a phosphotransfer cascade.[121] Various signaling pathways are deregulated in cancers and controlling them externally with selective kinase inhibitors can be used to achieve a desired physiological effect. The desired effect is typically to prevent growth, which can be accomplished by inhibiting a signaling pathway critical for cancer survival.[59, 122, 123]

Kinase inhibitors can be divided into three different types, simply called I, II and III. During the phosphate transfer reaction, the ATP binds to a pocket within the enzyme. The purine part of ATP is buried in the pocket, forming hydrogen-bonds with the enzyme backbone (Figure 12). Type I inhibitors are designed to interact with the same binding pocket, thus competing with ATP (Figure 13). These inhibitors often try to mimic ATP and usually have a heterocyclic ring system occupying the purine binding site. To gain a higher binding affinity than ATP, the inhibitors include substituents which interact with additional hydrophobic regions of the binding pocket. The ATP-binding pocket is rather conserved and one of the biggest challenges with type I inhibitors is to acquire selectivity among the 500 kinases. Kinase adaptation is another problem with type I inhibitors. Selective point mutations (single amino acid exchange) have been demonstrated to introduce sterically demanding amino acids, blocking the hydrophobic binding sites vital for inhibitor-kinase interaction. Nonetheless, the

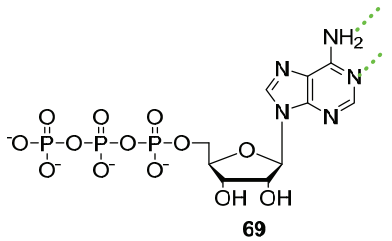

69

Figure 12. ATP with hydrogen bonds formed between the purine and kinase backbone.

applicability of this inhibitor type is well appreciated and a number are currently available on the market for cancer treatment.[121]

While type I target active kinases, type II target inactive (also called DFG out). In the inactive form, kinases have an additional hydrophobic pocket adjacent to the ATP-binding site. Type II inhibitors bind to this additional pocket in addition to the ATP-site, trapping the kinase in its inactive form (Figure 13). Targeting the inactive form has been proposed to furnish more selective inhibitors and developing protocols for designing type II inhibitors is an ongoing endeavor.[124, 125] Type III inhibitors bind outside the ATP-binding pocket, to an *allosteric* site. The binding can induce a conformational change in the kinase, preventing constructive interaction with ATP or the substrate (Figure 13). Allosteric inhibitors generally exhibit better selectivity than the previously described inhibitor types, as the allosteric sites are kinase specific.[121]

Scytonemin has been reported to inhibit kinases, albeit with poor selectivity. In a study including totally seven kinases, scytonemin inhibited five with similar potency. The mode of interaction was investigated in kinetic studies which concluded scytonemin to be a mixed inhibitor, i.e. the inhibition has both competitive and non-competitive components.[37] Consequently, scytonemin is not acting purely as a type I inhibitor.

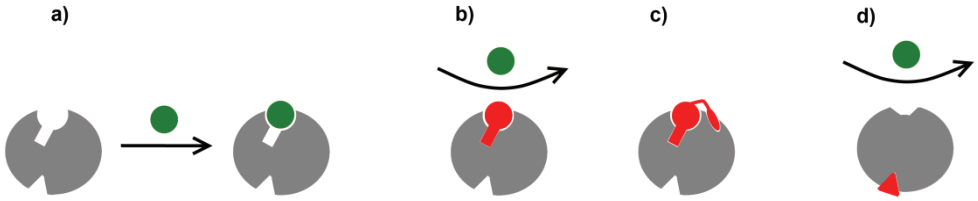

Figure 13. Schematic illustration of different kinase-inhibitor interactions. Kinase (grey), ATP (green), inhibitor (red). a) ATP coordinate to the kinase in the absence of an inhibitor. b) A type I kinase inhibitor, interacting with the ATP binding pocket and a hydrophobic site within, preventing ATP to bind. c) A type II inhibitor binding to an inactive kinase by interacting with the ATP binding site and the adjacent hydrophobic pocket. d) A type III inhibitor binding to an allosteric site, inducing a conformational change of the ATP binding pocket, preventing ATP to bind.

4 Results and discussion

This chapter presents retrosynthetic analysis of the target molecular structure, followed by an account over the synthetic results. Photophysicochemical- and biological studies of the synthesized compounds are thereafter presented. Results described in the papers are only discussed shortly here and the reader is referred to the papers for more details.

4.1 Retrosynthetic analysis of target scaffolds 16 and 17

The retrosynthetic analysis of scytonemin scaffold **16** and nostodione A scaffold **17** have numerous solutions. It is worth mentioning that just one possible solution is presented here. Also, the retrosynthesis is presented in a condensed form, omitting the synthons and directly presenting the equivalent reagents.

An initial disconnection at C-1 of **16** and **17** produced the common structure **70** (SCHEME 13). It was anticipated that **70** could be dimerized under oxidative conditions into a reduced form of the scytonemin scaffold **16**, as well as oxidized into the nostodione A scaffold **17**. Additionally, it was believed that enolate chemistry could be used to introduce various substituents at C-1 of **70**, giving other types of synthetic derivatives.

The synthetic intermediate **70** have several possible disconnections that efficiently simplify the skeleton and minimize appendages. For this project, the detachment at C-3a was considered promising due to:

1) several stereo- and regiospecific chemical transformations corresponding to this disconnection appeared viable, *vide infra.*

2) a further disconnection at the carbonyl carbon revealed a synthon corresponding to the commercially available indole-3-acetic acid (**74**).

We expected that a number of methods could be used to fuse the cyclopentone onto the indole. Introducing a halide in the 2-position of the indole provide a handle to initiate a Heck

SCHEME 13. Retrosynthetic analysis of scytonemin scaffold 16 and nostodione scaffold 17 with the goal of producing a concise and flexible synthetic route (X = halide).

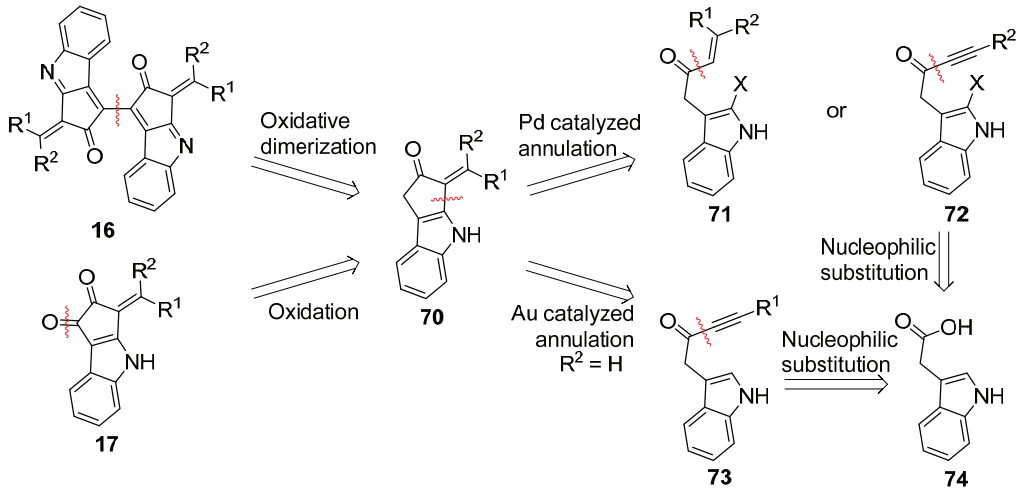

type reaction. The stereochemistry of the alkene in substrate **71** controls the stereochemical outcome of the annulation. A more versatile option is formed when performing the Heck cyclization with an alkyne of type **72** instead of an alkene. In this case, the palladium cannot undergo β-hydride elimination after cyclization, forming a trapped vinylic palladium intermediate (see chapter 3.1.2). Performing the reaction in presence of a transmetallation reagent generates a palladium species that instead undergo reductive elimination. When using boronic acid derivatives as transmetallation reagent, the reaction is known as a tandem/cascade Heck-Suzuki reaction. Considering the huge supply of boronic acid reagents, we envisioned this to be a very powerful method for producing numerous 3-alkenyl-cyclopenta[*b*]indole-2-one derivatives. Similarly, introducing a hydride source instead of a transmetallation reagent, it is possible to introduce a hydrogen in the R^1-position (reductive Heck reaction).

As an alternative to palladium catalysis, gold catalysis was also considered. Here, the gold will activate the alkyne of **73** toward interaction with the nucleophilic indole system. It is therefore not necessary to prepare the indole with a halide, affording a more efficient synthesis. However, the flexibility of the synthetic route will be lower as the *Z*-substituent (R^2) of the exocyclic double bond is limited to a proton.

It is interesting to note that the cyclopentanone formation via annulation of a 3-substituted indole is analogues to the biosynthesis of scytonemin (see chapter 1.2.3), albeit we propose a metal catalyzed reaction instead of an enzymatically catalyzed.

The 3-alkynyl/alkenyl indoles **71**, **72** and **73** required for the annulation were expected to be readily synthesized via a nucleophilic substitution on indole-3-acetic acid (**74**) or a derivative thereof.

4.2 Synthesis of 3-alkenyl-cyclopenta[*b*]indole-2-one intermediate 70 (Paper I-III)

From the retrosynthetic analysis, **70** was proposed as a key intermediate in the synthesis of both scytonemin and nostodione A (SCHEME 13). Three different approaches for the synthesis of **70**, all based on annulations of 3-substituted indole derivatives, are presented here. These include a cascade Heck-Suzuki sequence, a reductive Heck reaction and a gold-catalyzed Friedel-Craft reaction. Focus will be on the cascade Heck-Suzuki reaction, which offer the greatest possibility for diversity oriented synthesis.

4.2.1 Cascade Heck-Suzuki reaction (Paper I and III)

Intermediate **77** required for the proposed cascade Heck-Suzuki reaction was synthesized from the commercially available indole-3-acetic acid (**74**) (SCHEME 14). Here, an initial transformation of the acid functionality into the corresponding Weinreb Amide **75** was followed by a Lewis-acid activated electrophilic aromatic substitution, introducing an iodide in the 2-position of the indole, giving **76**. Finally, a substitution at the carbonyl carbon by lithium TMS-acetylide gave compound **77** which could be explored in the tandem Heck-Suzuki reaction. The choice of TMS-acetylene was based on 1) it is a stable, easily handled liquid, 2) a bulky substituent on the alkyne has been demonstrated as beneficial during palladium catalyzed cyclization on similar substrates[85] and 3) the outlook of removing it at a later stage to furnish mono-substituted exocyclic double bonds similar to what is found in scytonemin and nostodione A.

SCHEME 14. Synthesis of starting material for the cascade Heck-Suzuki reaction.

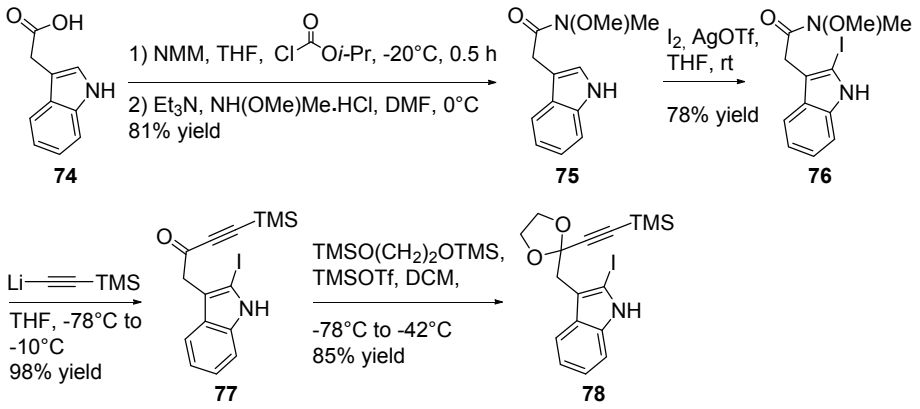

Initial reaction conditions were based on studies from the Fu laboratory and involved a palladium(0) precatalyst and a sterically demanding phosphine ligand. The system has previously been applied successfully to both Heck and Suzuki reactions.[126-128] However, treating substrate **77** with phenylboronic acid and the catalytic system only produced minimal amount of product, while consuming the starting material (TABLE 1, entry 1). Transforming the ketone to a ketal (SCHEME 14) produced substrate **78** which was more compatible with the reaction conditions (entry 2). A possible explanation resides either within the electronic nature of the alkyne or the steric properties of the ketal. Compared with the electron poor alkyne in **77**, the alkyne in **78** can potentially form a more constructive interaction with the electron deficient palladium(II) species obtained after oxidative addition.

TABLE 1. Initial investigation of tandem Heck-Suzuki sequence for the construction of intermediate 70.

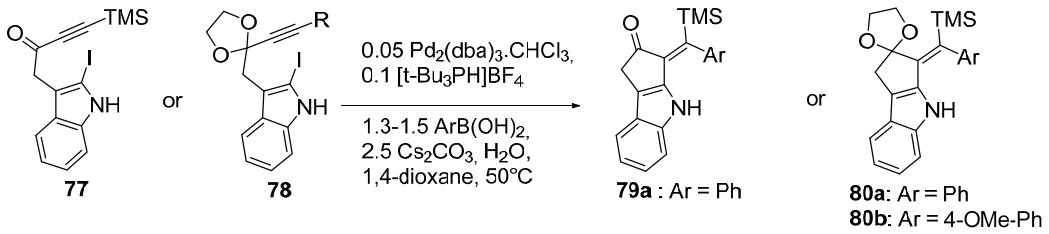

77 **78**

Entry	Substrate	H_2O equiv.	Ar	Product	Yield
1	**77**	0	Ph	**79**	13%
2	**78**	0	Ph	**80a**	70%
3	**78**	0	Ph	**80a**	30%[a]
4	**78**	1	Ph	**80a**	72%[b]
5	**78**	1	4-OMe-Ph	**80b**	30%

[a]Reaction run on a 50mg scale [b]Reaction run on a 500mg scale.

Interestingly, we had problems with reproducing this result on a larger scale. Going from 50 mg substrate (entry 2) to 500 mg (entry 3) reduced the conversion considerably, leaving most of substrate **78** unreacted, and consequently resulting in a low yield. The observed difference in reactivity was ascribed to water, which proved to have an essential effect on the reaction. We attempted to run the reactions anhydrous during the first experiments (entry 1-3), but were apparently not able to eliminate water completely. Small scale reactions are for experimental reasons prone to contain higher concentrations of water than large scale reactions, which explain the scale-dependent reactivity. Running the experiment again, but this time with the addition of water (entry 4) resulted in a much more active reaction. The observations agree with recent reports on the impact of water in Suzuki reactions as well as the influence of ions in Heck reactions (see chapter 3.1).

The possibility of producing different derivatives simply by using different boronic acid reagents is a great advantage with this reaction. However, already when switching from phenylboronic acid to the closely related *para*-methoxy derivative, a significant impact on the reaction outcome was observed (entry 5). One reason was the formation of 2-aryl substituted indole (of type **84**, SCHEME 15), which originates from a pure Suzuki cross-coupling between substrate **78** and the boronic acid. The compound **84** is produced when the intermolecular transmetallation of intermediate **81** competes efficiently with the intramolecular carbopalladation, and the reductive elimination of **83** is faster than the carbopalladation. The reductive elimination is rarely the rate limiting step and the direct coupling is likely due to the competing reactions of **81**.

To make the reaction a viable option for diversity oriented synthesis, further reaction optimization was clearly needed and a Design of Experiments (DoE) investigation was pursued (see chapter 3.3). The objective of the study was to obtain reaction conditions working with a variety of boronic acids. The measured response was the ratio between yield and conversion (y/c), representing how much starting material that is converted to product. The response will not discard reactions with low yields as poor if the byproduct formation is

SCHEME 15. Possible routes to byproduct formation.

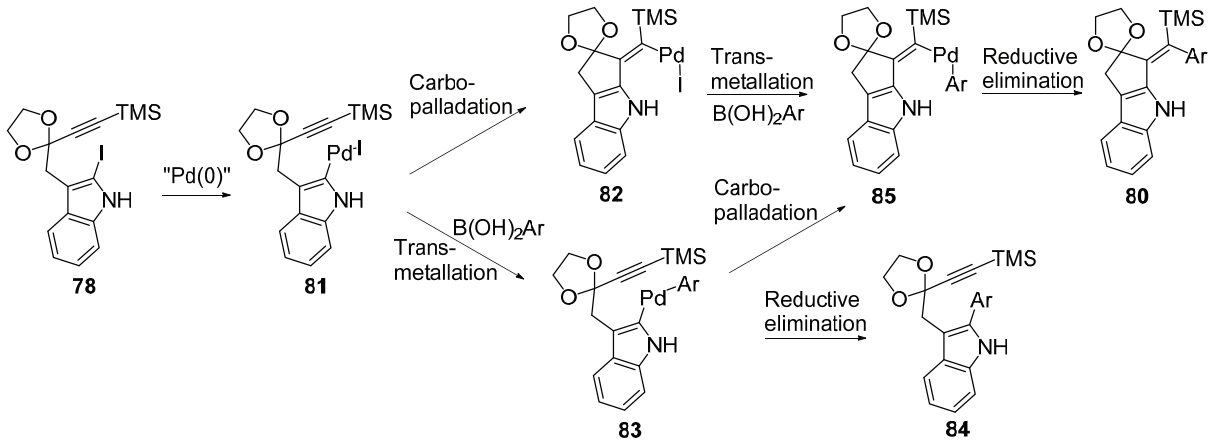

low, i.e. the conversion is similar to the yield. The conversion can often be increased simply by using longer reaction times or higher catalyst loading.

A detailed list over variables anticipated to affect the reaction is presented in paper III. Six variables were investigated while maintaining the others at constant values. To model a diversity oriented reaction, the electronic property of the boronic acid was introduced as one variable. The Hammett constant (*Ham*) of *para*-substituted phenylboronic acids was used to explain the electronic properties (Figure 14). Concentration (*C*) and the amount of boronic acid (*Bor*) were introduced as variables to tune the relative rate between carbopalladation and transmetallation, since the first is intramolecular and latter is intermolecular. To avoid the direct-coupled byproduct (SCHEME 15) the rate of carbopalladation should be higher than the rate of transmetallation. Further, water has been demonstrated to affect the reactivity, which steered us to opt for the amount of water (H_2O) as another variable. Ligands are well known to strongly affect catalytic reactions (see chapter 3.1). As discussed in chapter 3.3.3, discrete variables such as the ligand can efficiently be introduced in DoE as latent variables obtained from principal component analysis (PCA). Jover et al. recently published PCA of a P-donor ligand dataset comprising 348 ligands described by 28 quantum mechanically calculated descriptors (properties).[129] The two first latent variables (*t1* and *t2*) explain 65% of the variance and were here used to describe the ligands. By inspecting the relations between descriptors and latent variables, Jover et al. described *t1* to roughly capture the electronic properties and *t2* to roughly capture the size of the ligands (large t1: electron rich, small t1: electron deficient, large t2: small ligand, small t2: large ligand). Four ligands, forming a rectangle covering a major part of the ligand space were chosen, together with an additional ligand for the center point (Figure 15). The selection procedure resulted in an array of ligands

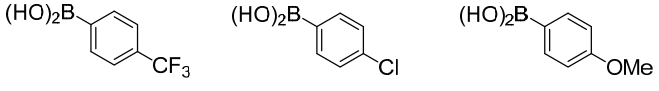

Figure 14. Boronic acids used in the DoE study to model the influence of electronic properties, quantified by the Hammett constant (Ham). 86 and 88 are used as extreme values and 87 as the center point.

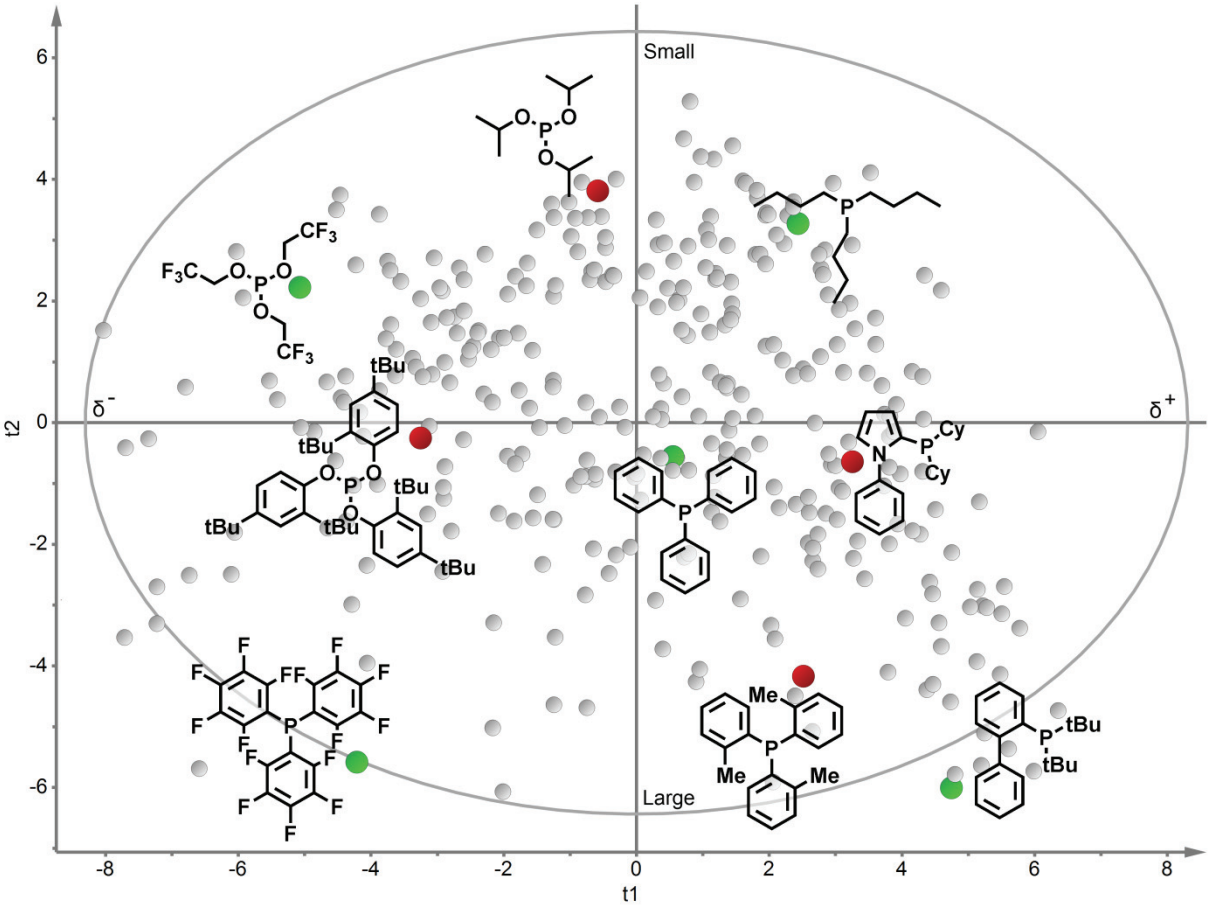

Figure 15. Ligand space described by two latent variables, t1 and t2. according to Jover et al. Initially chosen ligands are represented by green dots and ligands complemented to investigate quadratic effects as red dots.

varying from the universal triphenylphosphine to the bulky, electron rich biaryl phosphine to a more unorthodox electron deficient phosphite. As the ligand required two descriptive variables, the number of investigated factors were totally six.

A 2^{6-1} fractional factorial design was chosen for the initial investigation, which efficiently reduce the number of experiments to 32 from 64 necessary in a full factorial design. The design still allows both main and second order interaction effects to be elucidated with high confidence. Nine additional experiments were included to determine the experimental error, totaling 41 experiments (for a thorough explanation of included experiments, see supporting information for paper III). The experiments were run in a randomized order and analyzed with HPLC using external calibration curves, as well as NMR using an internal standard. The two analysis methods agreed well, indicating a reliable readout of the reaction. However, multiple linear regression could not fit a linear interaction model to the experimental data. Considering the high response of the center point, this is hardly surprising (Figure 16). As discussed in chapter 3.3.1, the center point should have an intermediate value to fit a linear model. Thus, the outcome of the initial 41 experiments prompted us to investigate possible quadratic effects and a central composite face design was adopted.

Axial points for the Hammett constant, the concentration, the amount of boronic acid and the

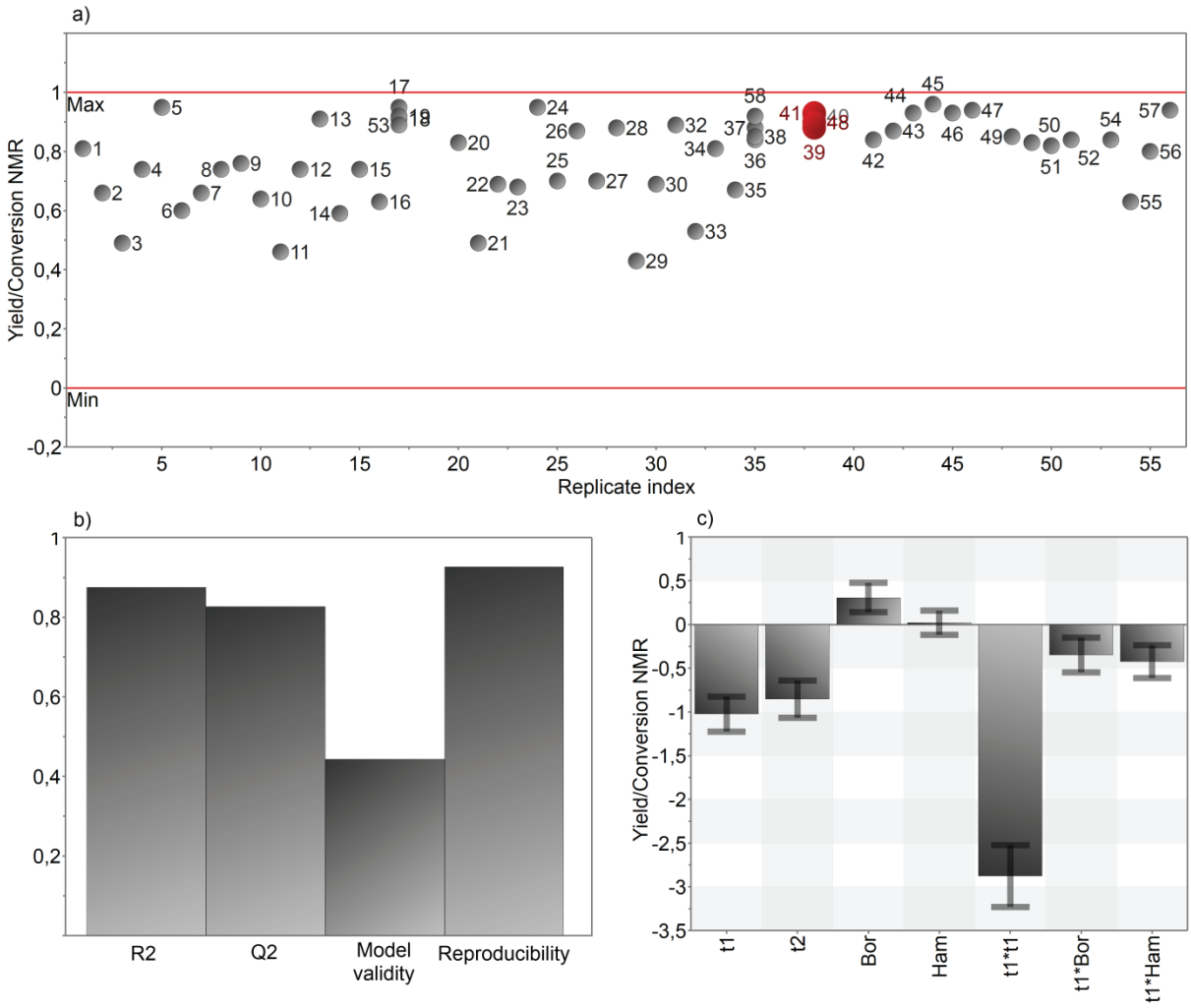

Figure 16. a) Replicate plot of performed experiments. Replicates of the center point in red. b) Evaluation of model performance after transforming the response according to $e^{2(y/c)}$. c) Significant factor coefficients at 95% confidence level.

amount of water were introduced in an ordinary manner, i.e. adopting extreme values on the variable investigated for quadratic effects, while maintaining intermediate values on the other variables. Axial points for the ligand variables, *t1* and *t2*, required four additional ligands to be investigated (Figure 15). After randomizing, executing and analyzing the additional 17 experiments, a satisfactory model was acquired by introducing a quadratic *t1* term and transforming the response according to $e^{2(y/c)}$ (Figure 16). The model explained 88% of the observed variation, displayed good predictive power and was only accompanied by a small model error. Introducing other quadratic terms (e.g. $t2^2$ and Bor^2) produced inferior models.

By dissecting the model, information related to reaction performance could be acquired. It is clear that the ligand is the most influential of the investigated factors. All but one of the significant effects include a ligand variable. The combination of negative coefficients for $t1^2$ and *t1* indicate that electron neutral to slightly electron deficient ligands are favored. Further, the negative *t2* effect signifies that large ligands are preferred over small. The pure ligand effects are easiest visualized with response surface maps (Figure 17). Complementary to the pure ligand effects, the model revealed interesting ligand interaction effects. The interaction

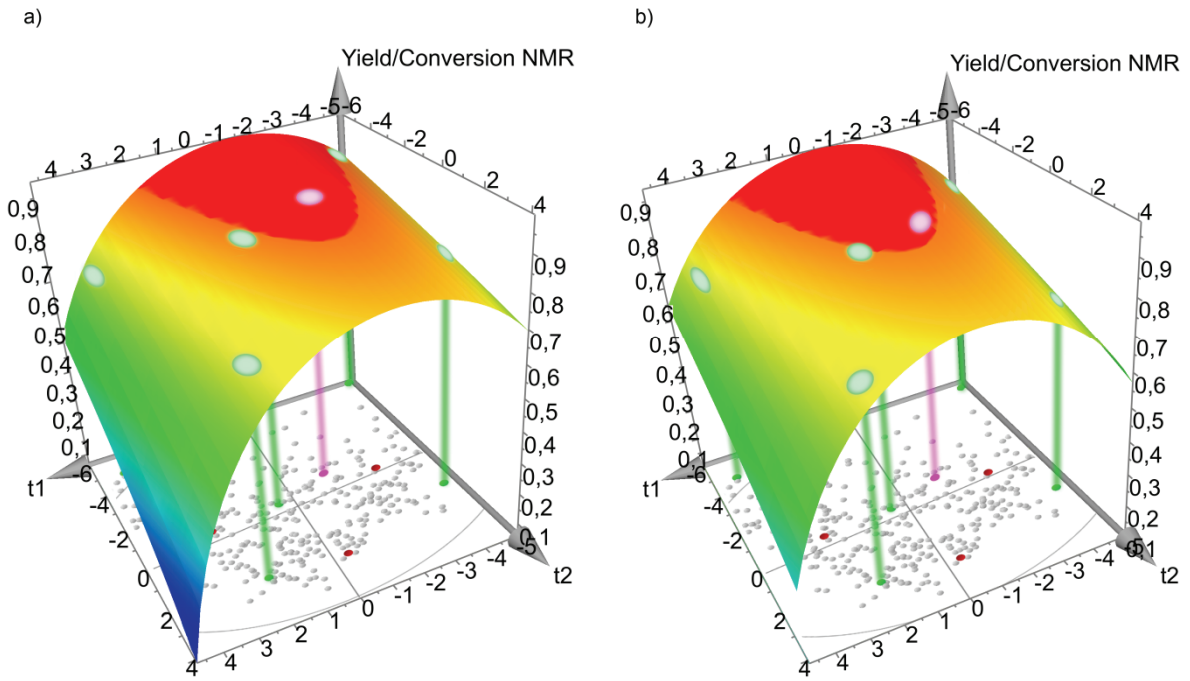

Figure 17. Response surface maps displaying the effects of t1 and t2 on the response for a) Ham = 0.54 and b) Ham = -0.27. The initially chosen ligands (represented as green dots in the two dimensional ligand space) are projected onto the response surface. The optimal ligand tris(4-trifluorophenyl)phosphine (89) is represented as a purple dot.

between *t1* and *Ham* point toward a preference for electron deficient ligands when using electron poor boronic acids and electron rich ligands when using electron rich boronic acids (Figure 18). This subtle interaction effect is however largely surpassed by the overall reaction preference for electron neutral ligands. The combination of *Bor* and the interaction between *Bor* and *t1* indicate an overall favorable effect of high boronic acid loadings, but together with increasingly more electron rich ligands, the positive effect is diminished (Figure 18). The other investigated variables had insignificant effects on the reaction.

To maximize the amount of product, the substrate need to follow the right reaction pathway (SCHEME 15), which is controlled by the relative rates of carbopalladation, transmetallation and reductive elimination. Oxidative addition to a carbon-iodide bond is fast and it should consequently not affect the reaction. To tune the complex reaction path, we investigated a number of variables with DoE. In particular, we envisioned that controlling the relative carbopalladation/transmetallation rate would be the key to an efficient reaction, and therefore investigated the reaction concentration and the loading of boronic acid. However, the first variable had an insignificant effect and the latter a minor. Instead, we found that the reaction outcome was controlled almost completely by the ligand. The reaction model revealed a complex relation between ligand and response, where steric and electronic properties of the ligand affected the reaction both linearly and quadratically. The ligand should be large but neither too electron rich, nor too electron poor to properly guide the substrate through the correct reaction pathway. As large ligands are favored, it is possible that mono-ligated palladium complexes are involved in the reaction. Larger ligands favor mono-ligated palladium, while smaller are more prone to exist as bi-ligated complexes.

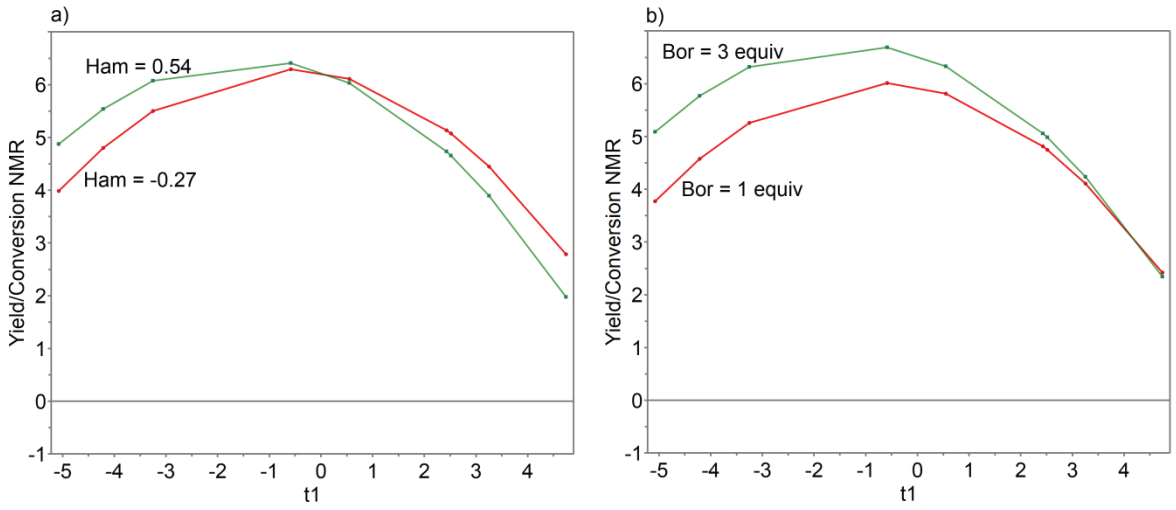

Figure 18. Calculated interaction effect plots for a) Ham × t1 and b) Bor × t1 at mid values on the other factors.

The optimal ligand also depended on the amount of boronic acid and its electronic properties, indicating that these reaction variables affect the relative rate of the catalytic steps. Indeed, a high loading of boronic acid will increase the rate of transmetallation. Accordingly, an optimal ligand should demonstrate an antagonistic effect, restoring the transmetallation rate to its native, slower state. When using increasingly higher boronic acids loadings, the model predicts optimal behavior from ligands with increasingly more electron deficient characteristics, i.e. electron poor ligands should decrease the transmetallation rate. The boronic acid electronic properties are harder to rationalize as both the rate of transmetallation and reductive elimination are affected.[76] However, it has been proposed that electron poor boronic acids increase the rate of transmetallation and as discussed above, the ligand should counteract the increased rate. When using increasingly more electron poor boronic acids, the model predicts optimal behavior from ligands with increasingly more electron deficient characteristics, i.e. electron poor ligands should decrease the transmetallation rate. Taken together, both interaction effects propose reduced transmetallation rates from ligands with low *t1*, i.e. electron deficient. Interestingly, a computational study recently proposed electron deficient ligands to accelerate transmetallation, contradictory to what is argued above.[72] There are several possible reasons for the divergent observations. Firstly, it is important to point out that *t1* has been assumed to account for purely electronic effects during the discussion. This is not true, as it also explains steric properties of the ligand to some degree. Hence, care should be taken when discussing latent variables as pure physical properties. Secondly, the electronics of the boronic acid will affect several of the catalytic steps, not just transmetallation. Although we cannot be sure of the underlying mechanism explaining the observed ligand influence, the model can be used to find optimal reaction conditions.

As discussed above, the ligand was the most crucial component of the investigated reaction, and consequently the most important parameter to optimize. Response surface maps were used to guide the choice of a ligand applicable to both electron rich and electron poor substrates (Figure 17). There are unfortunately no commercial ligands at the top of the parabolas, but the electron deficient tris(4-trifluorophenyl)phosphine (**89**) was in close

proximity. The model also predicts high loadings of boronic acids to be slightly beneficial. However, the benefit needs to be balanced against the cost, which can be rather high for certain boronic acids, and 1.5 equivalents were used in subsequent experiments. Intermediate values were used for the non-influential variables.

Optimal reaction conditions thus consisted of the precatalyst $Pd_2(dba)_3$, the ligand tris(4-trifluorophenyl)phosphine, boronic acid (1.5 equivalent), H_2O (2 equivalents), Cs_2CO_3 (2.5 equivalents), and 1,4-dioxane (0.06 M with regard to substrate) at a temperature of 50°C.

The optimal reaction conditions were assayed in a scope and limitation study, in which totally 20 boronic acids were tested (see paper III for full details). The reaction had some clear limitations. Firstly, strong electron withdrawing substituents conjugated with the reactive center (the $B(OH)_2$ substituted carbon) did in most cases not produce sufficient material to be isolated. Secondly, *ortho*-substituted aryls were too sterically congested to constructively participate in the reaction. Thirdly, coordinating groups such as phenols and carboxylates did either not react at all or only produced minor amounts of products. Apart from these limitations, the reaction proceeded well with various phenyl derivatives, thiophenes and pyridines.

The obtained derivatives could be transformed into the desired fragment **70** in moderate to good yields by acetal hydrolysis under acidic conditions followed by TMS-excision using TBAF in THF (SCHEME 16, see paper III for full details). Interestingly, the compounds isomerized spontaneously around the exocyclic double bond after removing the silyl group, and a thermodynamic equilibrium mixture of isomers was obtained. The equilibrium strongly favored the original configuration with less than 2% of the *Z*-isomer observed in most cases. However, when the double bond was conjugated with a strongly electron withdrawing group,

SCHEME 16. a) Final steps in the synthesis of fragment 70 via the tandem Heck-Suzuki route. b) Observed isomeric equilibrium of fragment 70. c) HOMO-LUMO of 70b with arrows pointing to the exo-cyclic double bond.

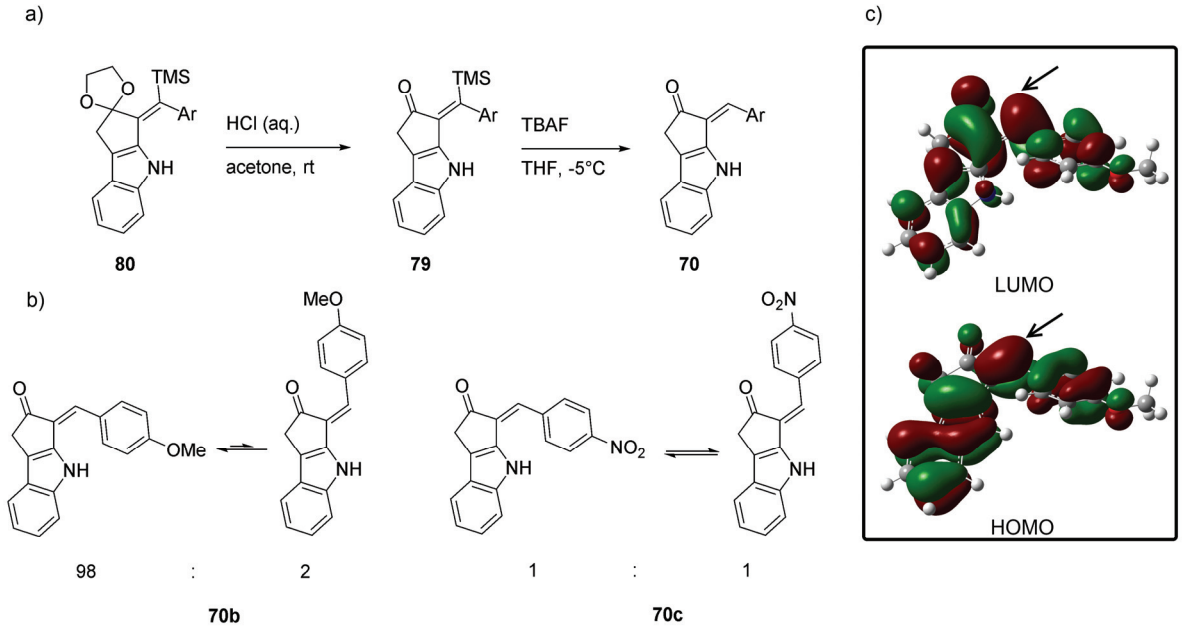

the equilibrium shifted into an equal distribution of isomers (SCHEME 16). The isomerization mechanism was investigated with quantum mechanical excited state calculations using time-dependent DFT. The strongest electronical transition for **70b** was predicted to 419 nm and corresponded to a pure HOMO-LUMO transition. Examining the molecular orbitals, the double-bond is characterized by a binding π -orbital in HOMO, while LUMO adopts an anti-bonding π-orbital (SCHEME 16). A HOMO-LUMO excitation should consequently reduce the bonding order of the double bond, potentially weakening it enough to allow an isomerization process.

Another observed structure-activity phenomena concerned fluorescence, which was highly dependent on the *para*-substituent of the phenyl ring. While a *para*-methoxy substituted compound displayed weak fluorescence, a *para*-chlorinated was brightly fluorescent (visually observable). All attempts to quantify the fluorescence (measure quantum yields) were fruitless due to observable changes in the absorption spectrum and to emission intensity during measurements. We hypothesize that the spectral changes are related to the *E*/*Z*-isomerization process described above, but further studies are necessary to elucidate the observed photophysical behavior.

4.2.2 Reductive Heck reaction (Paper II)

The reductive Heck strategy was originally intended for synthesizing the unnatural stereoisomer of scytonemin. As the project progressed, it soon became apparent that the ketone conjugated exocyclic double bond isomerized spontaneously under ambient conditions to the thermodynamically most stable isomer, as previously described (see chapter 4.2.1). However, the reductive Heck methodology can still be used as a complement to the cascade Heck-Suzuki reaction.

Starting materials were synthesized by nucleophilic substitution at the carbonyl carbon of Weinreb amide **76** (SCHEME 17). Treating **76** with phenylethynyl lithium gave ketone **89a**. The same reaction using (4-methoxyphenyl)ethynyl lithium resulted in unstable product **89b**, which spontaneously oxidized into spiro-indolinone **91**. However, treating **89b** with $NaBH_4$/

SCHEME 17. Synthesis of starting materials for the reductive Heck cyclization reaction.

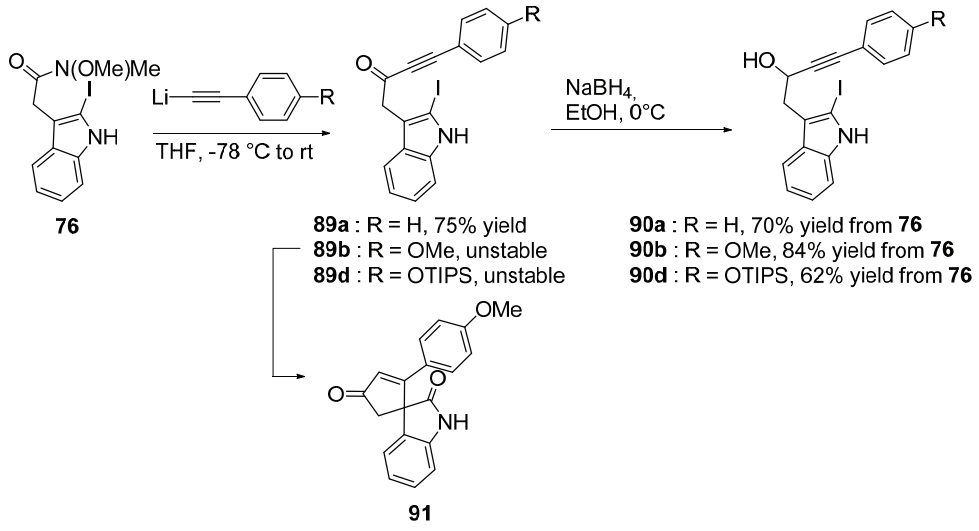

EtOH directly after workup gave alcohol **90b** as a stable intermediate. The same method could be used to synthesize precursor **90d**, which likewise was unstable as a ketone. The alcohol **90a** was also constructed for comparison. The regeneration of the ketone functionality was anticipated to be conceivable after cyclization of alcohol precursors **90a**, **b** and **d**.

Subjecting alcohol **90b** to typical reductive Heck conditions[130-134] (TABLE 2, entry 1) gave the desired product **92b** together with a number of uncharacterized byproducts. Switching solvent from THF to DMF gave better selectivity, resulting in a higher yield and less byproducts (entry 2) We have not been able to rationalize the observed difference in selectivity between DMF and THF. The TIPS-protected substrate **90d** was ring closed under the same reaction conditions (entry 3). TIPS-groups can be removed under mild and selective conditions to give free hydroxyl groups,[135-138] which could be utilized in the synthetic endgame of scytonemin and nostodione A. Unfortunately, the TIPS-group was slightly too labile for the developed reaction conditions, giving a mixture of the desired product **92d** and its TIPS-cleaved counterpart **92e**. Finally, ring-closing ketone **89a** resulted in a low yield (entry 4), similar to what was observed for the tandem Heck-Suzuki reaction (see chapter 4.2.1).

In a recent report, a procedure involving acetate salts in DMF has been used to cleave phenolic silyl ethers.[137] Based on this study, the acetate ions from the precatalyst and the formate ions used as hydride source both seemed likely to cause TIPS-excision in the reductive Heck reaction. Consequently, the applicability of another precatalyst and other hydride sources were investigated. Initially, promising results were obtained when treating substrate **90a** with the previously developed reaction conditions but in the presence of another precatalyst, $Pd(PPh_3)_2Cl_2$ (TABLE 3, entry 1). Next, to exclude the presence of formate ions, different hydride sources were tested. The use of phenylsilane (entry 2), proton sponge (entry 3) and Hantzsch ester (entry 4) as sources of hydrides have previously been reported in reductive Heck reactions,[139, 140] while 1,4-cyclohexadiene (entry 5) is a wild-card.

TABLE 2. Initial studies of the reductive Heck reaction.

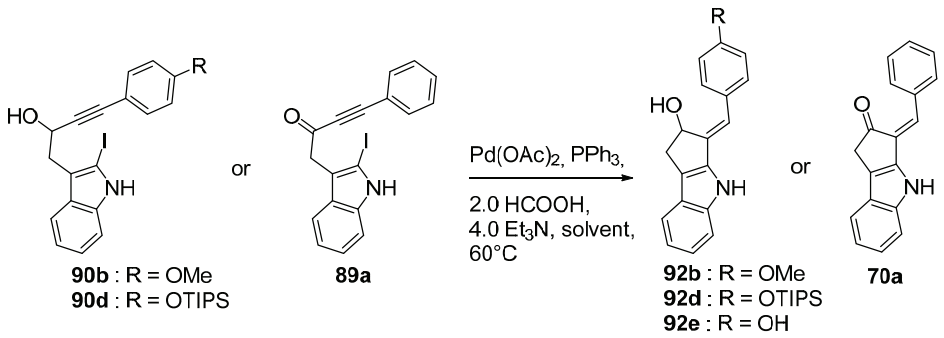

90b : R = OMe
90d : R = OTIPS

89a

92b : R = OMe
92d : R = OTIPS
92e : R = OH

70a

Entry	Substrate	$Pd(OAc)_2$	PPh_3	Solvent	Product	E/Z	Yield
1	**90b**	0.2 equiv.	0.4 equiv.	THF	**92b**	n.d.	44%
2	**90b**	0.2 equiv.	0.4 equiv.	DMF	**92b**	1:10	90%
3	**90d**	0.2 equiv.	0.4 equiv.	DMF	**92d/e**[a]	1:9	78%
4	**89a**	0.1 equiv.	0.2 equiv.	THF	**70a**	n.d.	15%

[a]28 % with TIPS and 50 % without TIPS.

TABLE 3. Screening of different hydride sources for the reductive Heck reaction.

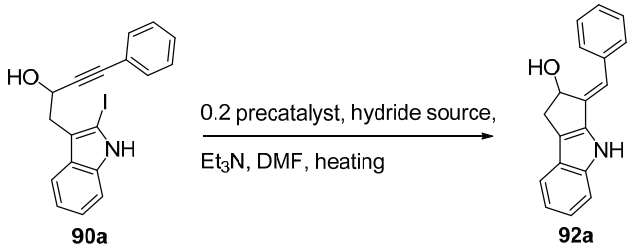

90a **92a**

Entry	Precatalyst	Hydride source	Temp.	Et_3N	Yield[a]
1	$Pd(PPh_3)_2Cl_2$	HCOOH	60°C	3 equiv.	75%
2	$Pd(PPh_3)_2Cl_2$	Phenylsilane	60°C	2 equiv.	9%
3	$Pd(PPh_3)_2Cl_2$	Proton sponge	60°C	-	0%
4	$Pd(PPh_3)_2Cl_2$	Hantzsch ester	60°C	2 equiv.	0%
5	$Pd(PPh_3)_2Cl_2$	Cyclohexadiene	60°C	2 equiv.	0%
6	$Pd(OAc)_2/(PPh_3)_2$	Proton sponge	95°C	-	6%
7	$Pd(OAc)_2/(PPh_3)_2$	Hantzsch ester	95°C	2 equiv.	8%

[a] Yield measured by NMR against 1,3,5-trimethoxybenzene and hexamethylbenzene as internal standards.

Only phenylsilane did actively participate in a constructive manner, albeit yielding a limited amount of product **92a**. When increasing the temperature and using $Pd(OAc)_2$ as precatalyst, the protons sponge (entry 6) and Hantzsch ester (entry 7) produced the desired product, but also in very poor yields.

Of the tested hydride sources, none could compete with formic acid. Phenylsilane has been reported to operate via a radical mechanism and a mechanistic comparison with formate ions is therefore difficult. However, both the proton sponge and the Hantzsch ester likely work mechanistically similar to formate ions in the hydride delivery step, and their incompatibility was slightly surprising. Some speculative explanations to the observed outcome can however be made. First, the sluggish proton sponge reaction may be rationalized by thermodynamical considerations. The generation of gaseous carbon dioxide is a strong entropic driving force when using formates (SCHEME 18a). The formation is likely also a strong enthalpic driving force. The proton sponge form oxidation product **96** which is neither as enthalpically nor entropically favorable as carbon dioxide (SCHEME 18b). On the other hand, the Hantzsch ester oxidation has a good driving force, going from a non-aromatic system to an aromatic (SCHEME 18c). The poor reaction outcome can potentially be ascribed to the allyl anion formation required for β-hydride elimination. The allyl anion **98** can only be formed by an initial nitrogen-palladium coordination and a subsequent deprotonation by Et_3N. The palladium-nitrogen coordination is inherently weak, which is further amplified by the deactivating ester substituents of the Hantzsch ester. Consequently, complex **97** is likely only a minor species, resulting in a slow formation of the allyl ion species **98**. This can be compared to formates and the proton sponge which can β-hydride eliminate without any external involvement.

It should be noted that each hydride source has been tested in a limited part of the reaction space and that suitable conditions could likely be obtained in a more thorough study, taking

SCHEME 18. Comparison of the hydride transfer step using a) formate ion, b) proton sponge and c) Hantzsch ester.

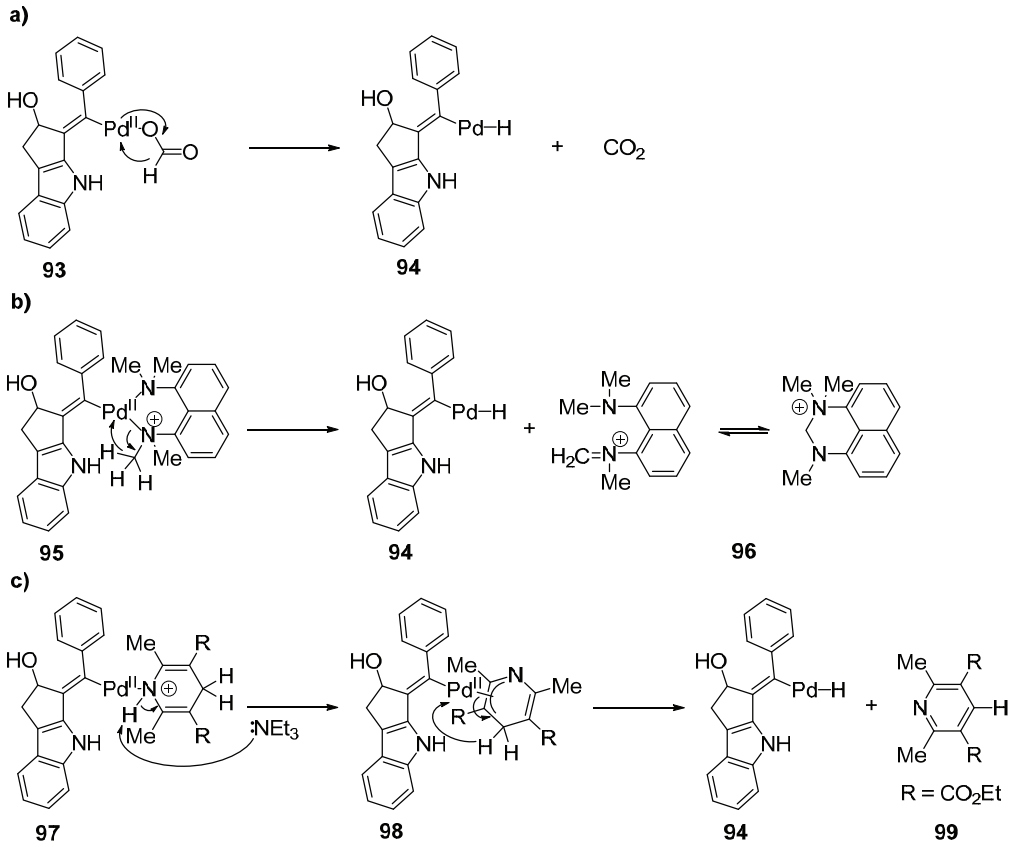

other reaction parameters, such as solvents, ligands, and bases, into account. This could preferentially be done with DoE.

The syntheses of fragment **70** derivatives **b**, **d** and **e** were completed by oxidation of the hydroxyl group (SCHEME 19). Several conditions were tested for this final functional group transformation. Due to the oxidation-sensitive nature of indoles, most of the conditions (e.g. Swern and Dess-Martin) simply degraded the starting material. Finally, we found that the Shvo catalyst (**101**) selectively oxidized the hydroxyl under Oppenauer-type reaction conditions.[141-143] The so formed ketones in their *Z* isomeric forms spontaneously isomerized to the favorable *E*-isomers as anticipated. Interestingly, we noticed that compound **70e** isomerized at a much higher rate compared to **70b** and **d**. While the isomerizations of **70b** and

SCHEME 19. Final step in syntheses of fragment 70 via the reductive Heck route.

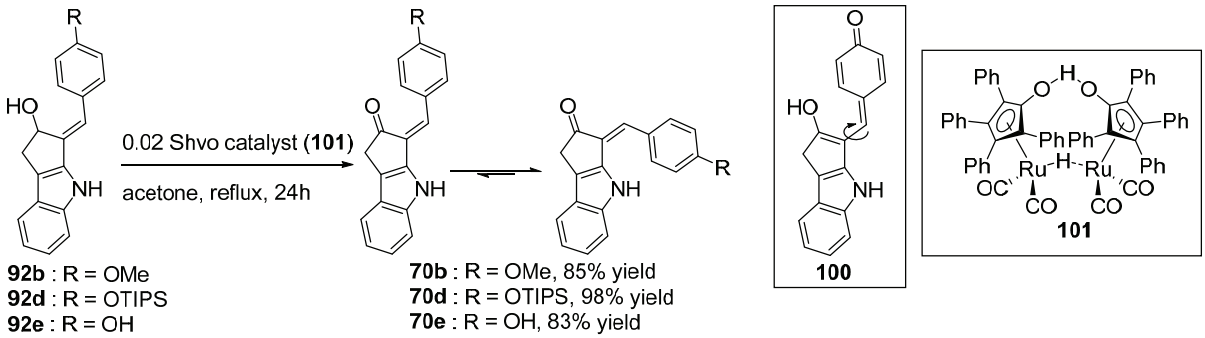

70d are likely limited to light driven processes, the free hydroxyl allows compound **70e** to tautomerize into **100**, which can rotate around the exocyclic bond and then tautomerize back into the *E*-isomer (SCHEME 19). The co-operation of two mechanisms may explain the increased isomerization rate.

4.2.3 Gold catalyzed Friedel-Craft annulation (Unpublished)

A last strategy for obtaining key intermediate **70** used the alkynophilic properties of gold in a catalytic Friedel-Craft type of aromatic annulation. Efficient use of this reaction would give a concise route to the molecular target. However, we realized that the annulation offered a double challenge in terms of selectivity. First, the initial cyclization needs to form the 4-*exo-dig* spiro intermediate regioselectively, a reactivity which has not been encountered previously (see chapter 3.2). Secondly, the spiro intermediate need to proceed via a selective 1,2-shift to form the 3-alkenyl-cyclopenta[*b*]indole-2-one and not the 1-alkenyl counterpart.

Two different model substrates were synthesized to investigate the selectivity of the reaction. Substrate **102** was obtained by nucleophilic substitution at the carbonyl of Weinreb amide **75** (SCHEME 20). It seemed likely that the α,β-unsaturated system of alkynyl ketone **102** would direct the nucleophilic attack toward a classical Michael addition, giving the undesired regioisomer. The ketone **102** was therefore reduced into alcohol **103**.

SCHEME 20. Synthesis of starting materials for the gold-catalyzed Friedel-Craft annulation.

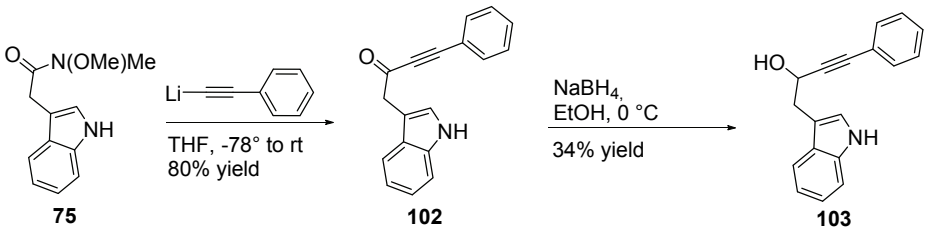

Three stereoelectronically different commercially available gold catalysts (SCHEME 21) were used together with alkynyl ketone **102** in a small screening study. The catalysts ranged from the very bulky **106** and **107**, to the less sterically demanding **108**. The electronics ranged

SCHEME 21. Screening of different gold catalysts for the annulation of 102.

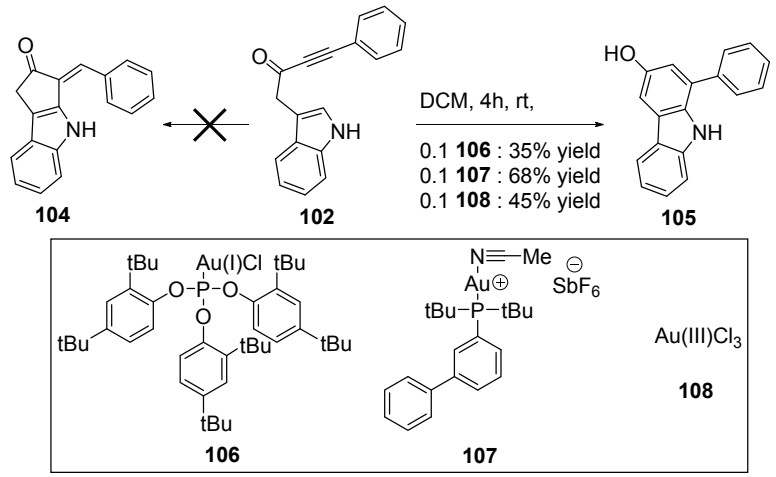

from the electron rich phosphine complex **107** to the more electron poor phosphite **106** to a gold species in a higher oxidation state, **108**. We observed varying efficiencies between the catalysts, with **107** giving the best result and **106** the worst. Unfortunately, all experiments exclusively produced six membered rings instead of the desired five membered ring-closed product **104**. The cyclization was followed by a keto-enol tautomerization to give **105**, which belongs to another class of natural products, namely carbazoles. We noted that the 1,2-shift proceeded with retention of the initial skeleton arrangement, i.e. the carbon connected to the indole in substrate **102** did *not* migrate in the 1,2-shift.

Next, alkynyl alcohol **103**, which lack the Michael acceptor functionality of **102**, was used as substrate (SCHEME 22). As previously discussed, the electronic preference to form 5-*endo-dig* spiro intermediates was hypothesized to be lower for this substrate. However, no change in the ring-size selectivity was observed, neither with **107** nor **108** as catalysts. An aromatic carbazole was instead obtained by dehydration of the alcohol. It is worth noting that the 1,2-shift proceeded exclusively with retention of the initial skeleton arrangement in all cases, a reactivity pattern which has recently been reported as completely reversed for a similar substrate.[103]

SCHEME 22. Gold catalyzed annulation of 103.

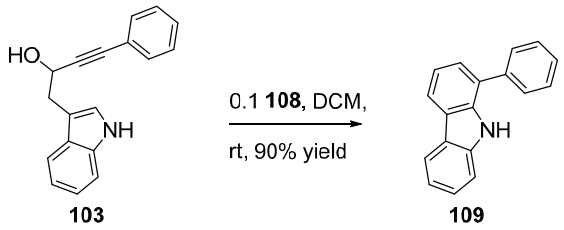

103 **109**

4.3 Total synthesis of nostodione A (Paper II) and scytonemin monomers (Paper IV)

The synthesis of nostodione A was anticipated to be achieved via a Yonemitsu oxidation[144] of a 3-alkenyl-cyclopenta[*b*]indole-2-one derivative (**70**). The Yonemitsu reaction use DDQ to oxidize the indole into an α,β-unsaturated imine of type **110** (SCHEME 23). A succeeding attack by water form **111** and an additional oxidation establish the dione functionality present in nostodione A. Compound **70d** obtained via the reductive Heck route was expected to furnish nostodione A via a Yonemitsu oxidation and a succeeding mild deprotection. Submitting **70d** to standard Yonemitsu reaction conditions, using DDQ in a THF/H_2O solvent system, produced only trace amount of product. Through the course of reaction optimization, we found a strong solvent dependence and switching to MeCN/H_2O furnished the desired product **112** in good yields (SCHEME 23). A final deprotection using TBAF yielded nostodione A. Compound **70e**, having a free phenolic hydroxyl group, was not compatible with the Yonemitsu conditions. However, it could be reprotected in excellent yield using TIPSCl and then transformed into nostodione A. In this way, all the product obtained from the reductive Heck reaction of **90d** (TABLE 2) could be funneled into nostodione A.

While investigating the Yonemitsu reaction, DDQ in THF was found to efficiently oxidize **70d**. However, the subsequent attack by water on the formed α,β-unsaturated imine was very

SCHEME 23. a) Synthesis of nostodione A from compound 70d and e, obtained from the reductive Heck route. b) Tentetative mechanism for the Yonemitsu oxidation.

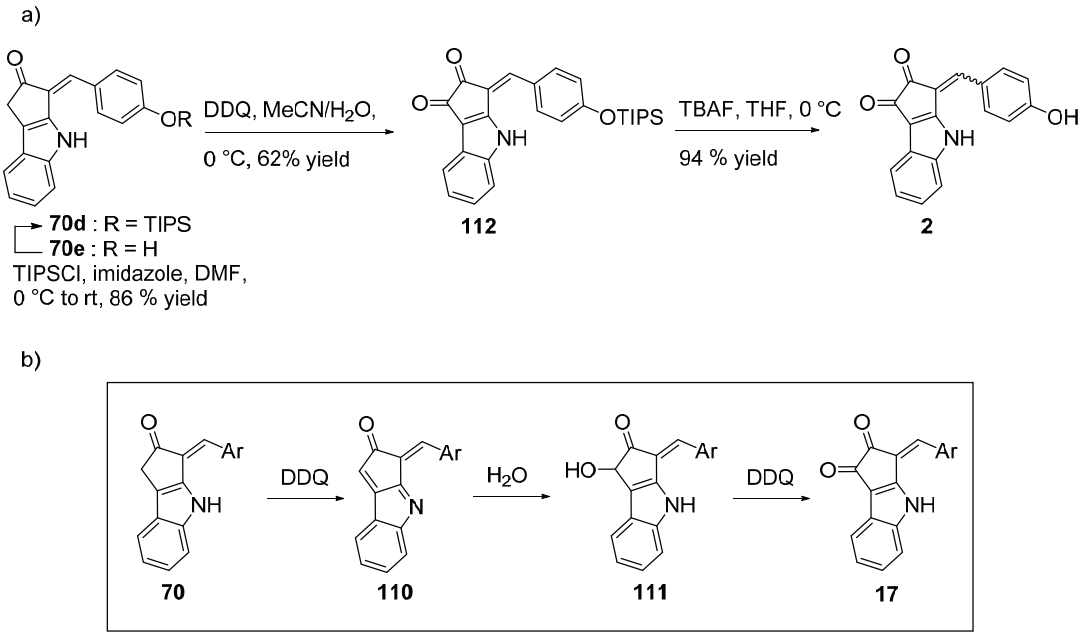

slow. The observed reactivity was realized when α,β-unsaturated imine **110d** was isolated from the reaction mixture (SCHEME 24). Possibly, MeCN has a stabilizing effect on the polarized electrophilic-nucleophilic transitions state during the addition of water, consequently lowering the reaction energy barrier. Although isolation of the enimine intermediate was not the desired result, it was none the less a pleasing outcome. The compound is the monomeric counterpart of scytonemin and in that sense interesting for photophysical studies. The direct comparison between monomer and dimer can potentially give information to the relaxation behavior of scytonemin. For this purpose, two more monomers were synthesized (SCHEME 24).

SCHEME 24. Synthesis of scytonemin monomer derivatives.

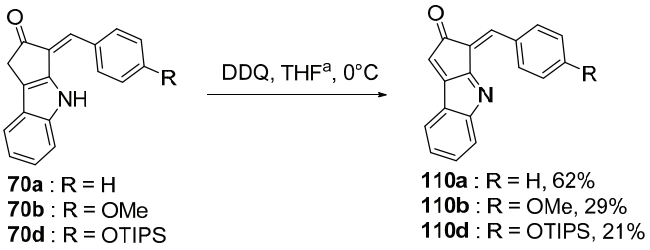

[a] Solvent was THF/H_2O 9:1 for **70d**

4.4 Total synthesis of scytonemin (Paper I)

In the retrosynthetic analysis, the dimeric structure of scytonemin was anticipated to be synthesized via oxidative coupling of two monomer fragments. Oxidative coupling of lithium enolates and silyl enol ethers are well documented in the literature and were envisioned as a possibility.[145-151] Indeed, deprotonation of monomer **70a** with LDA and sequential treatment with an oxidant formed the dimeric compound **113a** as an inconsequential mixture of

SCHEME 25. a) Oxidative enolate dimerization and subsequent oxidation.b) Suggested mechanism for the oxidative enolate coupling using iron(III).

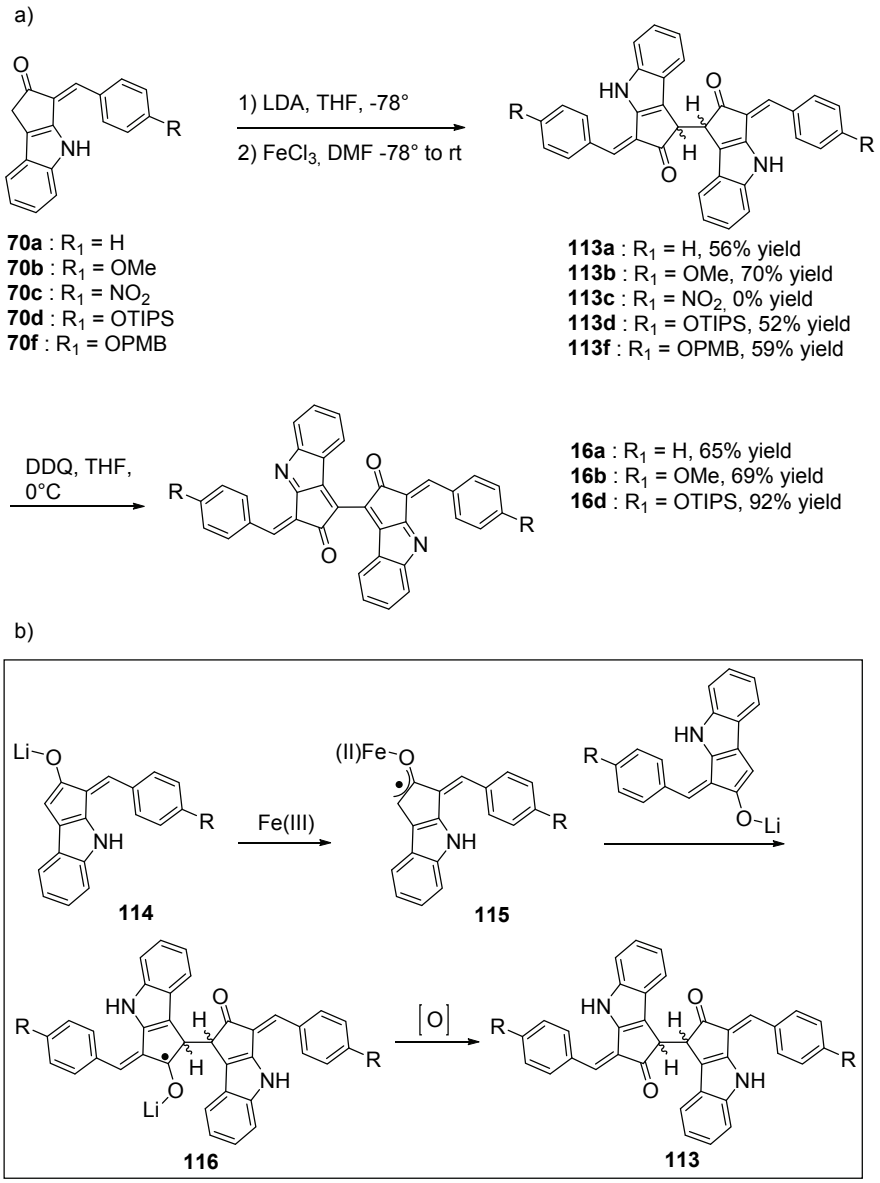

diastereoisomers (SCHEME 25). Four different oxidants were screened (please see paper I). Irontrichloride clearly outperformed the other oxidants and was used for the remainder of the study. Oxidative couplings involving iron(III) have been suggested to proceed via a single electron transfer (SET) mechanism, where an initial transmetallation between lithium and iron forms complex **115** (SCHEME 25).[146] The complex can be seen as an oxidized enolate with a single electron delocalized over the four atom system. The oxidation converts the nucleophilic enolate into an electrophile, which can react with a lithium enolate forming radical **116**. Another oxidation by iron(III) give the desired dimer **113**.

The coupling strategy was also applied to the electron rich monomer **70b**, which worked even better than **70a**. On the other hand, applying the method to electron deficient monomer **70c** yielded no product at all. The strong influence by the electronic properties concur with published reports.[146] Three additional dimeric compounds with different phenolic protective

groups were synthesized through the course of the project. Further, the diastereoisomeric mixtures could be oxidized by DDQ, forming single compounds containing the scytonemin core skeleton (**16**) (SCHEME 25).

The synthetic endgame of scytonemin did to a large extent revolve around the phenolic protective group. The dimeric compounds proved to be sensitive toward both basic and acidic reaction conditions, and most protective group excision strategies resulted in decomposition. First, we used borontribromide on compound **16b** (SCHEME 26). However, the attempted methyl group excision was unsuccessful due to severe decomposition. The reduced form **113b** proved to be more stable and submitting it to the same conditions gave phenolic compound **113e**, albeit in a mixture with many uncharacterized byproducts. Nonetheless, DDQ oxidation and preparative HPLC yielded scytonemin, but as expected in low yields.

Para-methoxybenzyl protective groups, which can be removed by DDQ and water, were investigated next. As DDQ was found to efficiently oxidize the isomeric mixture into the desired scytonemin skeleton, we envisioned that compound **113f** could be transformed into scytonemin by a single operation (SCHEME 27). Unfortunately, the strategy was unsuccessful and resulted in substrate decay. Substrate **113f** could however be deprotected with borontribromide and oxidized into scytonemin, although without increasing the yield compared to the methyl protective group (SCHEME 26).

With the moderate success of removing ether groups, we were inclined to investigate a more labile precursor. Considering the successful synthesis of nostodione A, a TIPS-protected derivative was investigated (SCHEME 28). The TIPS-excision was attempted from both the reduced and oxidized form with the latter being most successful. Using a more labile

SCHEME 26. Synthesis of scytonemin from ether precursors.

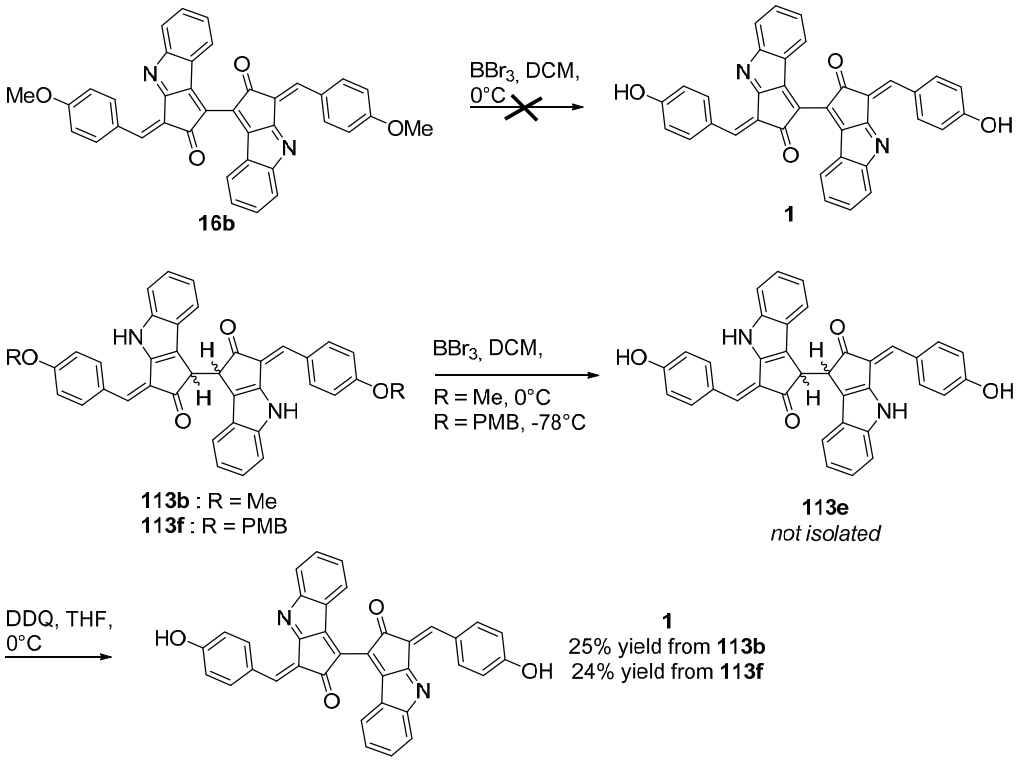

SCHEME 27. Unsuccessful attempt to combine oxidation and PMB-excision.

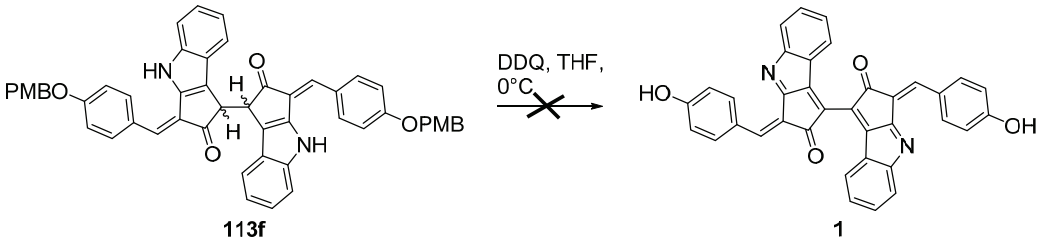

113f **1**

protective group was indeed more productive, with less product decay compared to methyl and PMB protective groups.

SCHEME 28. Synthesis of scytonemin from a TIPS-protected precursor.

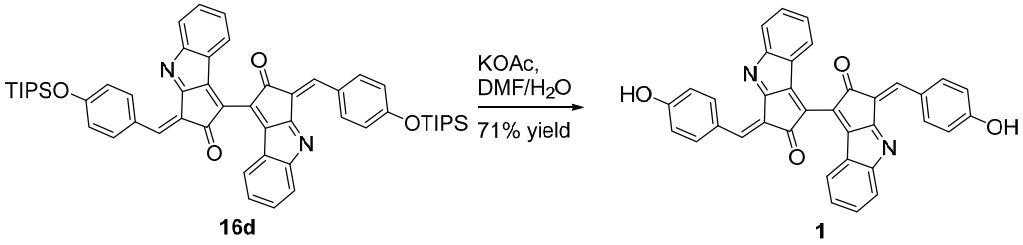

16d **1**

[a] Yield is reported for a not completely pure product

4.5 Photophysicochemical behavior of scytonemin (Paper IV)

Scytonemin (**1**) is well known to protect cyanobacteria from UV-light. In fact, its accumulation in the extra cellular sheaths allows the bacteria to thrive in locations highly exposed to solar radiation.[8] Further, scytonemin is proposed to be an ancient metabolite, suggesting inherent optimal traits which cannot be improved upon by the evolutionary mechanism.[18] It is often referred to as photo-stable and has been reported to be non-fluorescent, which taken together indicate inherently fast non-radiative relaxation processes.[8, 17, 19] Despite these traits, interesting for the development of sunscreens, the photophysics of scytonemin has yet been left almost completely unexplored. Against this background, we initiated a study of the photophysical behavior of scytonemin.

Scytonemin is a fairly complex molecule and several possible excited state deactivation mechanisms contributing to the non-emissive $S_1 \rightarrow S_0$ relaxation can be envisioned. These are discussed theoretically in chapter 3.4. First, there are several possible conformational changes. Rotation around single-bonds will affect the conjugated system and can possibly affect the excited state behavior (Figure 19). Further, the exocyclic double-bond could potentially participate in a stilbene type of deactivation, isomerizing between *cis* and *trans* configurations. There are also electron donor/acceptor moieties, which could be involved in internal charge transfer processes. Finally, the phenol group is likely to become much more acidic upon excitation, forming a phenoxy anion **1b** under neutral aqueous conditions. The particular amphoteric structure of scytonemin allows further protonation, forming an excited tautomer **1c** in analogy with 6-hydroxyquinine (chapter 3.4).

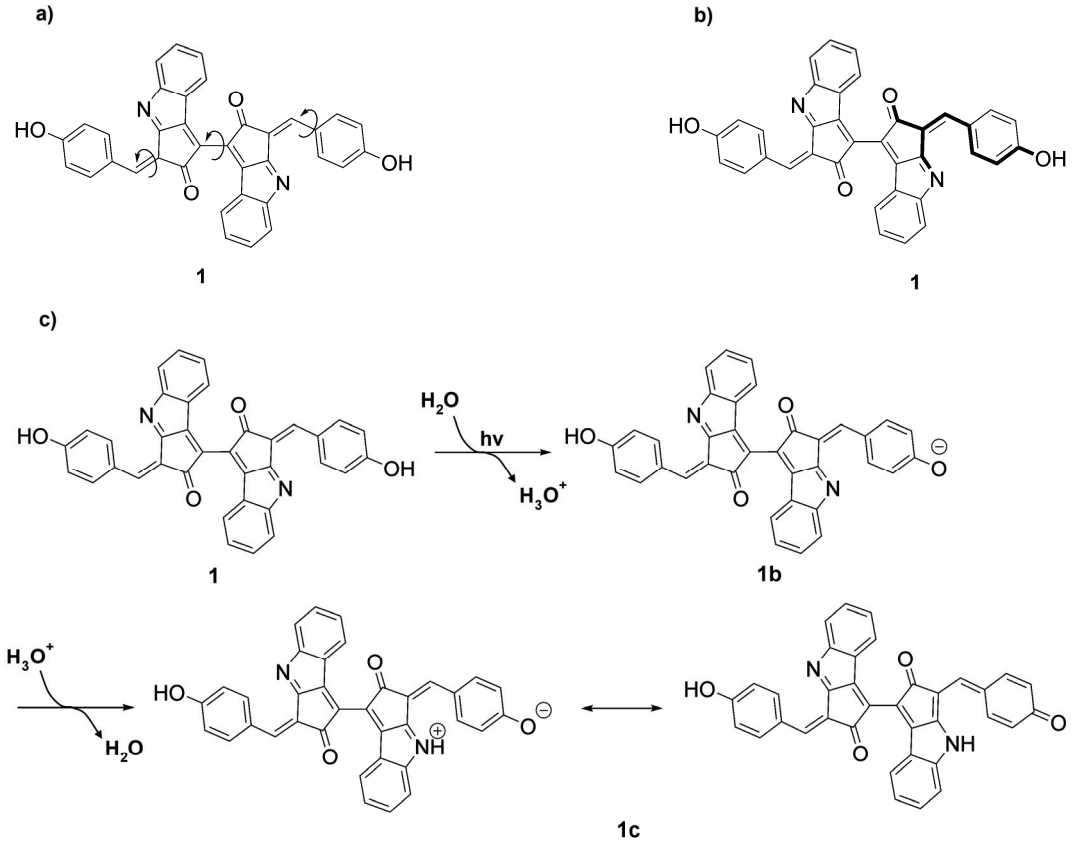

Figure 19. a) Possible conformational changes and isomerization processes affecting the excited state. b) Electron donor/acceptor moiety in bold. c) Deprotonation/protonation cascade possible in the excited state.

Scytonemin was here investigated together with four different derivatives, two dimeric and two monomeric (Figure 20). We initially studied the absorption processes using an organic solvent of medium polarity, 2-methyltetrahydrofuran (Me-THF). Scytonemin and its corresponding methoxy derivative **16b** are characterized by a broad absorption in the UVA-region with an absorption maximum at 380nm (Figure 21). Compound **16a** displayed similar behavior, but having a blue-shifted absorption maximum. The two monomeric derivatives, **110a** and **110b**, displayed absorption spectra comparable to the dimeric counterparts. All compounds displayed a characteristic weak absorption far into the visible light region. The peculiar absorption is a weak HOMO-LUMO transition, as established by quantum mechanical calculations.

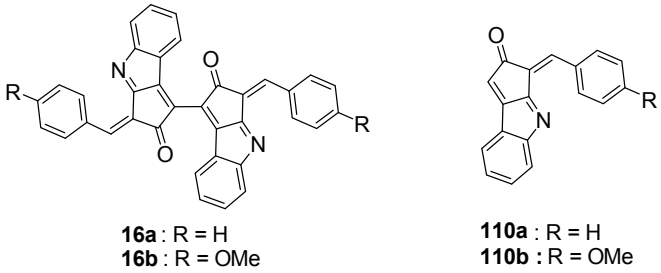

Figure 20. Investigated derivatives of scytonemin.

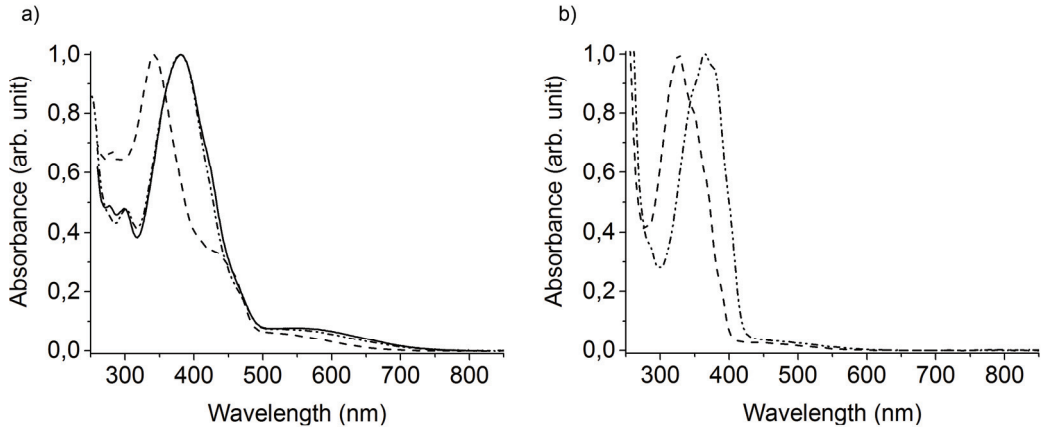

Figure 21. a) Absorption spectra of scytonemin (—), derivative 16a (- -) and methoxy derivative 16b (·--·) in Me-THF. b) Absorption spectra of monomer 110a (- -) and 110b (·--·) in Me-THF.

Next, the relaxation pathways were investigated. Fluorescence was measured after sequentially blocking the hypothetical deactivation routes outlined above. A change in fluorescence indicates whether or not a pathway is important for non-radiative relaxation. Any acid-base effects in the excited state should be suppressed in Me-THF, simplifying the hypothetical relaxation behavior. Further, methoxy derivative **16b** cannot, independently of solvent effects, participate in a phenolic acid-base pathway. However, the absence of fluorescence for both scytonemin and its methoxy derivative in Me-THF indicated that other non-radiative processes were present beside acid-base effects. The impact of conformational changes was explored next using the monomeric derivatives, which cannot relax via rotation around the center bond (Figure 19). Unfortunately, fluorescence measurements of these molecules were difficult. Fluorescence was observed, but was not consistent with the absorption spectra. It also increased during measurements, indicating a decay of the parent compound into fluorescent substances. Relaxation due to center bond rotation could neither be confirmed nor disconfirmed from these measurements. Instead, low temperature studies were pursued. However, freezing methoxy derivative **16b** in a solid Me-THF glass at 110K did not increase the fluorescence. In this state, no conformational changes can occur, indicating that there are other non-radiative pathways beside single-bond rotations and exocyclic double-bond *cis*/*trans*-isomerization.

The fluorescent studies were hampered by very fast photo-induced decay. For the unstable monomers, the buildup of fluorescent species was observed at room temperature. For the dimeric compound **16b**, decay was observed during the low temperature studies. One or two emission spectra were enough to form new substances, which displayed a temperature dependent fluorescence. The observed photochemistry could be indicative of a long lived excited state, i.e. both the non-radiative relaxation processes and relaxation via fluorescence are slow.

The photochemistry observed during the fluorescence measurements was studied further using a sun-lamp. Both scytonemin and the methoxy derivative **16b** displayed a rapid loss of absorption when irradiated by the sun-lamp in Me-THF. The combination of light and oxygen is known to oxidize ethers into hydroperoxides via a radical reaction.[152] Considering the anti-

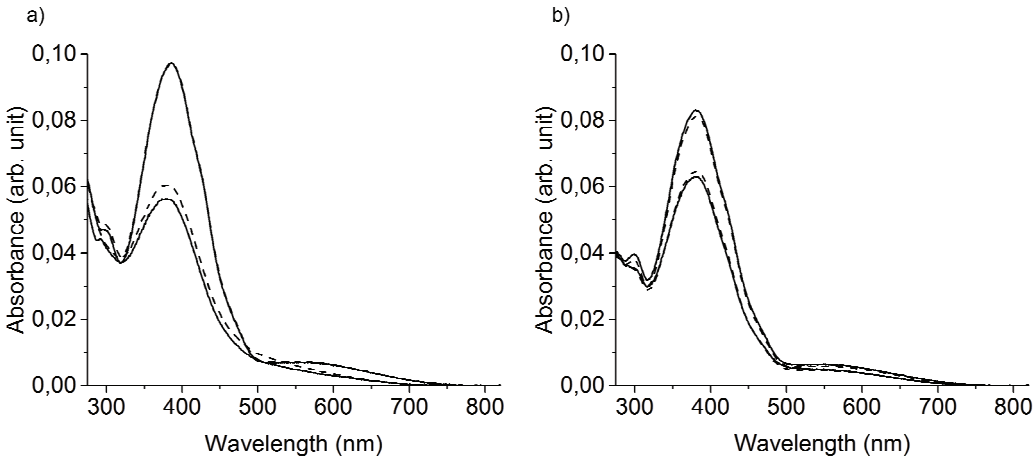

Figure 22. Photo-decay of scytonemin in presence (—) and absence (- -) of air. a) Measured in Me-THF before and after 1h of sun-lamp irradiation. b) Measured in EtOAc before and after 3h of sun-lamp irradiation.

oxidative activity of scytonemin, the decay could result from a radical reaction with the solvent. To exclude specific Me-THF effects, the experiment was repeated in ethyl acetate (EtOAc). Scytonemin was indeed more stable in EtOAc, albeit still displaying decay. To further investigate oxidative effects on the degradation, scytonemin was irradiated in the absence of oxygen. However, neither oxygen free Me-THF nor oxygen free EtOAc had any significant effect on the decomposition of scytonemin, thus eliminating the involvement of any oxygen associated reactions (Figure 22).

To further monitor and characterize the decay of scytonemin, HPLC coupled mass-spectrometry was used. Experiments were run in EtOAc and in 95% aqueous EtOH. Scytonemin displayed a linear decay in both solvents (Figure 23). No single degradation product could be observed and scytonemin likely decompose into a plethora of different substances, each one only present in minute quantities. Interestingly, the aqueous ethanol system had a stabilizing effect on scytonemin, resulting in a two and a half time slower decay compared to EtOAc. The relative stability of scytonemin can be concluded to be Me-THF < EtOAc < EtOH.

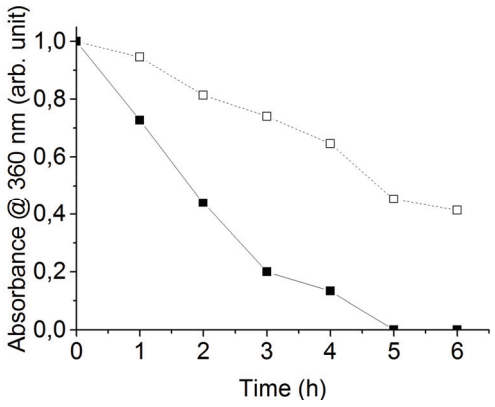

Figure 23. Sun-lamp induced photo-decay of scytonemin in EtOAc (—) and 95% aqueous EtOH (- -) analyzed by HPLC.

To attain a qualitative apprehension of the photo-induced decay of scytonemin, it was compared with two commercially available UV-screening agents; bemotrizinol and avobenzone (Figure 24). The first is considered to be highly photo-stable, while the latter display the opposite behavior.[153] The absorbance of bemotrizinol was constant over an irradiation period of six hours while avobenzone displayed a small decay. However, the absorbance of scytonemin was almost completely eradicated during the same period (Figure 24). Consequently, scytonemin displayed a decay rate several magnitudes greater than that of the unstable sunscreen avobenzone.

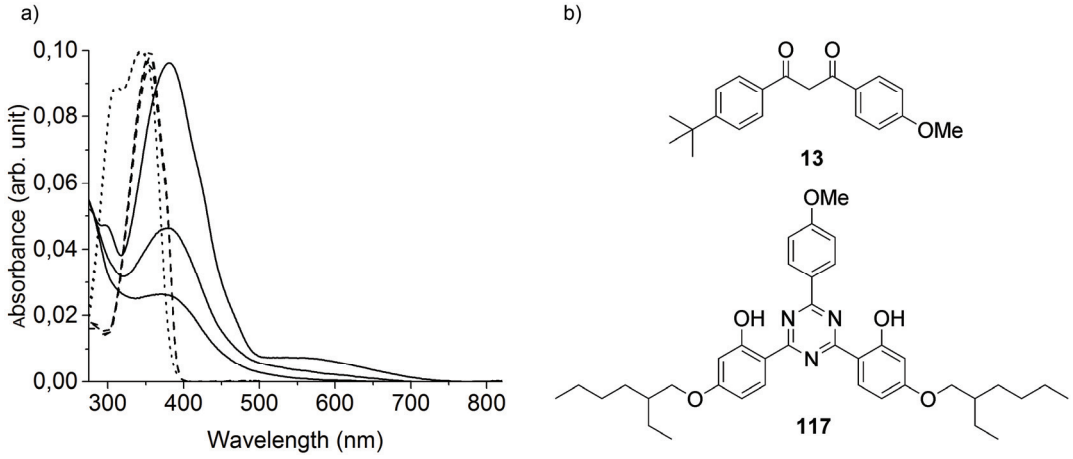

Figure 24.a) Photo-decay of scytonemin (—), avobenzone (- -) and bemotrizinol (··) in EtOAc at 0h, 3h and 6h of sun-lamp irradiation. b) Structures of avobenzone (13) and bemotrizinol (117).

To conclude, scytonemin and its methoxy derivative **16b** do not show any fluorescence in organic solvents. Further, derivative **16b** displayed an absence of fluorescence even in a conformationally frozen state. Under these conditions, excited state relaxations due to isomerizations or conformational changes are blocked, as well as excited state acid-base reactions. Regardless of the deactivation pathway, scytonemin and the derivative **16b** were found to be highly photo-unstable in organic solvents, possibly indicating a long lived excited state. Dissolution of scytonemin in aqueous ethanol had a stabilizing effect, a phenomenon which could have a number of different explanations. The highly polar solvent could stabilize an excited charge separated species and thereby introducing a new relaxation pathway. Another possibility is an excited state acid-base reaction. Phenol proton disassociations demonstrate a strong dependence on water, and the aqueous conditions could open up that pathway.[118] Unfortunately, we were unable to test methoxy derivative **16b** in EtOH, which could further strengthen or rule out a proton dissociative pathway. Nonetheless, the photo-stability of scytonemin seems to be very dependent on its surroundings.

In cyanobacteria, scytonemin is surrounded by a viscous matrix consisting of glycan polysaccharides and proteins.[9, 10] The environment offers plenty hydrogen bonding opportunities as well as more specific interactions. For instance, the scytonemin producing specie *Nostoc Commune* accumulates the water stress protein WspA in its extracellular matrix. Scytonemin and WspA have been demonstrated to non-covalently interact with one another, possibly indicating a synergistic effect in the bacteria.[10] Considering the environmental susceptibility described by us, together with the specific *in vivo* environment of

scytonemin, the reported *in vivo* photo-stability may be highly dependent on interactions with components of the extracellular matrix, explicit interactions which are not available upon dissolution in organic solvents.

The results presented here questions the proposed application of scytonemin as a sunscreen. Scytonemin has likely been "developed", i.e. evolutionary selected, to function specifically in a cyanobacterial environment. If it is ever to be used efficiently as sunscreen for personalized use, the sunscreen formulation (matrix) may need to mimic the cyanobacterial extra cellular matrix. This does not necessarily implicate using exactly the same mixture of polysaccharides and proteins, but rather that the formulation needs to mimic the stabilizing effect displayed by these components.

4.6 Biological studies of the 3-alkenyl-cyclopenta[*b*]indole skeleton (Paper III)

Scytonemin has in several studies demonstrated an inhibiting effect on cancer cell growth. Its ability to inhibit kinases via a mixed competitive/non competitive mechanism has also been established.[37] Despite recent breakthroughs in the treatment of advanced melanoma by targeting the kinase BRAF, tumor adaptation and adverse side effects are still problematic.[58, 60] Developing new scaffolds targeting melanoma-relevant kinases has been proposed as a strategy for improving the treatment. Against this background, we investigated the possibility of developing anti-melanoma relevant kinase inhibitors based on the scytonemin skeleton. We initially screened scytonemin, nostodione A and the reduced scytonemin monomer **70e** (Figure 25) against 20 cancer related kinases. Peculiarly, we were not able to repeat the reported kinase inhibitory effect of scytonemin against polo-like kinase 1 (PLK1).[37] Scytonemin has a reported IC_{50} of 2 μM, but no effect was observed even at the screening concentration of 10 μM. While the reported PLK1 assay used a reaction medium containing 4% DMSO, the assay used in our case only contained 2% DMSO. The observed difference may simply be due to the poor solubility of scytonemin. The kinases Aurora A and IKKβ were however inhibited by scytonemin, indicating that it was at least in part solubilized.

Continuing from the rather discouraging results concerning scytonemin, we were pleased with a number of exciting observations connected to the monomer **70e**. It displayed inhibitory properties against the kinases Aurora A, Aurora B, BRAF V600E and IRAK4. The Aurora kinases are intimately involved in cell mitosis, and frequently over expressed in cancers, e.g. melanoma. The close oncogenic relation has initiated an intense research around Aurora kinase inhibitors.[154] BRAF V600E is one of the most promising targets for melanoma and has been previously discussed (see chapter 1.4). IRAK4 is primarily related to inflammatory signaling pathways, but is also involved in cell survival and differentiation. In melanoma, inhibition of IRAK4 has been demonstrated to amplify the therapeutic effects of other anti-cancer agents.[155]

Encouraged by the results, we initiated cell studies to determine the compatibility of compound **70e** with biological systems. Detailed results are presented in paper III. In summary, the monomer displayed low toxicity with an IC_{50} of 20 μM. Very strong interaction with other cellular targets could thereby be ruled out. Further, flow cytometry revealed an

apoptotic mechanism to be responsible for the cellular growth inhibition, which agrees with inhibition of Aurora A, Aurora B and BRAF. At last, the fluorescent properties of compound **70e** (see chapter 4.2.1) were used to determine its cellular localization. The inhibitor was cell permeable and localized both in the cytosol and nucleus, concurring with the cellular localization of BRAF and IRAK4 (cytosol) as well as Aurora A and B (nucleus).

The initial cell studies were regarded as promising and a small structure-activity examination was pursued. Totally 14 derivatives with structural differentiation at the exocyclic double bond were assayed against Aurora A, Aurora B, BRAF and IRAK4 (Figure 25). A few interesting structure-activity observations will be highlighted here, please see paper III for the complete results. Small structural changes had a major impact on the kinase inhibition of BRAF and IRAK4 while inhibition of the Aurora kinases was more robust throughout the series. The observation is illustrated well by derivative **70b**. The methoxy derivative retains its inhibitory effects against Aurora A and B, while it is totally ineffective against BRAF. Interestingly, not only is its inhibitory effect against IRAK4 abolished, but it does paradoxically activate the enzyme. Derivative **70b** likely binds to an allosteric site of IRAK4, where it induce a conformational change that further activates the kinase.

Concerning inhibition of BRAF V600E, derivative **70g**, having a hydroxyl group in the *meta*-position proved to be equally potent to the *para*-compound **70e**. Acetamide derivative **70h**, having a hydrogen-bond donor in the same position as parent monomer **70e**, displayed a comparably poor inhibition of BRAF. The acetamide group modifies the ligand-kinase interactions primarily through the translocation of the hydrogen-bond acceptor and through the sheer bulk of the substituent. Pyridine **70i**, lacking a hydrogen-bond donor but having a hydrogen-bond acceptor demonstrated inhibition of BRAF, but less so than parent compound **70e**. The more bulky hydrogen-bond accepting molecules **70c** and **70j** displayed weak inhibition. Finally, the fluorinated derivative **70k**, unable to form hydrogen-bonds, displayed no activity at all. Taken together, the inhibitors appear to benefit from hydrogen bond-donating and accepting moieties on the aryl ring. The most potent compound **70e** and **70g** have both a donor and an acceptor, possibly indicating a synergistic effect. Further, the inhibitor seemed to be slightly flexible within the binding pocket of BRAF, as judged by the similar potencies of *meta*-substituted **70g** and *para*-substituted **70e**. The flexibility did however not render the compound insensitive to steric alterations of the hydrogen-bonding moieties, compare hydrogen-bond donating compound **70e** and **70h** as well as hydrogen bond accepting compounds **70c**, **70i** and **70j**.

Concerning IRAK4, *meta*-hydroxyl derivative **70g** displayed a reduced potency compared to *para*-compound **70e**. The pyridine **70i** was on the other hand almost as active as **70e**. Nitro compound **70c** demonstrated a weak interaction while the bulky hydrogen-bond donating substance **70h** and substances **70j** and **70k** were inactive. IRAK4 inhibition can be concluded to benefit from hydrogen bond accepting functional groups. Further, the position is important, compare **70e**, **70g** and **70i**. Compounds of more lipophilic character did not inhibit any of the investigated kinases, indicating that water solubility likely is a limiting factor.

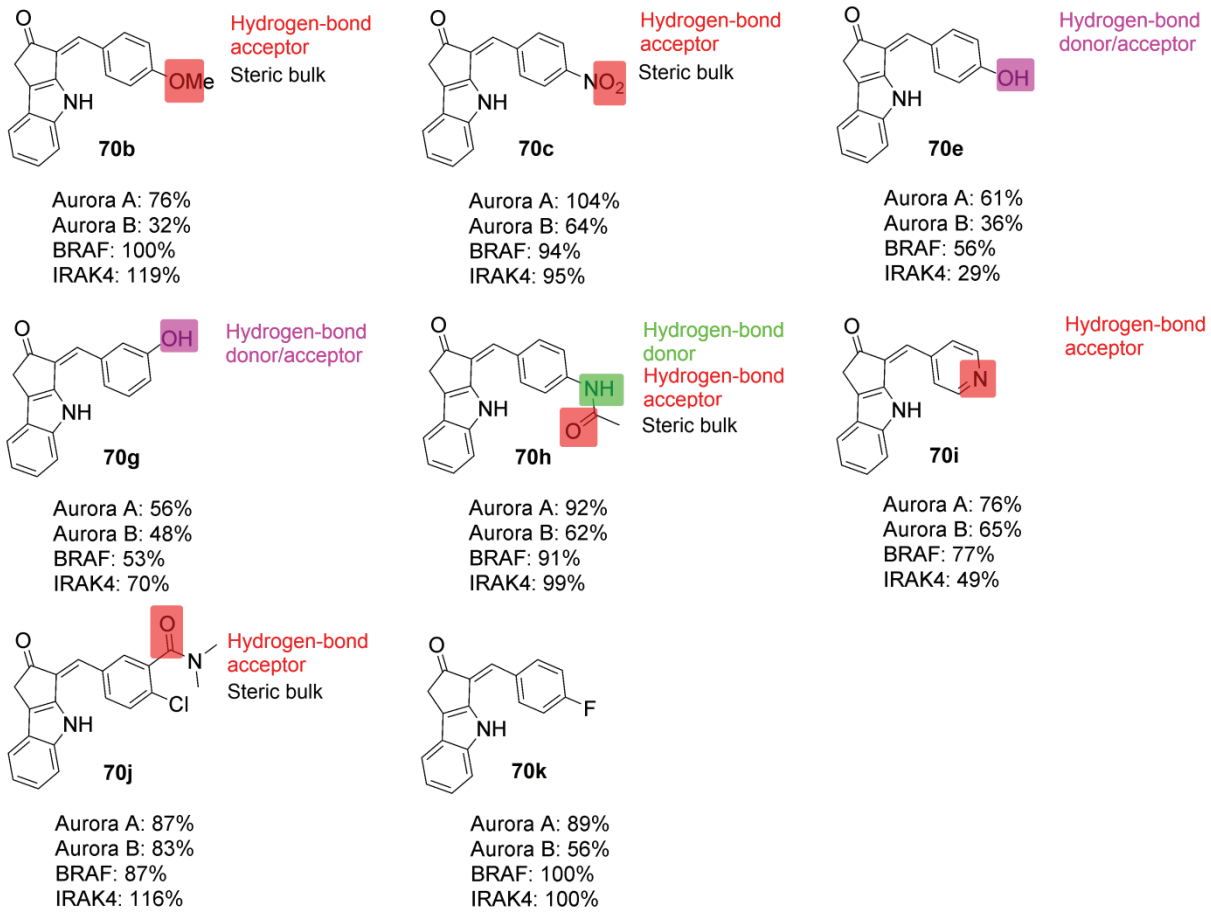

Figure 25. Selected kinase inhibitors from the structure-activity study. Kinase inhibition is reported as percent kinase activity remaining after treatment with 10μM compound at [ATP]≈K_m.

The promising cellular behavior of **70e** and its inhibition of BRAF V600E, which is a clinically proven target for melanoma treatment, were the most interesting observations in this study. The combination of hydrogen-bond donor/acceptor moieties at the exocyclic alkenyl substituent proved vital for BRAF inhibition. Compounds of type **70l**, **70m**, **70n** and **70o** (Figure 26) could possibly exhibit synergistic effects which warrant future investigations. Introducing water solubilizing substituents in positions not affecting the binding can also improve performance and deserves future studies. It is also of interest to elucidate the mode of kinase interaction, determining whether it is of type I, II or III.

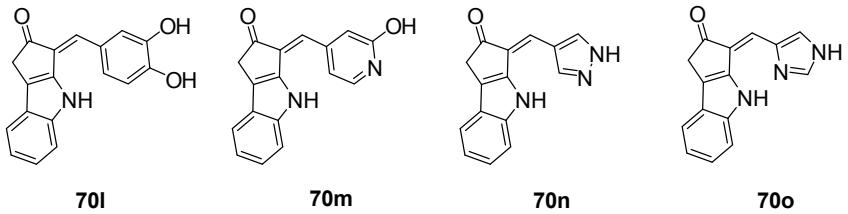

Figure 26. Potentially interesting BRAF V600E inhibitors.

5 Summary and conclusions

This thesis touches upon several different subjects, ranging from natural product synthesis and statistical reaction optimization to spectroscopy and cell studies. Our work was initially concerned with the synthesis of scytonemin, nostodione A and related derivatives. The compounds were subsequently utilized in the development of kinase inhibitors and in the photophysicochemical characterization of scytonemin. The results therefore have implications on many different areas, and will hopefully be useful for both synthetic and medicinal chemists, as well as biologists working with the ecology of cyanobacteria.

Our synthesis of scytonemin and nostodione A involved a key monomeric fragment (**70**), composed of a 3-alkenyl-cyclopenta[*b*]indole skeleton. The key fragment **70** was obtainable from the commercially available indole-3-acetic acid via either a seven or a six step synthetic pathway, both based on a palladium catalyzed annulation of the indole. The seven step synthetic route revolved around a cascade Heck-Suzuki reaction, which can be used to create compounds with structural diversity at the exocyclic alkenyl substituent. The reaction is a set of successive palladium catalyzed steps, which must occur in a specific order to secure a successful reaction outcome. Statistical experimental design (Design of Experiments, DoE) was used to optimize six variables likely to affect the multifaceted reaction. The palladium ligand was included as two latent variables obtained from principal component analysis (PCA), enabling it to be described in a quantitative, continuous manner. A very complex dependence on the ligand was found, which also was the most influential reaction variable. Using the obtained DoE-model, optimal reaction conditions were selected and utilized to synthesize 13 derivatives of **70**. The study demonstrate how a complex reaction, in which the underlying mechanism is not completely understood, can be rationally optimized using DoE. We also demonstrate the significance of including ligand as a continuous variable using PCA. It was very influential and the complex ligand effect can likely not be described by any other method.

Both scytonemin and nostodione A could be readily synthesized from the monomeric structure **70**. An oxidative coupling produced the dimeric structure of scytonemin, while a Yonemitsu reaction generated the dione moiety of nostodione A. We here demonstrate the versatility of our synthetic pathway, which is able to produce both scytonemin and nostodione A derivatives from a common intermediate **70**. The synthesis of **70** is also diversity oriented, having the possibility to introduce different substituents at the exo-cyclic alkenyl group. With the ability to construct unnatural derivatives, structural properties of the natural products can be investigated and for instance placed into an evolutionary perspective. It can also be used to enhance specific properties, such as bioactivity.

Contradictory to the reported *in vivo* photo-stability of scytonemin (i.e. whilst in the extra cellular matrix of the cyanobacteria), we have demonstrated that scytonemin is highly photo-unstable in organic solvents. The instability displayed a solvent dependence according to: Me-THF < EtOAc < EtOH, with scytonemin being most stable in EtOH. The presence of air did not influence the stability, indicating that an oxygen mediated effect was not responsible for the degradation. Further, a number of possible excited state deactivation pathways of scytonemin were investigated. The study was unfortunately unsuccessful as no fluorescence of the methoxy derivative **16b** could be observed in Me-THF, even when blocking all envisioned relaxation pathways. However, considering the solvent effects, the deactivation pathways of scytonemin seem to be dependent on its surroundings. For instance, the stabilizing effect displayed by aqueous EtOH could point toward efficient relaxation via acid-base reactions or internal charge transfers. Regardless of deactivation route, the observed solvent effect has implications on cyanobacterial ecology. The viscous extra cellular matrix of cyanobacteria consists of polysaccharides and proteins, offering a unique environment. The reported *in vivo* stability of scytonemin is likely due to specific matrix interactions, possibly providing an efficient excited state deactivation pathway that is not available upon dissolution in organic solvents.

We found an *in vitro* inhibitory activity of 3-alkenyl-cyclopenta[*b*]indole-2-one monomer **70** against four kinases, Aurora A, Aurora B, BRAF V600E and IRAK4, all relevant for combating melanoma. Inhibition of the kinase BRAF V600E has been clinically demonstrated to revert advanced melanoma, and finding new scaffolds for its inhibition is of particular interest. Totally 17 of our synthesized compounds, including scytonemin and nostodione A, were assayed against the kinases in a small structure-activity study. A number of interesting traits, which can be used in further inhibitor developments, were found. One of the more promising compounds, phenolic compound **70e**, was studied in a cellular context using peripheral blood mononuclear cells (PBMC). It induced cell apoptosis, agreeing with inhibition of investigated kinases. The cytotoxicity was low, indicative of only weak off-target interactions. It was further cell permeable and distributed both in the cytosol and nucleus, coinciding with the cellular location of the investigated kinases.

6 Future studies

The developed synthetic pathways can in future studies be utilized to synthesize tailored compounds of interest. The routes can also be elaborated to fulfill future need of complementary derivatization according to the following suggestions:

- Enolate chemistry can be utilized to introduce substituents at C-1 of 3-alkenyl-cycopenta[*b*]indole-2-one scaffold **70**. Attractive examples of enolate chemistries include condensations (e.g. aldol), transition metal catalyzed cross-couplings and oxidative hetero-couplings.
- Substitution on the indole nitrogen.
- Using different alkynes in the nucleophilic substitution of the Weinreb amide **76** to produce compounds that via the cascade Heck-Suzuki reaction generate additional diversity at the exocyclic double bond.

The photo-instability of scytonemin was not anticipated and should be investigated further, with the final goal of elucidating the environmental stabilizing/destabilizing mechanism. For this purpose, the following solvent based studies are proposed:

- Study scytonemin in non-protic solvents of various polarity. It will give insight to effects not involving hydrogen transfer reactions and hydrogen bonding.
- Study scytonemin in acetone, DMF or DMSO solutions with increasingly higher water content. The study can be indicative of stabilizing/destabilizing effects specifically involving hydrogens.
- Study different relevant additives, such as polysaccharides and proteins. The study can be thought of as a simulation of the cyanobacterial extracellular matrix. It may give valuable insight into the photo-stability.

Inhibition of BRAF V600E and the favorable cellular behavior of 3-(4-hydroxybenzylidene)-cyclopenta[*b*]indole-2-one monomer **70e** were the most interesting results from the anti-

melanoma study. The 3-alkenyl substituent of the scaffold **70** has been investigated and suggestions of better performing substituents in this position have been presented. To improve the scaffold further, future studies should focus on elucidating the binding mode by:

- Using a kinase inhibition assay differentiating between type I and type II inhibitors.
- Co-crystallization of BRAF V600E and **70e**
- Using computational ligand-protein docking simulations.

With an established mode of binding, rational design can be used to:

- Introduce water solubilizing substituents in a position which will not affect the inhibition. The inhibitors displayed water solubility as a limiting factor, and the proposed modification will likely be beneficial.
- Strengthen the kinase-protein binding by introducing new substituents which actively interact with the protein.

7 Acknowledgement

This work was funded by the **Swedish Research Council** and the **Wilhelm and Martina Lundgrens research foundation**.

None of the work presented herein would have been possible without the help and support from the following people: My supervisor **Jerker Mårtensson**, your knowledge and never-ending enthusiasm has encouraged me in every step of this project. **Shiming Li**, your continuous and valuable advices in the lab have been truly helpful. **Isabella Karlsson**, for getting my PhD studies off to a good start. Without your help, things would have taken much longer. **Anna Börje**, for all your help with everything from HPLC to feedback on papers. **Peter Sandin**, for your tireless work with the photochemically odd molecules. **Nina Kann**, for your help throughout my studies and especially for helping out the last week before the printing of this thesis. **Paul Helquist**, for a great, educating stay at the University of Notre Dame. The master students **Ye Pan**, **Rudi Mete**, **Asma Arshad** and **Lucy Idowu Ajakaiye**, for your contributions to the palladium and gold catalyzed reaction development. **All people at floor nine**, keep up the good work and bizarre lunch conversations.

The lunch group **Emil**, **Jesper**, **Maria**, **Alex**, **Johan** and **Mattias**, for all the pasta, husmanskost, kebab etc. we shared, good times!

Berne and **Marita**, big thanks for the nice holidays, great dinners, all the help with Belle and much more! **My family**, for 30 years of endless support, this thesis would not have been written without it. And of course **Kicki**, for, well..everything!

8 Literature

1. E. Kinne-Saffran and R. K. H. Kinne, *Am J Nephrol*, 1999, **19**, 290-294.

2. G. Fraenkel, *Science*, 1959, **129**, 1466-1470.

3. D. H. Williams, M. J. Stone, P. R. Hauck and S. K. Rahman, *J Nat Prod*, 1989, **52**, 1189-1208.

4. B. B. Buchanan, W. Gruissem and R. L. Jones, *Biochemistry & molecular biology of plants*, American Society of Plant Physiologists, Rockville, Md. ; [Great Britain], 2000.

5. K. C. Nicolaou and S. A. Snyder, *Classics in total synthesis. Vol. 2, More targets, strategies, methods*, Wiley-VCH ; [Chichester : Wiley], Weinheim, 2003.

6. P. M. Dewick, *Medicinal natural products : a biosynthetic approach*, Wiley-Blackwell, Oxford, 2009.

7. C. W. v. Naegeli, *Gattungen einzelliger Algen physiologisch und systematisch bearbeitet. Mit acht lithographirten Tafeln*, Zurich, 1849.

8. F. Garciapichel and R. W. Castenholz, *J Phycol*, 1991, **27**, 395-409.

9. R. F. Helm, Z. Huang, D. Edwards, H. Leeson, W. Peery and M. Potts, *J Bacteriol*, 2000, **182**, 974-982.

10. D. J. Wright, S. C. Smith, V. Joardar, S. Scherer, J. Jervis, A. Warren, R. F. Helm and M. Potts, *J Biol Chem*, 2005, **280**, 40271-40281.

11. P. J. Proteau, W. H. Gerwick, F. Garciapichel and R. Castenholz, *Experientia*, 1993, **49**, 825-829.

12. A. Kobayashi, S. I. Kajiyama, K. Inawaka, H. Kanzaki and K. Kawazu, *Z Naturforsch C*, 1994, **49**, 464-470.

13. A. Ploutno and S. Carmeli, *J Nat Prod*, 2001, **64**, 544-545.

14. S. H. Shim, G. Chlipala and J. Orjala, *J Microbiol Biotechn*, 2008, **18**, 1655-1658.

15. V. Bultel-Ponce, F. Felix-Theodose, C. Sarthou, J. F. Ponge and B. Bodo, *J Nat Prod*, 2004, **67**, 678-681.

16. C. S. Grant and J. W. Louda, *Org Geochem*, 2013, **65**, 29-36.

17. F. Garciapichel, N. D. Sherry and R. W. Castenholz, *Photochem Photobiol*, 1992, **56**, 17-23.

18. J. G. Dillon and R. W. Castenholz, *J Phycol*, 1999, **35**, 673-681.

19. Q. Gao and F. Garcia-Pichel, *Nat Rev Microbiol*, 2011, **9**, 791-802.

20. J. G. Dillon, C. M. Tatsumi, P. G. Tandingan and R. W. Castenholz, *Arch Microbiol*, 2002, **177**, 322-331.

21. K. Matsui, E. Nazifi, Y. Hirai, N. Wada, S. Matsugo and T. Sakamoto, *J Gen Appl Microbiol*, 2012, **58**, 137-144.

22. T. Soule, K. Palmer, Q. Gao, R. M. Potrafka, V. Stout and F. Garcia-Pichel, *BMC Genomics*, 2009, **10**, 336.

23. T. Soule, V. Stout, W. D. Swingley, J. C. Meeks and F. Garcia-Pichel, *J Bacteriol*, 2007, **189**, 4465-4472.

24. E. P. Balskus and C. T. Walsh, *J Am Chem Soc*, 2008, **130**, 15260-15261.

25. E. P. Balskus and C. T. Walsh, *J Am Chem Soc*, 2009, **131**, 14648-14649.

26. S. Malla and M. O. A. Sommer, *Green Chem*, 2014, **16**, 3255-3265.

27. L. Franceschetti, A. Garzonaburbeh, M. R. Mahmoud, B. Natalini and R. Pellicciari, *Tetrahedron Lett*, 1993, **34**, 3185-3188.

28. G. Henrion, T. E. J. Chavas, X. Le Goff and F. Gagosz, *Angew Chem Int Edit*, 2013, **52**, 6277-6282.

29. J. A. Jordan, G. W. Gribble and J. C. Badenock, *Tetrahedron Lett*, 2011, **52**, 6772-6774.

30. E. T. Li, C. W. Li, J. Wang, J. Q. Wang, L. H. Dong, X. H. Guo, C. J. Song and J. B. Chang, *Tetrahedron*, 2014, **70**, 874-879.

31. J. M. Lopchuk, I. L. Green, J. C. Badenock and G. W. Gribble, *Org Lett*, 2013, **15**, 4485-4487.

32. M. Salim and A. Capretta, *Tetrahedron*, 2000, **56**, 8063-8069.

33. Q. Tang, X. K. Chen, B. Tiwari and Y. R. Chi, *Org Lett*, 2012, **14**, 1922-1925.

34. A. Ekebergh, A. Börje and J. Mårtensson, *Org Lett*, 2012, **14**, 6274-6277.

35. A. Ekebergh, I. Karlsson, R. Mete, Y. Pan, A. Börje and J. Mårtensson, *Org Lett*, 2011, **13**, 4458-4461.

36. J. McNulty, K. Keskar, C. Bordon, R. Yolken and L. Jones-Brando, *Chem Commun*, 2014, **50**, 8904-8907.

37. C. S. Stevenson, E. A. Capper, A. K. Roshak, B. Marquez, C. Eichman, J. R. Jackson, M. Mattern, W. H. Gerwick, R. S. Jacobs and L. A. Marshall, *J Pharmacol Exp Ther*, 2002, **303**, 858-866.

38. Z. F. Duan, D. N. Ji, E. J. Weinstein, X. Z. Liu, M. Susa, E. Choy, C. Yang, H. Mankin and F. J. Hornicek, *Cancer Lett*, 2010, **293**, 220-229.

39. G. J. Zhang, Z. Zhang and Z. G. Liu, *Tumor Biol*, 2013, **34**, 1887-1894.

40. G. J. Zhang, Z. Zhang and Z. G. Liu, *Tumor Biol*, 2013, **34**, 2241-2247.

41. Z. Zhang, G. J. Zhang and C. Z. Kong, *Urol Oncol-Semin Ori*, 2013, **31**, 1222-1230.

42. C. S. Stevenson, E. A. Capper, A. K. Roshak, B. Marquez, K. Grace, W. H. Gerwick, R. S. Jacobs and L. A. Marshall, *Inflamm Res*, 2002, **51**, 112-114.

43. J. S. Kang, S. A. Cho, S.-B. Han, K. Lee and H. M. Kim, *The Journal of Immunology*, 2011, **186**, 112.113.

44. E. Garcion, N. Wion-Barbot, C. N. Montero-Menei, F. Berger and D. Wion, *Trends Endocrin Met*, 2002, **13**, 100-105.

45. M. F. Holick, E. Smith and S. Pincus, *Arch Dermatol*, 1987, **123**, 1677-&.

46. S. Q. Wang, Y. Balagula and U. Osterwalder, *Dermatol Ther*, 2010, **23**, 31-47.

47. A. Osterlind, M. A. Tucker, B. J. Stone and O. M. Jensen, *Int J Cancer*, 1988, **42**, 319-324.

48. J. C. van der Pols, G. M. Williams, N. Pandeya, V. Logan and A. C. Green, *Cancer Epidem Biomar*, 2006, **15**, 2546-2548.

49. S. Schauder and H. Ippen, *Contact Dermatitis*, 1997, **37**, 221-232.

50. S. Schauder and H. Ippen, *Photodermatology*, 1986, **3**, 140-147.

51. I. Karlsson, Chemical and Dermatological Aspects of UV-absorbing Compounds, University of Gothenburg, 2011.

52. I. Karlsson, L. Hillerstrom, A. L. Stenfeldt, J. Martensson and A. Borje, *Chem Res Toxicol*, 2009, **22**, 1881-1892.

53. C. Garbe and U. Leiter, *Clin Dermatol*, 2009, **27**, 3-9.

54. C. M. Balch, A. C. Buzaid, S. J. Soong, M. B. Atkins, N. Cascinelli, D. G. Coit, I. D. Fleming, J. E. Gershenwald, A. Houghton, J. M. Kirkwood, K. M. McMasters, M. F. Mihm, D. L. Morton, D. S. Reintgen, M. I. Ross, A. Sober, J. A. Thompson and J. F. Thompson, *J Clin Oncol*, 2001, **19**, 3635-3648.

55. H. Tsao, *New Engl J Med*, 2004, **351**, 2461-2461.

56. H. Davies, G. R. Bignell, C. Cox, P. Stephens, S. Edkins, S. Clegg, J. Teague, H. Woffendin, M. J. Garnett, W. Bottomley, N. Davis, N. Dicks, R. Ewing, Y. Floyd, K. Gray, S. Hall, R. Hawes, J. Hughes, V. Kosmidou, A. Menzies, C. Mould, A. Parker, C. Stevens, S. Watt, S. Hooper, R. Wilson, H. Jayatilake, B. A. Gusterson, C. Cooper, J. Shipley, D. Hargrave, K. Pritchard-Jones, N. Maitland, G. Chenevix-Trench, G. J. Riggins, D. D. Bigner, G. Palmieri, A. Cossu, A. Flanagan, A. Nicholson, J. W. C. Ho, S. Y. Leung, S. T. Yuen, B. L. Weber, H. F. Siegler, T. L. Darrow, H. Paterson, R. Marais, C. J. Marshall, R. Wooster, M. R. Stratton and P. A. Futreal, *Nature*, 2002, **417**, 949-954.

57. B. B. Friday and A. A. Adjei, *Clin Cancer Res*, 2008, **14**, 342-346.

58. P. Lito, N. Rosen and D. B. Solit, *Nat Med*, 2013, **19**, 1401-1409.

59. J. Tsai, J. T. Lee, W. Wang, J. Zhang, H. Cho, S. Mamo, R. Bremer, S. Gillette, J. Kong, N. K. Haass, K. Sproesser, L. Li, K. S. M. Smalley, D. Fong, Y. L. Zhu, A. Marimuthu, H. Nguyen, B. Lam, J. Liu, I. Cheung, J. Rice, Y. Suzuki, C. Luu, C. Settachatgul, R. Shellooe, J. Cantwell, S. H. Kim, J. Schlessinger, K. Y. J. Zhang, B. L. West, B. Powell, G. Habets, C. Zhang, P. N. Ibrahim, P. Hirth, D. R. Artis, M. Herlyn and G. Bollag, *P Natl Acad Sci USA*, 2008, **105**, 3041-3046.

60. P. B. Chapman, A. Hauschild, C. Robert, J. B. Haanen, P. Ascierto, J. Larkin, R. Dummer, C. Garbe, A. Testori, M. Maio, D. Hogg, P. Lorigan, C. Lebbe, T. Jouary, D. Schadendorf, A. Ribas, S. J. O'Day, J. A. Sosman, J. M. Kirkwood, A. M. M. Eggermont, B. Dreno, K. Nolop, J. Li, B. Nelson, J. Hou, R. J. Lee, K. T. Flaherty, G. A. McArthur and B.-S. Grp, *New Engl J Med*, 2011, **364**, 2507-2516.

61. J. A. Sosman, K. B. Kim, L. Schuchter, R. Gonzalez, A. C. Pavlick, J. S. Weber, G. A. McArthur, T. E. Hutson, S. J. Moschos, K. T. Flaherty, P. Hersey, R. Kefford, D. Lawrence, I. Puzanov, K. D. Lewis, R. K. Amaravadi, B. Chmielowski, H. J. Lawrence, Y. Shyr, F. Ye, J. Li, K. B. Nolop, R. J. Lee, A. K. Joe and A. Ribas, *New Engl J Med*, 2012, **366**, 707-714.

62. A. J. Sievert, S. S. Lang, K. L. Boucher, P. J. Madsen, E. Slaunwhite, N. Choudhari, M. Kellet, P. B. Storm and A. C. Resnick, *P Natl Acad Sci USA*, 2013, **110**, 5957-5962.

63. E.-i. Negishi, *Handbook of organopalladium chemistry for organic synthesis*, Wiley, New York ; [Great Britain], 2002.

64. T. N. Foundation, The Nobel Prize in Chemistry 2010, http://www.nobelprize.org/nobel_prizes/chemistry/laureates/2010/.

65. N. Miyaura, K. Yamada and A. Suzuki, *Tetrahedron Lett*, 1979, **20**, 3437-3440.

66. J. F. Fauvarque, F. Pfluger and M. Troupel, *J Organomet Chem*, 1981, **208**, 419-427.

67. A. Jutand and A. Mosleh, *Organometallics*, 1995, **14**, 1810-1817.

68. F. Barrios-Landeros, B. P. Carrow and J. F. Hartwig, *J Am Chem Soc*, 2009, **131**, 8141-8154.

69. K. C. Lam, T. B. Marder and Z. Y. Lin, *Organometallics*, 2007, **26**, 758-760.

70. R. Martin and S. L. Buchwald, *Accounts Chem Res*, 2008, **41**, 1461-1473.

71. M. Peruzzini and L. Gonsalvi, *Phosphorus compounds : advanced tools in catalysis and material sciences*, Springer, Dordrecht ; London, 2011.

72. J. Jover, N. Fey, M. Purdie, G. C. Lloyd-Jones and J. N. Harvey, *J Mol Catal a-Chem*, 2010, **324**, 39-47.

73. A. J. J. Lennox and G. C. Lloyd-Jones, *Angew Chem Int Edit*, 2013, **52**, 7362-7370.

74. C. Amatore, G. Le Duc and A. Jutand, *Chem-Eur J*, 2013, **19**, 10082-10093.

75. B. P. Carrow and J. F. Hartwig, *J Am Chem Soc*, 2011, **133**, 2116-2119.

76. G. Audran, P. Bremond, S. R. A. Marque, D. Siri and M. Santelli, *Tetrahedron*, 2014, **70**, 2272-2279.

77. A. L. Casado and P. Espinet, *J Am Chem Soc*, 1998, **120**, 8978-8985.

78. J. Louie and J. F. Hartwig, *J Am Chem Soc*, 1995, **117**, 11598-11599.

79. C. Amatore, A. Jutand and A. Suarez, *J Am Chem Soc*, 1993, **115**, 9531-9541.

80. A. Ariafard and B. F. Yates, *J Organomet Chem*, 2009, **694**, 2075-2084.

81. M. Perez-Rodriguez, A. A. C. Braga, M. Garcia-Melchor, M. H. Perez-Temprano, J. A. Casares, G. Ujaque, A. R. de Lera, R. Alvarez, F. Maseras and P. Espinet, *J Am Chem Soc*, 2009, **131**, 3650-3657.

82. R. F. Heck and J. P. Nolley, *J Org Chem*, 1972, **37**, 2320-&.

83. T. Mizoroki, K. Mori and A. Ozaki, *Bull. Chem. Soc. Jpn.*, 1971, **44**.

84. A. Arcadi, F. Blesi, S. Cocchi, G. Fabrizi, A. Goggiamani and F. Marinelli, *J Org Chem*, 2013, **78**, 4490-4498.

85. M. Arthuis, R. Pontikis and J. C. Florent, *Tetrahedron Lett*, 2007, **48**, 6397-6400.

86. M. Arthuis, R. Pontikis and J. C. Florent, *J Org Chem*, 2009, **74**, 2234-2237.

87. T. Castanheiro, M. Donnard, M. Gulea and J. Suffert, *Org Lett*, 2014, **16**, 3060-3063.

88. W. S. Cheung, R. J. Patch and M. R. Player, *J Org Chem*, 2005, **70**, 3741-3744.

89. R. L. Greenaway, C. D. Campbell, O. T. Holton, C. A. Russell and E. A. Anderson, *Chem-Eur J*, 2011, **17**, 14366-14370.

90. E. Marchal, J. F. Cupif, P. Uriac and P. van de Weghe, *Tetrahedron Lett*, 2008, **49**, 3713-3715.

91. B. M. Monks and S. P. Cook, *J Am Chem Soc*, 2012, **134**, 15297-15300.

92. K. Paul, K. Bera, S. Jalal, S. Sarkar and U. Jana, *Org Lett*, 2014, **16**, 2166-2169.

93. C. Amatore and A. Jutand, *Accounts Chem Res*, 2000, **33**, 314-321.

94. C. Backtorp and P. O. Norrby, *J Mol Catal a-Chem*, 2010, **328**, 108-113.

95. D. J. Gorin and F. D. Toste, *Nature*, 2007, **446**, 395-403.

96. C. Ferrer and A. M. Echavarren, *Angew Chem Int Edit*, 2006, **45**, 1105-1109.

97. C. Ferrer, C. H. Amijs and A. M. Echavarren, *Chem-Eur J*, 2007, **13**, 1358-1373.

98. D. B. England and A. Padwa, *Org Lett*, 2008, **10**, 3631-3634.

99. Y. Liu, W. Xu and X. Wang, *Org Lett*, 2010, **12**, 1448-1451.

100. G. Verniest, D. England, N. De Kimpe and A. Padwa, *Tetrahedron*, 2010, **66**, 1496-1502.

101. G. Cera, P. Crispino, M. Monari and M. Bandini, *Chem Commun (Camb)*, 2011, **47**, 7803-7805.

102. L. Wang, G. Li and Y. Liu, *Org Lett*, 2011, **13**, 3786-3789.

103. A. S. K. Hashmi, W. B. Yang and F. Rominger, *Chem-Eur J*, 2012, **18**, 6576-6580.

104. I. V. Alabugin, K. Gilmore and M. Manoharan, *J Am Chem Soc*, 2011, **133**, 12608-12623.

105. H. Abdi and L. J. Williams, *Wiley Interdisciplinary Reviews: Computational Statistics*, 2010, **2**, 433-459.

106. T. Lundstedt, E. Seifert, L. Abramo, B. Thelin, A. Nystrom, J. Pettersen and R. Bergman, *Chemometr Intell Lab*, 1998, **42**, 3-40.

107. D. C. Montgomery, *Design and analysis of experiments*, Wiley, Hoboken, NJ, 2008.

108. G.-J. Park, *Analytic methods for design practice*, Springer, London, 2007.

109. S. Wold, K. Esbensen and P. Geladi, *Chemometr Intell Lab*, 1987, **2**, 37-52.

110. R. Carlson and J. E. Carlson, *Org Process Res Dev*, 2005, **9**, 680-689.

111. J. D. Moseley and P. M. Murray, *J Chem Technol Biot*, 2014, **89**, 623-632.

112. P. M. Murray, S. N. G. Tyler and J. D. Moseley, *Org Process Res Dev*, 2013, **17**, 40-46.

113. L. Eriksson, *Design of experiments : principles and applications*, Umetrics, Umea, 2000.

114. J. R. Lakowicz, *Principles of fluorescence spectroscopy*, Springer, New York, 2006.

115. J. Chen, C. C. W. Law, J. W. Y. Lam, Y. Dong, S. M. F. Lo, I. D. Williams, D. Zhu and B. Z. Tang, *Chemistry of Materials*, 2003, **15**, 1535-1546.

116. D. C. Todd, J. M. Jean, S. J. Rosenthal, A. J. Ruggiero, D. Yang and G. R. Fleming, *J Chem Phys*, 1990, **93**, 8658-8668.

117. M. Sumitani, N. Nakashima, K. Yoshihara and S. Nagakura, *Chem Phys Lett*, 1977, **51**, 183-185.

118. M. M. Martin and J. T. Hynes, *Femtochemistry and femtobiology : ultrafast events in molecular science : VIth International Conference on Femtochemistry, Maison de la Chimie, Paris, France, July 6-10, 2003*, Elsevier, Amsterdam ; Oxford, 2004.

119. O. Poizat, E. Bardez, G. Buntinx and V. Alain, *The Journal of Physical Chemistry A*, 2004, **108**, 1873-1880.

120. G. L. Patrick, *An introduction to medicinal chemistry*, Oxford University Press, Oxford, 2005.

121. J. M. Zhang, P. L. Yang and N. S. Gray, *Nat Rev Cancer*, 2009, **9**, 28-39.

122. S. Lapenna and A. Giordano, *Nat Rev Drug Discov*, 2009, **8**, 547-566.

123. K. Strebhardt, *Nat Rev Drug Discov*, 2010, **9**, 643-U624.

124. I. Kufareva and R. Abagyan, *J Med Chem*, 2008, **51**, 7921-7932.

125. Y. Liu and N. S. Gray, *Nat Chem Biol*, 2006, **2**, 358-364.

126. A. F. Littke, C. Y. Dai and G. C. Fu, *J Am Chem Soc*, 2000, **122**, 4020-4028.

127. A. F. Littke and G. C. Fu, *J Org Chem*, 1999, **64**, 10-11.

128. M. R. Netherton and G. C. Fu, *Org Lett*, 2001, **3**, 4295-4298.

129. J. Jover, N. Fey, J. N. Harvey, G. C. Lloyd-Jones, A. G. Orpen, G. J. J. Owen-Smith, P. Murray, D. R. J. Hose, R. Osborne and M. Purdie, *Organometallics*, 2010, **29**, 6245-6258.

130. P. A. Donets and E. V. Van der Eycken, *Org Lett*, 2007, **9**, 3017-3020.

131. Z. Li, E. B. Watkins, H. Liu, A. G. Chittiboyina, P. B. Carvalho and M. A. Avery, *J Org Chem*, 2008, **73**, 7764-7767.

132. B. Schmidt and H. M. R. Hoffmann, *Tetrahedron*, 1991, **47**, 9357-9368.

133. B. M. Trost and F. D. Toste, *J Am Chem Soc*, 1999, **121**, 3543-3544.

134. R. Yanada, S. Obika, T. Inokuma, K. Yanada, M. Yamashita, S. Ohta and Y. Takemoto, *J Org Chem*, 2005, **70**, 6972-6975.

135. J. M. Bothwell, V. V. Angeles, J. P. Carolan, M. E. Olson and R. S. Mohan, *Tetrahedron Lett*, 2010, **51**, 3696-3696.

136. Z. Y. Jiang and Y. G. Wang, *Tetrahedron Lett*, 2003, **44**, 3859-3861.

137. B. Wang, H. X. Sun, B. Chen and Z. H. Sun, *Green Chem*, 2009, **11**, 1112-1114.

138. M. J. Wang, C. Li, D. L. Yin and X. T. Liang, *Tetrahedron Lett*, 2002, **43**, 8727-8729.

139. E. R. Fruchey and S. P. Cook, *Abstr Pap Am Chem S*, 2013, **246**.

140. A. Minatti, X. L. Zheng and S. L. Buchwald, *J Org Chem*, 2007, **72**, 9253-9258.

141. M. L. S. Almeida, M. Beller, G. Z. Wang and J. E. Backvall, *Chem-Eur J*, 1996, **2**, 1533-1536.

142. Y. Blum, D. Czarkie, Y. Rahamim and Y. Shvo, *Organometallics*, 1985, **4**, 1459-1461.

143. Y. Blum and Y. Shvo, *J Organomet Chem*, 1985, **282**, C7-C10.

144. Y. Oikawa and O. Yonemitsu, *J Org Chem*, 1977, **42**, 1213-1216.

145. A. G. Csaky and J. Plumet, *Chem Soc Rev*, 2001, **30**, 313-320.

146. M. P. DeMartino, K. Chen and P. S. Baran, *J Am Chem Soc*, 2008, **130**, 11546-11560.

147. R. H. Frazier and R. L. Harlow, *J Org Chem*, 1980, **45**, 5408-5411.

148. F. Guo, M. D. Clift and R. J. Thomson, *Eur J Org Chem*, 2012, **2012**, 4881-4896.

149. Y. Ito, T. Konoike and T. Saegusa, *J Am Chem Soc*, 1975, **97**, 2912-2914.

150. N. Kise, T. Ueda, K. Kumada, Y. Terao and N. Ueda, *The Journal of Organic Chemistry*, 2000, **65**, 464-468.

151. Y. Kobayashi, T. Taguchi and E. Tokuno, *Tetrahedron Lett*, 1977, 3741-3742.

152. S. Di Tommaso, P. Rotureau, O. Crescenzi and C. Adamo, *Phys Chem Chem Phys*, 2011, **13**, 14636-14645.

153. E. Chatelain and B. Gabard, *Photochem Photobiol*, 2001, **74**, 401-406.

154. M. Kollareddy, D. Zheleva, P. Dzubak, P. S. Brahmkshatriya, M. Lepsik and M. Hajduch, *Invest New Drug*, 2012, **30**, 2411-2432.

155. R. Srivastava, D. G. Geng, Y. J. Liu, L. Q. Zheng, Z. Y. Li, M. A. Joseph, C. McKenna, N. Bansal, A. Ochoa and E. Davila, *Cancer Res*, 2012, **72**, 6209-6216.

9 Appendix for unpublished experimental procedures

General procedures: All reactions were carried out under argon atmosphere with dry solvents in oven dried glassware, unless otherwise noted. Reagents and solvents were bought from commercial vendors and used as received, unless otherwise stated. Dry oxygen free THF was obtained through distillation over sodium under nitrogen gas. Dry oxygen free Et_3N was obtained through distillation over calcium hydride under nitrogen gas. DMF was purchased in anhydrous form and used without further purification. For the transition metal catalyzed reactions, oxygen free DMF and acetone were obtained by bubbling argon through the solvents for 30 min. Reactions were monitored by thin-layer chromatography (TLC) carried out on Merck silica gel plates ($60_{F\text{-}254}$) using UV light as visualizing agent. NMR spectra were recorded on samples in either deuterated chloroform ($CDCl_3$) or acetone (acetone-d_6) on either a JEOL Eclipse 400 MHz (101 MHz for ^{13}C) or an Agilent 400 MHz (101 MHz for ^{13}C) instrument. Residual undeuterated solvent was used as internal reference: chloroform (^1H: δ = 7.26 ppm, ^{13}C: δ = 77.0 ppm) and acetone (^1H: δ = 2.05 ppm, ^{13}C: δ = 29.8 ppm). The following abbreviations, or a combination thereof, were used to characterize the multiplicities: s = singlet, d = doublet, t = triplet, q = quartet, m = multiplet, br = broad. Melting points (mp) were recorded on a Mettler FP 90/82 melting point apparatus and are uncorrected. HRMS analysis were performed on either a Waters Micromass Q-Tof micro instrument or a QSTAR XL using positive electrospray ionization and a tandem quadropole time-of-flight mass analyzer (ESI+ qTOF). Preparative HPLC was performed using a Gilson pump model 305, a Gilson UV/VIS detector model 119 and a Zorbax Semi-Preparative column (250 mm × 9.4 mm, 5 μm particles, Agilent Technologies) by monitoring the compounds at 380 nm.

Synthesis of ketone 89a. A solution of *n*-BuLi in toluene (1.95 ml, 1.6 M, 3.1 mmol) was added dropwise to a stirred solution of phenyl acetylene (0.45 ml, 4.1 mmol) in THF (5 ml, 0.8 M) at -78°C. After being stirred for 1 hour at -78°C, the reaction mixture was warmed to rt, stirred for additional 15 minutes and then cooled to -78°C. The solution of lithium phenylacetylide was added to a solution of Weinreb amide **76** (0.42 g, 1.2 mmol) in THF (20

ml, 0.06 M) at -78°C via a transfer cannula. The yellow reaction mixture was stirred at -78°C for 30 minutes, then allowed to warm to rt and stirred for an additional hour. The reaction was cooled to -78°C and quenched with $NaHSO_4$ (30 ml, sat. aq.), then extracted with EtOAc (3 × 20 ml), washed with brine, dried over Na_2SO_4 and concentrated under reduced pressure. The crude product was purified by column chromatography (Petroleum ether/EtOAc 4:1) to give **89a** (0.35 g, 75 %) as pale yellow crystals; mp 137 - 139°C; δ_H(400 MHz, Chloroform-d) 4.00 (s, 2H), 7.10 – 7.18 (m, 2H), 7.28 - 7.40 (M, 6H), 7.56 - 7.58 (d, *J* = 7.68 Hz, 1H), 8.18 (br s, 1H); δ_C(101 MHz, chloroform-d) 184.5, 138.9, 133.3, 130.8, 128.6, 127.8, 122.8, 120.5, 120.0, 118.4, 114.4, 110.6, 92.5, 88.0, 80.7, 43.8.

Synthesis of alcohol 90a. A solution of *n*-BuLi in hexanes (2.5 ml, 2.5 M, 6.3 mmol) was added dropwise to a solution of phenylacetylene (0.72 ml, 6.6 mmol) in THF (13 ml, 0.5 M) at -78 °C. The reaction mixture was stirred for 25 min at -78 °C followed by 20 min at room temperature. The lithium phenylacetylide solution was added dropwise to a solution of Weinreb amide **76** (0.56 g, 1.6 mmol) in THF (65 ml, 0.025 M) at -78 °C. The reaction mixture was warmed to room temperature and stirred for 2 h, recooled to -78 °C and quenched with $NaHSO_4$ (50 ml, sat. aq./H_2O 1:1). The mixture was warmed to room temperature and the formed layers were separated. The aqueous layer was extracted with EtOAc (3 × 40 ml) and the combined organic phases were washed with brine (40 ml), dried over Na_2SO_4, filtered, and concentrated under reduced pressure until 20 ml remained. The solution was diluted with EtOH (30 ml), concentrated under reduced pressure to 20 ml, diluted with EtOH (30 ml) and finally concentrated to 20 ml again. To the solution under air atmosphere was added EtOH (45 ml) and $NaBH_4$ (72 mg, 1.9 mmol). The resulting solution was stirred for 1 h, quenched with NH_4Cl (25 ml, sat. aq.) and diluted with brine (25 ml). The mixture was extracted with DCM (2 × 40 ml) and the combined extracts were dried over Na_2SO_4, filtered and concentrated onto silica gel (7 g). The silica bound crude product was purified by column chromatography (DCM) to afford **90a** (0.44 g, 70% over 2 steps) as white crystals; R_f = 0.3 (DCM); δ_H(400 MHz, Chloroform-d) 8.19 (br s, 1H), 7.72 – 7.67 (m, 1H), 7.39 – 7.35 (m, 2H), 7.32 – 7.26 (m, 4H), 7.18 – 7.08 (m, 2H), 4.93 (apparent q, *J* = 6.3 Hz, 1H), 3.29 (dd, *J* = 14.2, 6.3 Hz, 1H), 3.25 (dd, *J* = 14.1, 6.6 Hz, 1H), 2.14 (d, *J* = 5.7 Hz, 1H).

Synthesis of alcohol 90b. A solution of *n*-BuLi in hexanes (2.8 ml, 2.5 M, 7.0 mmol) was added dropwise to a solution of 4-ethynylanisole (0.95 ml, 7.3 mmol) in THF (14 ml, 0.5 M) at -78 °C. The reaction mixture was stirred for 30 min at -78 °C followed by 15 min at room temperature. The lithium phenylacetylide solution was added dropwise to a solution of Weinreb amide **76** (1.1 g, 3.2 mmol) in THF (125 ml, 0.025 M) at -78 °C. The reaction mixture was warmed to room temperature and stirred for 2.5 h, recooled to -78 °C and quenched with $NaHSO_4$ (40 ml, sat. aq./H_2O 1:1). The mixture was warmed to room temperature and the formed layers were separated. The aqueous layer was extracted with EtOAc (3 × 50 ml) and the combined organic layers were washed with H_2O (50 ml) and brine (50 ml), dried over Na_2SO_4, filtered, and concentrated under reduced pressure until 10 ml remained. The solution was diluted with EtOH (50 ml) and concentrated under reduced pressure to 30 ml. To the solution under air atmosphere was added EtOH (100 ml) and $NaBH_4$ (129 mg, 3.4 mmol). The resulting solution was stirred for 1 h and 20 min, quenched with

NH_4Cl (40 ml, sat. aq.) and diluted with brine (50 ml). The mixture was extracted with DCM (2 × 60 ml) and the combined extracts were dried over Na_2SO_4, filtered and concentrated under reduced pressure to an oily residue. The crude product was purified by column chromatography (DCM) to yield **90b** (1.12 g, 84% over 2 steps) as slightly off-white crystals; R_f = 0.15 (DCM); mp = 47 – 49°C; δ_H(400 MHz, Chloroform-d) 8.11 (br s, 1H), 7.69 (ddt, *J* = 7.6, 1.6, 0.8 Hz, 1H), 7.34 – 7.28 (m, 3H), 7.17 – 7.12 (m, 1H), 7.12 – 7.08 (m, 1H), 6.84 – 6.78 (m, 2H), 4.91 (apparent q, *J* = 6.3 Hz, 1H), 3.27 (dd, *J* = 14.1, 6.3 Hz, 1H), 3.23 (dd, J = 14.1, 6.5 Hz), 2.02 (d, *J* = 5.9 Hz, 1H); δ_C(101 MHz, Chloroform-d) 159.6, 138.8, 133.2, 128.0, 122.4, 120.0, 118.6, 117.2, 114.7, 113.8, 110.3, 88.4, 85.3, 79.8, 63.3, 55.3, 35.6; HRMS (ESI+ qTOF) calcd for $C_{19}H_{17}INO_2$ [M + H] 418.0304, found 418.0312.

Synthesis of cyclopenta[*b*]indole-2-ol 92a. To a stirred solution of alcohol **90a** (0.41 mg, 0.11 mmol) and $PdCl_2(PPh_3)_2$ (16 mg, 0.022 mmol) in DMF (1.1 ml, 0.1 M) was added Et_3N (50 µl, 0.34 mmol) and HCOOH (8 µl, 0.21 mmol). The solution was heated to 60°C, stirred for 6 h and then cooled to rt. The mixture was run through a short pad of silica to remove the catalyst. The silica pad was eluted with EtOAc (10 ml) and the obtained solution was concentrated under reduced pressure and left under a stream of N_2 for a night to remove the DMF. Dissolution of the residue in deuterated acetone (0.7 ml) was followed by the addition of 1,3,4-trimethoxybenzene (1.61 mg, 9.6 µmol) and hexamethylbenzene (1.30 mg, 8.0 µmol) as internal standards. ^{1}H-NMR was run with a relaxation delay of 5 s. The yield was calculated by comparing product peaks at δ 6.88, 5.54 and 3.40 with those of 1,3,4-trimethoxybenzene δ 3.75 and hexamethylbenzene δ 2.17. The same method was used for all hydride sources. When the hydride source was a solid, it was added together with the substrate and catalyst.

Synthesis of cyclopenta[*b*]indole-2-ol 92b. To a stirred solution of alcohol **90b** (0.68 g, 1.6 mmol), $Pd(OAc)_2$ (72 mg, 0.32 mmol) and PPh_3 (0.17 g, 0.65 mmol) in DMF (32 ml, 0.05 M) was added Et_3N (0.70 ml, 4.8 mmol) and HCOOH (0.12 ml, 3.2 mmol). The solution was heated to 60°C, stirred for 6 h and then cooled to rt. The solution was run through a short pad of silica to remove the catalyst. The silica pad was eluted with EtOAc (100 ml) and the obtained solution was concentrated under reduced pressure at 80°C to remove most of the DMF. The oily crude product was purified by column chromatography (DCM) to give product **92b** in a mixture with DMF. The mixture was dissolved in DCM and washed with H_2O (5 × 15 ml), dried over Na_2SO_4, filtered and concentrated yield pure **92b** (0.39 g, 85 %) as tan crystals; R_f = 0.15 (DCM); mp = 187 – 190°C; δ_H(400 MHz, Acetone-d6) 10.25 (br s, 1H), 7.73 (AA' part of a AA'XX' system, 2H), 7.43 (ddt, *J* = 7.8, 1.4, 0.7 Hz, 1H), 7.35 (dt, *J* = 8.1, 1.0 Hz, 1H), 7.09 (ddd, *J* = 8.2, 7.1, 1.2 Hz, 1H), 7.01 (ddd, *J* = 7.8, 7.1, 1.1 Hz, 1H), 6.93 (XX' part of AA'XX' system, 2H), 6.72 (d, *J* = 1.4 Hz, 1H), 5.49 (ddt, *J* = 7.8, 6.1, 1.2 Hz, 1H), 4.41 (d, *J* = 8.0 Hz, 1H), 3.82 (s, 3H), 3.39 (dd, *J* = 15.8, 6.1 Hz, 1H), 2.87 (dd, *J* = 15.8, 1.1 Hz, 1H); δ_C(101 MHz, Acetone-d6) δ 159.6, 144.2, 143.2, 136.5, 131.99, 130.98, 126.0, 122.8, 122.5, 120.24, 120.23, 119.7, 114.6, 112.5, 76.9, 55.5, 36.7; HRMS (ESI+ qTOF) calcd for $C_{19}H_{18}NO_2$ [M + H] 292.1338, found 292.1336.

Synthesis of reduced scytonemin monomer 70b via Oppenaur type reaction. A solution of alcohol **92b** (0.39 g, 1.4 mmol) and Shvo catalyst (**101**) (27 mg, 0.026 mmol) in acetone

was refluxed for 24 h. The solution was cooled to rt and run through a plug of silica. The plug was further eluted with EtOAc (150 ml) and the combined solvent was concentrated onto silica (4 g). The silica bound crude product was purified by column chromatography (hexanes/DCM 1:4) to yield product **70b** (0.33 g, 85 %) as a yellow crystalline mixture of *E*/*Z*-stereoisomers. The isomers equilibrated in solution until *E/Z* 98:2 was reached. Spectroscopic data agreed with our previous report (see paper I).

Synthesis of ketone 102. A solution of *n*-BuLi in hexanes (3.2 ml, 2.5 M, 8.0 mmol) was added to a solution of phenylacetylene (1.0 ml, 9.1 mmol) in THF (11 ml, 0.8 M) at -78°C. The reaction mixture was stirred for 1 h at -78°C, then warmed to room temperature and stirred for additional 15 min. The reaction mixture was recooled to -78°C and transferred to a solution of Weinreb amide **75** (0.50 g, 2.3 mmol) in THF (32 ml, 0.07 M) at -78°C. The reaction mixture was stirred for 30 min, then warmed to room temperature and stirred for additional 75 min. The reaction was cooled again to -78°C and quenched by the addition of $NaHSO_4$ (50 ml, sat. aq.). After warming to rt, the mixture was extracted with EtOAc (3 × 40 ml) and the combined organic layers were washed with brine (80 ml), dried over $MgSO_4$ and concentrated under reduced pressure. The crude product was purified by column chromatography (Petroleum ether/EtOAc 1:1) to obtain **102** (0.48 g, 80%) as pale yellow crystals; δ_H(400 MHz, Chloroform-d) 8.16 (br s, 1H), 7.68 (ddt, *J* = 7.8, 1.4, 0.8 Hz, 1H), 7.44 – 7.29 (m, 6H), 7.26 – 7.21 (m, 2H), 7.17 (ddd, *J* = 7.7, 7.1, 1.1 Hz, 1H), 4.09 (d, *J* = 0.8 Hz, 2H).

Synthesis of alcohol 103. To a stirred solution of ketone **102** (0.28 g, 1.1 mmol) in ethanol (107 ml, 0.01 M) under air atmosphere was added $NaBH_4$ (40 mg, 1.1 mmol). The reaction mixture was stirred for 2 h at 0°C and then quenched with HCl (50 ml, 1 M, aq.). Brine (200 ml) was added and the mixture was extracted with EtOAc (50 ml) and DCM (50 ml). The combined organic layers were dried over Na_2SO_4, filtered and concentrated under reduced pressure. The crude product was purified by column chromatography (DCM) to yield **103** (97 mg, 34%) as brown crystals; δ_H(400 MHz, Chloroform-d) 8.13 (br s, 1H), 7.75 (ddt, *J* = 7.9, 1.4, 0.8 Hz, 1H), 7.42 – 7.36 (m, 3H), 7.34 – 7.28 (m, 3H), 7.23 (ddd, *J* = 8.3, 7.1, 1.2 Hz, 1H), 7.19 – 7.14 (m, 2H), 4.90 (t, *J* = 5.4 Hz, 1H), 3.35 (ddd, *J* = 14.4, 5.5, 0.8 Hz, 1H), 3.28 (ddd, *J* = 14.4, 6.6, 0.7 Hz, 1H), 2.25 (br s, 1H).

Synthesis of carbazole 105. To a stirred solution of gold catalyst **107** (18 mg, 0.02 mmol) in CH_2Cl_2 (5 ml) was added a solution of ketone **102** (52 mg, 0.20 mmol) in CH_2Cl_2 (1 ml). The reaction mixture was stirred for 4 h at rt and then run through a short silica plug, eluted with EtOAc. The solution was concentrated under reduced pressure and the obtained crude product was purified by column chromatography (DCM) to yield **105** (35 mg, 68%) as brown crystals; δ_H(400 MHz, Chloroform-d) 8.14 (br s, 1H), 8.02 (dq, *J* = 7.9, 0.8 Hz, 1H), 7.70 – 7.65 (m, 2H), 7.57 – 7.52 (m, 2H), 7.51 (dd, *J* = 2.4, 0.6 Hz, 1H), 7.47 – 7.36 (m, 3H), 7.21 (ddd, *J* = 8.0, 6.3, 1.8 Hz, 1H), 7.02 (d, *J* = 2.4 Hz, 1H), 4.82 (br s, 1H).

Synthesis of carbazole 109. To a stirred solution of gold catalyst **108** (6 mg, 0.02 mmol) in CH_2Cl_2 (5 ml) was added a solution of alcohol **103** (49 mg, 0.19 mmol) in CH_2Cl_2 (1 ml). The reaction mixture was stirred for 4 h at rt and then run through a short silica plug, eluted with

EtOAc. The solution was concentrated under reduced pressure and the obtained crude product was purified by column chromatography (petroleum ether/DCM 3:2) to yield **109** (41 mg, 90%) as brown crystals; δ_H(400 MHz, Chloroform-d) 8.32 (s, 1H), 8.13 (dq, *J* = 7.8, 0.9 Hz, 1H), 8.10 (ddd, *J* = 7.8, 1.2, 0.7 Hz, 1H), 7.74 – 7.69 (m, 2H), 7.61 – 7.55 (m, 2H), 7.49 – 7.40 (m, 4H), 7.34 (t, *J* = 7.6 Hz, 1H), 7.30 – 7.24 (m, 1H).

Synthesis of monomer 110d. To reduced monomer **70d** (60 mg, 0.14 mmol) in THF/H_2O (28 ml, 0.005 M) at 0°C under air atmosphere was added DDQ (73 mg, 0.32 mmol). The solution was stirred for 30 seconds, then diluted with EtOAc (50 ml). The solution was washed with $NaHCO_3$ (4 × 5 ml, sat. aq.) to remove DDQ-adducts. The organic layer was further washed with brine (10 ml), dried over Na_2SO_4, filtered and concentrated onto SiO_2 (1.5 g). The silica bound crude product was purified by column chromatography (petroleum ether/EtOAc 95:5) to yield monomer **110d** (13 mg, 21%) as a red oil; R_f = 0.55 (hexane/EtOAc 3:1); δ_H(400 MHz, Chloroform-d) 8.53 (AA' part of AA'XX' system, 2H), 7.69 (dt, *J* = 7.4, 1.0 Hz, 1H), 7.65 (dq, *J* = 7.8, 0.8 Hz, 1H), 7.53 – 7.48 (m, 2H), 7.22 (tt, *J* = 7.5, 0.9 Hz, 1H), 7.01 (XX' part of AA'XX' system, 2H), 6.86 (s, 1H), 1.36 – 1.25 (m, 3H), 1.13 (d, *J* = 7.4 Hz, 18H); δ_C(101 MHz, Chloroform-d) 197.3, 174.7, 162.7, 160.2, 159.6, 137.5, 135.2, 134.1, 127.3, 127.1, 126.3, 125.9, 124.2, 121.9, 120.4, 119.9, 17.9, 12.7; HRMS (ESI+ qTOF) calcd for $C_{27}H_{32}NO_2Si$ [M + 1] 430.2202, found 430.2229.

Synthesis of dimer 113d. LDA was freshly prepared by the addition of *n*-BuLi in hexanes (0.5 ml, 2.5 M, 1.24 mmol) to a stirred solution of diisopropylamine (0.19 ml, 1.4 mmol) in THF (11 ml, 0.12M) at -78°C. The solution was stirred for 30 min followed by a dropwise addition of reduced monomer **70d** (0.27 g, 0.62 mmol) in THF (11 ml, 0.06 M). The resulting enolate solution was stirred for 5 min and a solution of $FeCl_3$ (0.22 g, 1.36 mmol) in DMF (6.2 ml, 0.2 M) was added. The mixture was allowed to warm to rt, stirred for 23 h and quenched by the addition of HCl (20 ml, 0.5 M, aq.). The resulting phases were separated and the aqueous layer was extracted with EtOAc (3 × 15 ml). The combined organic layers were washed with H_2O (3 × 12 ml) and brine (10 ml), dried over Na_2SO_4, filtered and concentrated to a black oily residue. The crude product was purified by column chromatography (hexane/DCM 95:5 → 1:1) to yield **113d** (0.14 g, 52%) as an oily mixture of diastereoisomers; R_f = 0.2 (Hexane/DCM 1:1); HRMS (ESI+ qTOF) calcd for $C_{54}H_{65}N_2O_4Si_2$ [M + 1] 861.4483, found 861.4483; No NMR is reported due to the mixture of diastereoisomers, which produce a complex NMR-spectrum.

Synthesis of dimer 113f. LDA was freshly prepared by the addition of *n*-BuLi in hexanes (0.16 ml, 2.5 M, 0.39 mmol) to a stirred solution of diisopropylamine (60 µl, 0.40 mmol) in THF (2 ml, 0.2 M) at -78°C. The solution was stirred for 30 min followed by a dropwise addition of reduced monomer **70f** (76 mg, 0.19 mmol) in THF (6 ml, 0.03 M). The resulting enolate solution was stirred for 5 min and a solution of $FeCl_3$ (69 mg, 0.42 mmol) in DMF (2.2 ml, 0.2 M) was added. The mixture was allowed to warm to rt, stirred for 22 h and quenched by the addition of HCl (8 ml, 0.5 M, aq.). The resulting phases were separated and the aqueous layer was extracted with EtOAc (3 × 8 ml). The combined organic layers were washed with H_2O (3 × 8 ml) and brine (8 ml), dried over Na_2SO_4, filtered and concentrated to a brown solid. The crude product was purified by column chromatography (hexane/DCM 1:1

→ 0:1) to yield **113f** (45 mg, 59%) as an amorphous solid mixture of diastereoisomers; R_f = 0.25 (DCM); HRMS (ESI+ qTOF) calcd for $C_{52}H_{41}N_2O_6$ [M + 1] 789.2965, found 789.3104; No NMR is reported due to the mixture of diastereoisomers, which produce a complex NMR-spectrum.

Synthesis of TIPS-protected scytonemin 16d. To a stirred solution of isomeric mixture **113d** (84 mg, 0.1 mmol) in THF (10 ml, 0.01 M) at 0°C under air atmosphere was added DDQ (47 mg, 0.21 mmol). The resulting dark solution was stirred for 15 min and then diluted with EtOAc (40 ml). The mixture was washed with $NaHCO_3$ (4 × 10 ml, sat. aq.) to remove DDQ adducts and brine (10 ml), dried over Na_2SO_4, filtered and concentrated. The crude product was run through a pad of silica, eluted with DCM/EtOH (50 ml, 3:1), to further remove DDQ adducts. The solution was concentrated to yield rather pure **16d** (77 mg, 92%) as a dark solid; δ_H(400 MHz, Chloroform-d) 8.60 (AA' part of AA'XX' system, 2H), 7.68 (s, 1H), 7.63 (dt, *J* = 7.7, 0.8 Hz, 1H), 7.49 (td, *J* = 7.6, 1.2 Hz, 1H), 7.44 (ddd, *J* = 7.5, 1.3, 0.6 Hz, 1H), 7.15 (td, *J* = 7.5, 1.0 Hz, 1H), 7.04 (XX' part of AA'XX' system, 2H), 1.38 – 1.24 (m, 3H), 1.14 (d, *J* = 7.3 Hz, 18H).

Synthesis of scytonemin (1) from 16d. To a stirred solution of **16d** (58 mg, 0.067 mmol) in DMF/H_2O (6.7 ml, 20:1, 0.01 M) at 0°C under air atmosphere was added solid KOAc (27 mg, 0.27 mmol). The solution was warmed to rt, stirred for 15 min and then diluted with EtOAc (60 ml). The solution was washed with H_2O (4 × 20 ml) and brine (20 ml), dried over Na_2SO_4, filtered and concentrated to a black solid. The solid was dissolved in THF (2 ml) and precipitated by the dropwise addition of hexane (50 ml) over 5 h. The mixture was cooled to -20°C and after 14h, the motherliquid was removed using a pipette. The precipitate was dissolved in THF (16 ml), diluted with H_2O/MeCN (18 ml, 4:1) and divided into four equal portions. Each of the four solutions was purified on a column packed with C18-silica (0.5 g, pre-equilibrated with 3 ml MeOH and 3 ml H_2O/MeCN 4:1). The columns were eluted with additional H_2O/MeCN (4 ml, 4:1) and THF (5 ml) each. One fraction (**A**) was eluted with H_2O/MeCN and a second (**B**) with THF. The first fraction (**A**) was concentrated under reduced pressure to remove MeCN, diluted with EtOAc (100 ml) and brine (20 ml). The layers were separated and the aqueous phase was extracted with EtOAc (50 ml). The combined organic layers were washed with H_2O (3 × 15 ml) and brine (15 ml), dried over Na_2SO_4, filtered and concentrated under reduced pressure to yield scytonemin (20 mg) as a green/brown solid. The second fraction (**B**) was concentrated under reduced pressure to remove THF, diluted with EtOAc (60 ml), washed with H_2O (3 × 10 ml) and brine (10 ml), dried over Na_2SO_4, filtered and concentrated to a dark solid. The solid was dissolved in acetone (5 ml) and purified by preperative HPLC. Aliquots of 0.2 ml were injected and eluted with H_2O/MeCN (3:7) at a flow rate of 10 ml/min. The obtained solution was concentrated under reduced pressure to remove MeCN and the resulting aqueous solution was extracted with EtOAc (3 × 50 ml). The combined extracts were washed with brine (50 ml), dried over Na_2SO_4, filtered and concentrated to yield scytonemin (6 mg) as a green/brown solid. Totally 26 mg, 71 %, scytonemin was obtained; Spectroscopic data agreed with our previous reports.

Synthesis of scytonemin (1) from 113f. BBr_3 in DCM (0.13 ml, 1 M, 0.13 mmol) was added to a stirred solution of dimer **113f** (26 mg, 0.03 mmol) in DCM (3.3 ml, 0.01 M) at -78°C.

The dark solution was stirred for 50 min and then quenched with H_2O (3.3 ml). After warming the mixture to rt, EtOAc (12 ml) was added and the formed layers were separated. The aqueous layer was extracted with EtOAc (2 × 7 ml) and the combined organic phases were washed with brine (7 ml), dried over Na_2SO_4, filtered and concentrated under reduced pressure to a red/brown solid. The crude product was dissolved in THF (1.65 ml) under air atmosphere and cooled to -78°C. DDQ (16 mg, 0.07 mmol) was added and the resulting mixture was stirred for 20 min followed by concentration under reduced pressure. The black solid was dissolved in acetone (2 ml) and precipitated by the addition of hexane (10 ml). The solid precipitate was redisolved in acetone (5 ml) and purified by preparative HPLC. Aliquots of 0.1 ml were injected and eluted with H_2O/MeCN (3:7) at a flow rate of 7 ml/min. The obtained solution was concentrated under reduced pressure to remove MeCN and the resulting aqueous solution was extracted with EtOAc (3 × 20 ml). The combined extracts were washed with brine (20 ml), dried over Na_2SO_4, filtered and concentrated to yield scytonemin (4 mg, 24%) as a green/brown solid; Spectroscopic data agreed with our previous reports.